

NASA CR- 166750

ER-275

STUDY OF HOLLOW CORNER RETROREFLECTORS  
FOR USE IN A SYNCHRONOUS ORBIT

P. R. Yoder, Jr.  
The Perkin-Elmer Corporation  
Optical Technology Division  
Wooster Heights Road  
Danbury, Conn. 06810

(NASA-CR-166750) STUDY OF HOLLOW CORNER RETROREFLECTORS FOR USE IN A SYNCHRONOUS ORBIT Final Report, Sep. 1974 - Feb. 1975 (Perkin-Elmer Corp., Danbury, Conn.) 119 p  
HC A06/MF A01 N82-12931  
Unclas  
CSCL 20F G3/74 02630

March 1975  
Final Report for Period September - February 1974-1975  
Prepared under Contract NAS 5-20580

Prepared for  
GODDARD SPACE FLIGHT CENTER  
Greenbelt, Maryland 20771

1. Report No. ER-275	2. Government Accession No.	3. Recipient's Catalog No.	
4. Title and Subtitle STUDY OF HOLLOW CORNER RETROREFLECTORS FOR USE IN A SYNCHRONOUS ORBIT		5. Report Date March 1975	6. Performing Organization Code
		8. Performing Organization Report No. ER-275	
7. Author(s) P. R. Yoder, Jr.		10. Work Unit No.	11. Contract or Grant No. NAS 5-20580
9. Performing Organization Name and Address The Perkin-Elmer Corporation Optical Technology Division Wooster Heights Road Danbury, Conn. 06810		13. Type of Report and Period Covered Block III Sep 74/Feb 75	
		14. Sponsoring Agency Code	
12. Sponsoring Agency Name and Address Mr. Peter Minott Code 722 Goddard Space Flight Center Greenbelt, Maryland 20771			
15. Supplementary Notes			
16. Abstract <p>The purpose of this study was to determine how a hollow corner cube retro-reflector made up of three mutually perpendicular optically flat mirrors would perform when undergoing the thermal-mechanical strains induced by a spacecraft environment. Of particular interest was a device of 200 square centimeter optical aperture used on a satellite in a synchronous orbit. It was assumed that the reflector always faces the earth. The effects of direct solar irradiance, earthshine and albedo were considered. The results included the maximum mirror surface temperature during the orbit as well as the worst-case loss of optical performance due to thermally-induced mirror distortions.</p> <p>It was concluded that a device made of three suitably coated flat ULE mirrors, optically contacted to each other and supported mechanically in a nonrigid mount, would be expected to concentrate over 80 percent of the theoretical maximum energy in the central maximum of the far field diffraction pattern. Continued development of the device through a detailed design, fabrication and test phase is recommended.</p>			
17. Key Words (Selected by Author(s)) Corner Cube, Retroreflector, Thermal Analysis, Far Field Dif- fraction Effects, Synchronous Satellite Instrumentation		18. Distribution Statement	
19. Security Classif. (of this report) Unclassified	20. Security Classif. (of this page) Unclassified	21. No. of Pages 130	22. Price*

\*For sale by the Clearinghouse for Federal Scientific and Technical Information, Springfield, Virginia 22151.

## PREFACE

This report discusses a study under Contract NAS 5-20580 for NASA Goddard Space Flight Center which was conducted jointly by the Optical Technology Division and the Electro-Optical Division of The Perkin-Elmer Corporation on a hollow corner cube retroreflector (HCR). The purpose of the study was to determine how the HCR, made up of three optically flat mirrors, would perform when undergoing the thermal-mechanical strains induced by a spacecraft environment. Of particular interest was a device with an optical aperture of 200 square centimeters used on a satellite in a synchronous orbit. The satellite was assumed to be stabilized in three axes with the reflector on the earth-facing side and oriented so that its axis of symmetry was directed toward the earth's center. The effects of direct solar irradiance, earthshine and albedo were considered. The results included the maximum mirror surface temperature during the orbit as well as the worst-case loss of optical performance resulting from thermally-induced mirror distortions.

In order to conduct this thermal analysis as realistically as possible, Perkin-Elmer's efforts were first directed toward identifying various ways in which the HCR could be fabricated, comparing candidate materials for the mirrors and adhesives to be used in assembly, and considerations of the optical effects of defects in the device. After careful consideration, Perkin-Elmer established a preferred configuration employing a proven technique for fabricating the optical assembly and optical materials with relatively low sensitivity to the anticipated environment. The proposed preliminary design for the HCR was then analyzed using mechanical and thermal computer programs available at Perkin-Elmer. While not an exhaustive analysis, the results are considered representative of the actual worst-case condition in orbit.

It was concluded that a HCR made of three suitably coated flat ULE mirrors, optically contacted to each other and supported mechanically in a nonrigid mount, would be expected to perform quite well in the environment of a synchronous satellite in spite of the deleterious effects of solar irradiation

during the orbital period. The optical performance, measured in terms of the energy contained in the central maximum of the retroreflected diffraction pattern, should exceed 80 percent of that theoretically possible in the absence of defects.

The investigation presented here represents the combined efforts of many individuals within Perkin-Elmer. Mr. Herbert Wischnia was responsible for the initial planning phase of the investigation while Mr. Paul R. Yoder, Jr. was the project engineer and chief investigator during the actual study effort. Mr. Peter Minott, Code 722 of the Goddard Space Flight Center, was the NASA Technical Officer.

The chief Perkin-Elmer contributors to technical aspects of this program were Mr. Justin Kreuzer who investigated the diffraction effects in a hollow corner retroreflector, Dr. Herbert Yanowitz who analyzed the anticipated thermal distortions of the device in a specific space environment, and Mr. Francis Foster who calculated the retroreflected optical wavefront aberrations due to these thermal distortions. Messrs. Joseph Vrabel, Edwin Pelkey, Walter Augustyn, and Edward Strouse contributed many valuable suggestions in the areas of retroreflector design, surface coating technology, and component fabrication techniques.

Continuation of this program through a detailed design, fabrication and test phase is recommended. Under this follow-on effort, several prototype units would be fabricated and evaluated in a simulated orbital environment in order to provide practical experience and realistic performance data. It is believed that this is a logical and necessary next step toward the eventual application of the HCR to an operational satellite.

## TABLE OF CONTENTS

<u>Section</u>	<u>Title</u>	<u>Page</u>
1	DIFFRACTION INTEGRAL ANALYSIS .....	1-1
1.1	Hollow Corner Cube Retroreflector Far Field	
	Considerations .....	1-1
1.1.1	Normal Incidence .....	1-4
1.1.2	Oblique Incidence .....	1-5
1.1.3	Reflectance Variations .....	1-8
1.1.4	Dihedral Angle Errors .....	1-9
1.1.5	Mirror Plate Distortions .....	1-11
2	POTENTIAL HCR CONFIGURATIONS .....	2-1
2.1	Comparison of Candidate Configurations .....	2-1
2.1.1	Optically Contacted Plates .....	2-1
2.1.2	Epoxy Joined Plates .....	2-4
2.1.3	Internal Structure .....	2-6
2.1.4	External Structure .....	2-6
2.1.5	Core-Out Solid .....	2-6
2.1.6	Epoxy Replication .....	2-9
2.1.7	"Pelkey Prisms" .....	2-9
2.1.8	Exterior Structure with Replicated Surface ....	2-11
2.1.9	"Vrabel HCR" .....	2-11
2.2	Geometrical Relationships in a HCR .....	2-13
2.3	Properties of Potential HCR Materials .....	2-19
2.3.1	Dimensional Stability .....	2-19
2.3.2	Thermal Stability .....	2-26
2.3.3	Compatibility with Optical Fabrication .....	2-27
2.3.4	Optical Coating Considerations .....	2-28
2.4	Establishment of Preferred HCR Configuration ....	2-31
2.4.1	Optical Considerations .....	2-31
2.4.2	Some Considerations of Mechanical Mounting and Thermal Interface .....	2-33
3	THERMAL ANALYSIS OF HCR IN GEOSYNCHRONOUS ORBIT ....	3-1
3.1	Deformation Due to Unit Temperature Gradient ....	3-1
3.2	Input Thermal Flux Received During Orbit .....	3-8
3.3	Temperature Profile Analysis .....	3-23
3.4	Literature Search .....	3-23
4	OPTICAL EFFECTS OF THERMAL DISTORTIONS .....	4-1
5	CONCLUSIONS AND RECOMMENDATIONS .....	5-1
6	REFERENCES .....	6-1

## TABLE OF CONTENTS (Continued)

<u>Section</u>	<u>Title</u>	<u>Page</u>
APPENDIX A	SOME CONSIDERATIONS OF BONDED HCR AS MANUFACTURED BY PRECISION LAPPING & OPTICAL CO., INC. ....	A-1
APPENDIX B	HIGH PRECISION 10-CM APERTURE PENTA AND ROOF-PENTA MIRROR ASSEMBLIES .....	B-1
APPENDIX C	OUTLINE OF 58 NODE COMPUTER MODEL PROPOSED FOR MORE DETAILED THERMAL ANALYSIS OF THE HCR .....	C-1

## LIST OF ILLUSTRATIONS

<u>Figure</u>	<u>Title</u>	<u>Page</u>
1-1	HCR Aperture for an Oblique Incidence Wavefront .....	1-5
1-2	Far Field Coordinates .....	1-7
1-3	Wavefront Sectors .....	1-10
2-1	Optically Contacted Plates .....	2-3
2-2	Epoxy Joined Plates .....	2-5
2-3	Internal Structure .....	2-7
2-4	External Structure .....	2-8
2-5	Core-Out .....	2-8
2-6	Cast Epoxy Replication .....	2-9
2-7	The "Pelkey Prism" HCR .....	2-10
2-8	Exterior Machined Structure with Replicated Optical Surface .....	2-12
2-9	"Vrabel HCR" - Plates and Base in Optical Contact .....	2-12
2-10	Geometrical Relationships .....	2-14
2-11	Reflector Face Area Utilized at Infinity and Symmetrical Incidence .....	2-16
2-12	Photographs of Full-Sized Wooden Mock-Ups of Four Types of HCRs .....	2-17
2-13	Coefficient of Expansion of Typical Materials - Variation with Temperature .....	2-23
2-14	Hollow Corner Reflector .....	2-34
2-15	A Suggested Mechanical Interface with the HCR Assembly	2-36
3-1	Thermal Distortions of a Front-Irradiated HCR .....	3-3
3-2	Nodal Locations and Element Description for NASTRAN Analysis of HCR Plate Deflections .....	3-5
3-3	Results of Constrained-Plate NASTRAN Analysis (Deflection in Z Direction) .....	3-6
3-4	Results of Constrained-Plate NASTRAN Analysis (Deflection in Minus Z Direction ) .....	3-7
3-5	Solar and Albedo Fluxes Incident Upon an Earth Oriented Flat Plate in a Synchronous Orbit .....	3-9

## LIST OF ILLUSTRATIONS (Continued)

<u>Figure</u>	<u>Title</u>	<u>Page</u>
3-6	Schematic of 7-Node Model Used to Estimate Temperature Gradients Through the HCR Plates .....	3-10
3-7	Paths of Rays Incident Upon a Single Point A on the Surface of a HCR when all Surfaces are Illuminated ..	3-13
3-8	Typical Geometry for HCR in Synchronous Orbit .....	3-15
3-9A	Solar Flux Distribution, $\gamma = 200^\circ$ .....	3-18
3-9B	Solar Flux Distribution, $\gamma = 220^\circ$ .....	3-18
3-9C	Solar Flux Distribution, $\gamma = 240^\circ$ .....	3-19
3-9D	Solar Flux Distribution, $\gamma = 261^\circ$ .....	3-19
3-9E	Solar Flux Distribution, $\gamma = 279^\circ$ .....	3-20
3-9F	Solar Flux Distribution, $\gamma = 300^\circ$ .....	3-20
3-9G	Solar Flux Distribution, $\gamma = 320^\circ$ .....	3-21
3-9H	Solar Flux Distribution, $\gamma = 340^\circ$ .....	3-21
4-1	Coordinate System for HCR Wavefront Distortion Analysis .....	4-11
4-2A	OPD Map of Lower Right Quadrant of HCR Aperture - Hypothetical Case 1 .....	4-12
4-2B	OPD Map of Lower Right Quadrant of HCR Aperture - Hypothetical Case 2 .....	4-13
4-3A	Semi-Profiles of Concave Wavefront Reflected from Thermally Distorted HCR - Hypothetical Case 1 .....	4-15
4-3B	Semi-Profiles of Concave Wavefront Reflected from Thermally Distorted HCR - Hypothetical Case 2 .....	4-16
4-4	Variation of Central Maximum Intensity with RMS Wavefront Error .....	4-19

## LIST OF TABLES

<u>Table</u>	<u>Title</u>	<u>Page</u>
2-1	Comparative Configurations .....	2-2
2-2	Dimensions for a HCR with Aperture Area = $200 \text{ cm}^2$ .....	2-15
2-3	Size and Mass Comparisons of Two HCR Configurations ...	2-20
2-4	Published Physical Properties of Potential Hollow Corner Cube Materials .....	2-22
2-5	Reflectance Characteristics of Typical Optical Coatings .....	2-29
3-1	Material Properties of ULE Used in Analysis .....	3-4
3-2	Three Special Cases of HCR Irradiation .....	3-16
3-3	Calculated Worst-Case HCR Mirror Temperatures .....	3-17
4-1	Ray Trace Printout of Thermally Distorted HCR - Hypothetical Case 1 .....	4-3
4-2	Ray Trace Printout of Thermally Distorted HCR - Hypothetical Case 2 .....	4-7
4-3	Summary of Surface Distortions and Optical Effects ....	4-18

# SECTION 1

## DIFFRACTION INTEGRAL ANALYSIS

### 1.1 HOLLOW CORNER CUBE RETROREFLECTOR FAR FIELD CONSIDERATIONS

This section considers the pattern of the light reflected by a hollow corner cube retroreflector (HCR) far away from the corner cube, that is, for distances much greater than  $R^2\lambda$  where  $\lambda$  is the wavelength of light and  $R$  is the radius of the HCR aperture. At such large distances, the light pattern is called the far field pattern.<sup>1</sup> This pattern is not a function of distance from the cube; it is a function only of angular coordinates measured from the cube, the cube orientation, and the cube properties as well as defects in those properties.

For the purpose of this analysis, it is assumed that only one of the cube parameters departs from an ideal HCR. An ideal HCR consists of three mirrors which intersect at right angles in analogy to the corner formed by three adjacent sides of a cube. Each mirror is a perfectly flat, front surfaced reflector of infinite conductivity so that it is a perfect (i.e., 100 percent reflecting) mirror which produces no undesired changes in the polarization of the reflected light. The shape or aperture of the returned beam depends upon the angle of incidence and the contour which defines the nonintersecting portions of the three mirrors, as well as any aperture limiting structure in front of the HCR. Let it be assumed that each of the three mirrors is terminated by a similar curve. In particular, assume that the three mirrors are cut so that the reflector presents a circular aperture when viewed parallel to its axis.

It will be convenient to assume that the reflector is surrounded by a right circular cylindrical tube or mask whose front edge is just flush with the cube entrance face. Thus the HCR aperture at oblique incidence corresponds to the common area of two identical, sheared intersecting circles.

Assuming that a monochromatic plane wave is incident on the corner cube from the desired direction, the far field pattern will be calculated in two sequential steps. The first step will use conventional geometric optical techniques to calculate the returned wavefront just in front of the cube. This ignores internal diffraction within the corner cube. Such diffraction appears to occur in a single plane in the aperture of the corner cube. This will suffice in our case as it includes the first order effects of any departures from the ideal, such as gaps associated with the actual intersection of the mirrors and mirror irregularities, including nonflatness, reflectance variations and polarization properties.

The actual far field pattern is computed in the second step by taking the two-dimensional Fourier transform of the returned wave.

When polarization effects are considered, the returned wavefront polarization is calculated for each of two incident orthogonal polarizations, typically "horizontal and vertical" linear polarization. The far field is computed by taking the four Fourier transforms -- one of the horizontal component and one of the vertical component of the returned wavefront for each of the two incident polarizations.

The computation of the far field can be either analytically derived and then numerically evaluated or evaluated numerically directly. In general, the analytic expression is fairly complex even with only a single departure from our ideal retroreflector. The analytic expressions are useful in understanding the effect of various parameters upon performance, but are generally more complex to evaluate numerically than a direct numerical computation.

The analytic far field expressions will be derived with the aid of the following general expressions. The far field pattern energy density can be expressed as the function:

$$F(\rho, \phi) = \frac{I}{I_0} = \frac{I}{\lambda^2} |U(\rho, \phi)|^2 \quad (1-1)$$

where  $I$  is the far field angular energy density in watts per steradian and  $I_0$  is the incident light energy density just in front of the corner cube in watts per square meter.  $U(\rho, \phi)$  is the (scaled) two dimensional Fourier transform of  $U(r, \theta)$ , the returned wavefront near the cube written in terms of conventional polar coordinates  $(r, \theta)$  in the plane perpendicular to the direction of the incident and returned beams.

$$U(\rho, \phi) = \iint u(r, \theta) e^{-jk\rho r \cos(\phi - \theta)} r dr d\theta \quad (1-2)$$

where

$r$  is in meters

$\theta$  is in radians

$k = \frac{2\pi}{\lambda}$  is the wave number

$(\rho, \phi)$  are the corresponding polar (spherical) coordinates, respectively, in the far field. Both  $\rho$  and  $\phi$  are in radians with an origin at the cube and  $\rho = 0$  corresponding to the incident or returned beam.  $\rho$  corresponds to latitude and  $\phi$  corresponds to longitude.

The far field pattern is related to the classical radar cross section:

$$\sigma = 4\pi F \quad (1-3)$$

The Bradley or velocity aberration causes an additive angle offset in the far field patterns in the direction of motion. This is ignored here. The correction is easily made. In the absence of aberration, the energy density returned is

$$F(0,0) = \frac{A^2}{\lambda^2} \quad (1-4)$$

where  $A$  is the corner cube cross sectional area as seen by the transmitter. This area is a function of the cube orientation.

At large angles away from this region, we observe the complex fringe pattern normally associated with diffraction from a complex aperture. The energy density at larger angles is essentially a function of the aperture edge shape. When the fringes are averaged out, the energy decreases proportionally to  $\rho^{-n}$  where  $n = 2, 3$  or  $4$  in different directions, depending upon whether the diffraction arises from a straight or curved edge or vertex (corner) of the aperture.

### 1.1.1 Normal Incidence

The far field pattern at normal incidence of an HCR of aperture radius  $R$  is the Fourier transform of a circular aperture which is merely the conventional, well-known Airy diffraction pattern given by

$$F(\rho, \phi) = \frac{(\pi R^2)^2}{\lambda^2} \left( \frac{2J_\ell(P)}{P} \right)^2 \quad (1-5)$$

where, in general,  $J_\ell(P)$  is the  $\ell^{\text{th}}$  Bessel function.

Here it will be convenient to write

$$P = Rk\rho \quad (1-6)$$

to define a scaled polar far field radian angle. The center of the far field pattern in the direction of the geometric retroreturn is given by

$$F(0,0) = \frac{(\pi R^2)^2}{\lambda^2} \quad (1-7)$$

At large angles, the far field pattern can be approximated quite accurately by

$$F(\rho, \phi) \approx \frac{\lambda R}{\pi^2 \rho^3} \cos^2\left(P - \frac{3}{4}\pi\right) \quad (1-8)$$

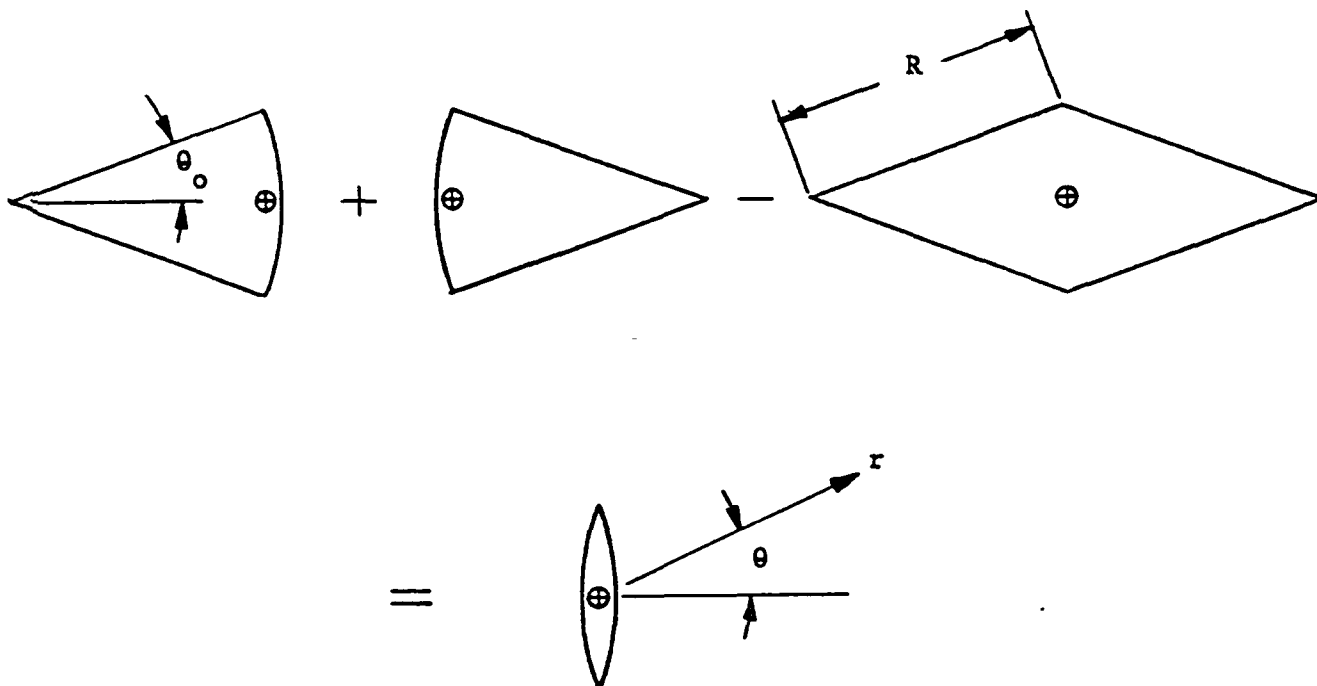
If we average out the interference fringes, the average far field energy is given by

$$F(\rho, \phi) \approx \frac{\lambda R}{2\pi^2 \rho^3} \quad (1-9)$$

Here it is seen that the energy falls off according to the cube of the angle away from the main return.

### 1.1.2 Oblique Incidence

The far field pattern of our ideal corner cube for oblique incidence is the Fourier transform of the common area of two sheared circles. The Fourier transform may be conveniently evaluated by utilizing the property of linearity and noting that the common area of two sheared circles can be represented by the sum of the areas of the two segments minus the area of the rhombus (see Figure 1-1). The Fourier transform of the circular segments is most easily



NOTE:  $\oplus$  INDICATES THE COMMON CENTER.

Figure 1-1. HCR Aperture for an Oblique Incidence Wavefront

derived in polar coordinates while the Fourier transform of the rhombus is most readily derived in Cartesian coordinates. The Fourier transforms of these three figures are then added with the appropriate phase corresponding to their position. The scaled Fourier transform of the two sectors with the common center shown in Figure 1-1 is

$$U_s(\rho, \phi) = 4\theta_o R^2 \sum_{\ell=0}^{\infty} G_{\ell}(P) \operatorname{sinc} \ell \theta_o \cos(P \cos \theta_o \cos \phi + \ell \frac{\pi}{2}) \cos \ell \phi \quad (1-10)$$

where it is convenient to define the functions  $\operatorname{sinc} x \equiv \sin x/x$ ;  $\operatorname{sinc}(0) \equiv 1$  and

$$G_{\ell}(P) = \begin{cases} \frac{2}{P^2} \int_0^P j_{\ell}(x) x dx & \text{for } \ell \neq 0 \\ \frac{1}{P^2} \int_0^P j_0(x) x dx = \frac{J_1(P)}{P} & \text{for } \ell = 0 \end{cases} \quad (1-11)$$

and the following relates the sector angle  $\theta_o$  to the angle of incidence or return  $i$  to the corner cube normal:

$$\theta_o = \cos^{-1} (\sqrt{2} \tan i) \quad (1-12)$$

The scaled Fourier transform of the rhombus is

$$U_r(\rho, \phi) = R^2 \sin^2 \theta_o \operatorname{sinc} \left[ \frac{1}{2} P \cos (\theta_o + \phi) \right] \operatorname{sinc} \left[ \frac{1}{2} P \cos (\theta_o - \phi) \right] \quad (1-13)$$

Thus the far field pattern at oblique incidence is given by Equation (1-1) and

$$U(\rho, \phi) = U_s(\rho, \phi) - U_r(\rho, \phi) \quad (1-14)$$

This is a complex expression. It is informative to consider briefly two special cases separately -- one for the peak retroreflection and a second expression for large angles. The central peak return of the far field pattern is proportional to the square of the cross-sectional area presented by the hollow corner cube.

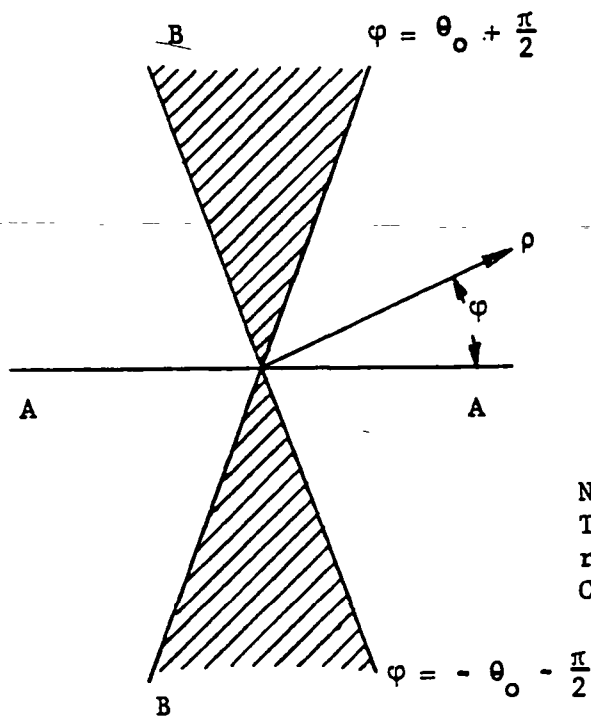
This is given by

$$A = \pi R^2 \left( \frac{2\theta_0}{\pi} \right) (1 - \text{sinc } 2\theta_0) \quad (1-15)$$

The far field pattern at large angles may be derived from the asymptotic expressions for diffraction. The energy at larger angles in the far field is found to fall off the cube of the off-axis angle in Region A of Figure 1-2 and with the fourth power of that angle in Region B.

The far field pattern at larger angles is associated primarily with diffraction from the edges of the corner cube. We have assumed that there are no "gaps" where the corner mirrors meet within the reflector. If there were, these would contribute to the far field pattern at large angles for both normal and oblique incidence. Asymptotic expansion of the far field pattern for larger angles with the fine interference fringes averaged out yields for Region A:

$$F(\rho, \phi) \approx \frac{\lambda R}{2\pi^2 \rho^3} \quad \text{for } |\rho| \gg \frac{\lambda}{R \cos \theta_0} \quad (1-16)$$



NOTE: THE VECTOR  $\rho$  HAS THE SAME ORIENTATION AS  $r$  IN FIGURE 1.1 SO  $\theta = \theta_0$  CORRESPONDS TO  $\phi = 0$ .

Figure 1-2. Far Field Coordinates

This is the same as Equation (1-9). Likewise, we find for Region B:

$$F(\rho, \phi) \approx \frac{\lambda^2}{8\pi^4} \frac{\sin^2 2\theta_0}{\cos^2(\theta_0 + \phi) \cos^2(\theta_0 - \phi)} \frac{1}{\rho^4} \quad \text{for } \rho \gg \frac{\lambda}{R \sin \theta_0} \quad (1-17)$$

The smaller value of Equations (1-16) or (1-17) applies in Region B near the four boundary lines.

Diffraction from Region A is associated with the curved portion of the aperture, while that in Region B is associated with the two vertices of the aperture.

### 1.1.3 Reflectance Variations

Mirror reflectance variations will be associated directly with polarization effects. These effects should be combined directly with the associated polarization effects and the far field computed numerically as previously mentioned. Here, reflectance variations will be considered alone. Uniform differences in reflectance for each of the three mirrors that are not a function of the angle of incidence do not show separately in the wavefront because all of the rays bounce from all three mirrors. The most significant effect is that the returned energy will be lowered by the triple reflection. In general, the associated polarization effects will be even more important. The reduction in the central returned beam energy is a complex function of the angle of incidence, the basic reflector and any dielectric coatings which may be placed over the reflector to improve the reflectance at certain wavelengths and to control polarization changes.

Next, we will consider briefly the effect of small reflectance variations (mottling) over the surface of a mirror. Such mottling will scatter light out of the main returned beam in analogy to the effect of small random wavefront errors. A single flat mirror reflecting light near normal incidence will be considered now.

Let the mirror have a mean energy reflectance  $R_0$  and a small random reflectance variation with a standard deviation  $\Delta R_{\text{rms}}$ . Likewise, let the mirror

surface have a small random low spatial frequency depth variation with a standard deviation  $\Delta D_{\text{rms}}$ . The reflected wavefront has twice the deformation. The reflectance and depth variations are uncorrelated. The main returned beam energy from such a simple mirror is proportional to

$$R_o \left[ 1 - \frac{1}{4} \left( \frac{\Delta R_{\text{rms}}}{R_o} \right)^2 - 16\pi^2 \left( \frac{\Delta D_{\text{rms}}}{\lambda} \right)^2 \right] \quad (1-18)$$

in analogy to the conventional phase-dependent Strehl intensity. Here we see that reflectance variations are not important. For example, if  $R_o = 1$ , a reflectance standard deviation of  $\Delta R_{\text{rms}} = 0.2$  reduces the main return by only one percent, which corresponds to the reduction due to a surface depth standard deviation of  $\Delta D_{\text{rms}}/\lambda = 8 \times 10^{-3}$  waves corresponding to a wavefront phase deformation of twice this amount. The reflectance is not likely to be this non-uniform, and the mirrors are not likely to be so smooth. Thus reflective variations seem unimportant.

#### 1.1.4 Dihedral Angle Errors

Here the far field pattern of our ideal cube at normal incidence with small dihedral angle errors will be considered. We will follow the notation and use the results of Yoder and Chandler.<sup>2,3</sup> The dihedral angle errors,  $\alpha$ ,  $\beta$ ,  $\gamma$  are the angles in radians in excess of  $\pi/2$  radians between the three mirrors labeled a, b and c, respectively, in Figure 1-3.

The far field can be written with the aid of Equation (1-1) as a sum of six scaled Fourier transforms, one from each  $\pi/3$  radian sector.

$$U(\rho, \phi) = \sum_{\ell=1}^6 U_{\ell}(\rho, \phi) \quad (1-19)$$

Each sector has a linear phase due to the plate angle errors. The phase is negative in opposite segments. The returned wavefront phase is continuous at

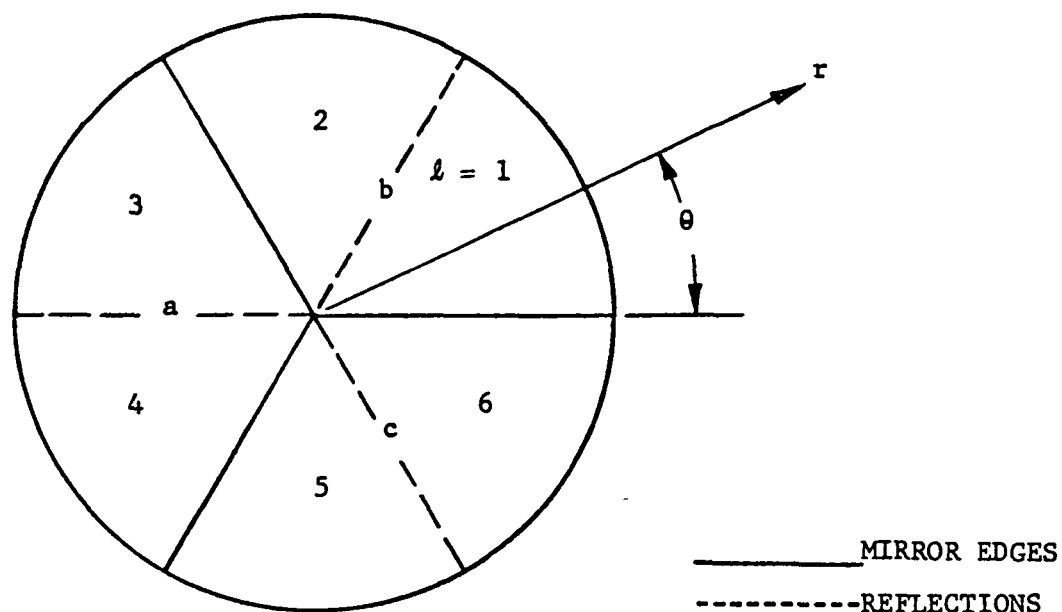


Figure 1-3. Wavefront Sectors

the center of the cube. The scaled Fourier transform of the returned wave from the  $\ell^{\text{th}}$  segment is

$$U_{\ell}(\rho, \phi) = \frac{\pi}{3} R^2 \sum_{m=0}^{\infty} \text{sinc} \left( m \frac{\pi}{6} \right) e^{-jm \frac{\pi}{2}} \cos \left[ m \left( \frac{2\ell-1}{6} - \phi_{\ell} \right) \right] G_m(P_{\ell}) \quad (1-20)$$

where

$$P_{\ell} = kR \sqrt{\rho^2 + A_{\ell}^2 - 2\rho A_{\ell} \cos(\phi - \theta_{\ell})} \quad (1-21)$$

and

$$\phi_{\ell} = \tan^{-1} \left[ \frac{\rho \sin \phi - A_{\ell} \sin \theta_{\ell}}{\rho \cos \phi + A_{\ell} \cos \theta_{\ell}} \right] \quad (1-22)$$

are linearly translated polar coordinates. The translation is due to the wavefront linear phase error. Here

$$A_{\ell} = 2 \sqrt{(\alpha^2 + \beta^2 + \gamma^2) - \frac{1}{3} B_{\ell}} \quad (1-23)$$

may be considered to give the magnitude or latitude of the error in radians and

$$\theta_{\ell} = \sin^{-1} \left[ \frac{1}{A_{\ell}} \sqrt{\frac{2}{3}} C_{\ell} \right] \quad (1-24)$$

gives the corresponding orientation or longitude.

The symmetry of the cube yields

$$\begin{aligned} A_1 &= A_4 & A_2 &= A_5 & A_3 &= A_6 \\ \theta_1 &= \theta_4 + \pi & \theta_2 &= \theta_5 + \pi & \theta_3 &= \theta_6 + \pi \end{aligned} \quad (1-25)$$

and the actual wavefront errors are related to the plate angle errors by

$$\begin{aligned} B_1 &= \alpha - \beta + \gamma & B_2 &= \alpha - \beta - \gamma & B_3 &= \alpha + \beta - \gamma \\ C_1 &= 2\alpha + \beta - \gamma & C_2 &= 2\alpha + \beta + \gamma & C_3 &= 2\alpha - \beta + \gamma \end{aligned} \quad (1-26)$$

#### 1.1.5 Mirror Plate Distortions

Small random low spatial frequency mirror surface distortions or departures from flatness will reduce the central returned beam by sending some energy into large angles as mentioned in Section 1.3.3. At normal incidence, the beam returned by a single distorted mirror is reduced by

$$\delta = 16\pi^2 \left( \frac{\Delta D_{\text{rms}}}{\lambda} \right)^2 \quad (1-27)$$

where, as before,  $\Delta D_{\text{rms}}$  is the standard deviation of the surface depth distortion. The wavefront deformation is twice this amount. Three consecutive

reflections at near normal incidence from different mirrors with different independent random distortions reduce the returned beam by  $3\delta$ . However, at normal incidence the retro mirrors are not normal to the beam. This reduces the wavefront distortion in analogy to the way slightly rough surfaces look smooth and become mirrors at grazing incidence. In our case, the returned beam is reduced by only  $2\delta$  for three reflections. Thus three mirror surfaces, each with a standard deviation of about 0.01 wave root mean square, reduce the main returned beam by about 3 percent while a 0.02 wave reduces the return by about 13 percent.

## SECTION 2

### POTENTIAL HCR CONFIGURATIONS

#### 2.1 COMPARISON OF CANDIDATE CONFIGURATIONS

There are many ways in which a HCR can be fabricated. Nine candidate configurations and several variations were considered under this study. Each involved different manufacturing processes and varying degrees of difficulty in providing the required precision. Some configurations were superior to others in regard to their potentiality for retaining mutual perpendicularity of the mirror surfaces in orbit over a three- to five-year life span.

It should be noted that, if the optical precision requirement were to be relaxed substantially from a level limited primarily by diffraction in the visible spectrum, then technical problems would become secondary. Any of the HCR configurations suggested here could provide this reduced performance and the choice between them would shift to economic considerations -- we would be interested only in which HCR can be produced at lowest cost. For the immediate purpose of this study, we are confronted by the more complex problem of finding the most cost effective way of making a high precision HCR which will perform adequately in the environment of a synchronous satellite.

In the paragraphs which follow, each of the nine basic configurations that were investigated are briefly considered. Table 2-1 compares the characteristics of these concepts in summary form.

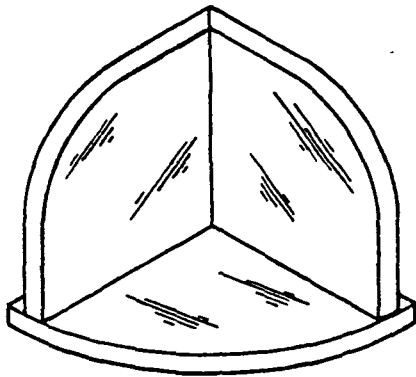
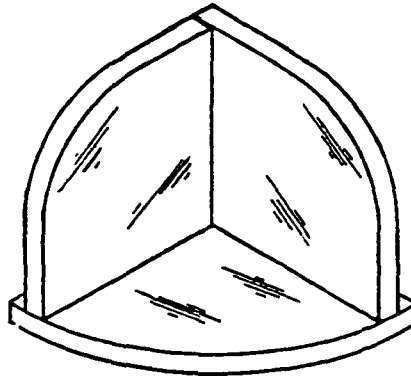
##### 2.1.1 Optically Contacted Plates (Figure 2-1)

This is an obvious HCR candidate. Even though there are four precise angles to generate, the most difficult task would be the assembly of the compound, or bias, joint. The plates may be plane-parallel or sculptured as shown. The appropriate approach would be to assemble two plates, together with the required mutual perpendicularity, and then to grind and polish the base of the "V"

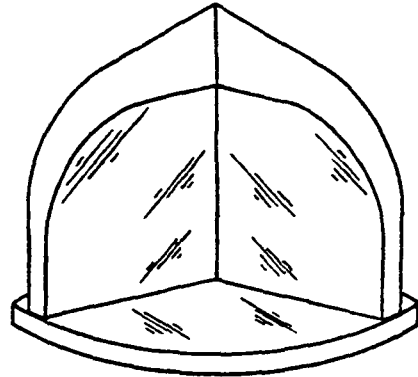
TABLE 2-1  
COMPARATIVE CONFIGURATIONS

CONCEPT CONFIGURATIONS	NUMBER OF COMPOUND JOINTS	NUMBER OF SIMPLE SURFACE SETS TO JOIN TOGETHER	NUMBER OF PRECISE ANGLES TO CONTROL SIMULTANEOUSLY IN ASSEMBLY	NUMBER OF SIMPLE PRECISE ANGLES TO GENERATE	NUMBER OF OPTICAL FLAT SURFACES TO FIGURE
Optically Contacted Plates	1	1	2	4	6
Epoxy Joined Plates	1	1	2	4	6
Internal Structure	1	2	2	4	8
External Structure	0	0	3	0	3
Core-Out Solid	0	0	0	3	3
Epoxy Replication	0	0	3 on stripping replica from mandrel	3	3
"pelkey Prisms" in Optical Contact	0	2	1	2	5
Exterior Mechanical Structure with Replicated Surface	0	0	3 on stripping replica from mandrel	3	3
"v-rabel HCR" (Plates and Base in Optical Contact)	0	2	0	3 on base plate only	5

CONCEPT 1A  
EDGE-CONTACTED  
PLATES



CONCEPT 1B  
EDGE-CONTACTED PLATES WITH  
BIAS JOINT



CONCEPT 1C  
EDGE-CONTACTED PLATES WITH  
TAPERED PLATES AND BIAS JOINT

Figure 2-1. Optically Contacted Plates

assembly to obtain a common surface to mate with the third mirror. The base polished surface must be mutually perpendicular to the other two reflector surfaces. The process of optically working the "bonded" assembly would be expected to be difficult because the bond will tend to separate. If this potential manufacturing problem could be solved, the device should be quite satisfactory.

The bottom optical flat is a simple precise flat. Joining the "V" to the flat seems to be a reasonably easy task.

The main advantage of this concept is the simplicity of the assembled structure. However, since it is conceptually related to the configuration of Figure 2-9 and that configuration avoids the potential manufacturing problem, this configuration is not recommended for further consideration.

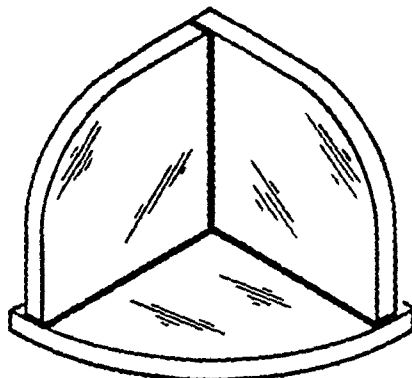
#### 2.1.2 Epoxy Joined Plates (Figure 2-2)

This is a variation of the optically contacted plates (refer to Paragraph 2.1.1), but here the difficulty of generating precise angles is replaced by problems of holding alignment during setting up of the bonding agent (epoxy). The approach with its variations implies that the strength of the structure to maintain its integrity is dependent upon the agent used. The assembly process would use a precise, hard manufacturing tool or fixture, which would permit adjustment of the reflector plates while the epoxy is hardening. In order to execute adjustment while the epoxy is setting, an interferometer is used to establish the proper adjustment.

The technique has much to recommend it if the epoxy joint is temporally stable at temperatures that the HCR is likely to encounter. It must be noted that this is one of the basic principles of the reflectors manufactured by Precision Lapping and Optical Company, Inc. (Valley Stream, Long Island, New York), and their products have been acceptable for many applications (see Appendix A). At this time, we have no conclusive evidence to support Precision Lapping's advertising literature... "Operation is unaffected by humidity, dust, salt spray or temperatures from 0°F to 140°F...". It has been Perkin-Elmer's experience

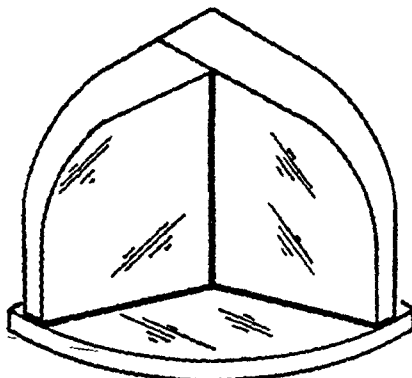
EPOXY JOINT

CONCEPT 2A



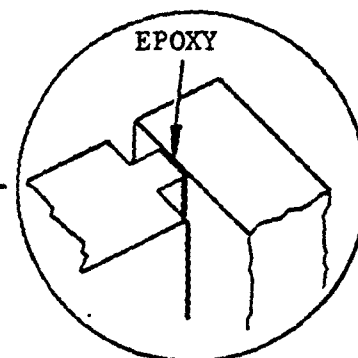
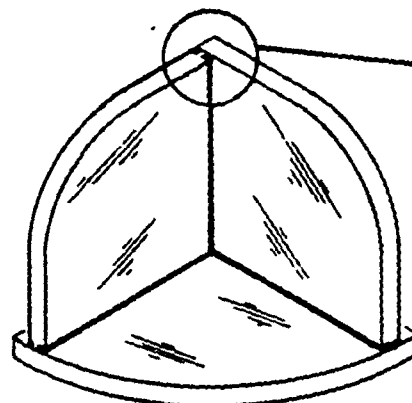
EPOXY JOINT (SCULPTURED PLATES)

CONCEPT 2B



EPOXY JOINT (SCULPTURED JOINT)

CONCEPT 2C



TYPICAL JOINT CONFIGURATION

Figure 2-2. Epoxy Joined Plates

that even small epoxy seams on very stiff low-expansion glass plates induce stresses which cause the plates to distort in time with temperature and humidity variations. The epoxies we have tested are hygroscopic to some degree. Some epoxies also outgas in a vacuum. Apparently, Precision Lapping has overcome these difficulties, at least in part, through use of proprietary techniques and/or materials.

#### 2.1.3 Internal Structure (Figure 2-3)

The obvious disadvantages of this concept are (1) that there is a central obscuration and (2) that there are eight optical flats to polish plus four precise angles to generate. The concept is fundamentally deficient in that the internal structure is located near the apex and, consequently, the plates are cantilevered out. The internal structure arrangement is complex and very sensitive to exact procedures on assembly. Perkin-Elmer does not recommend further consideration of this approach.

#### 2.1.4 External Structure (Figure 2-4)

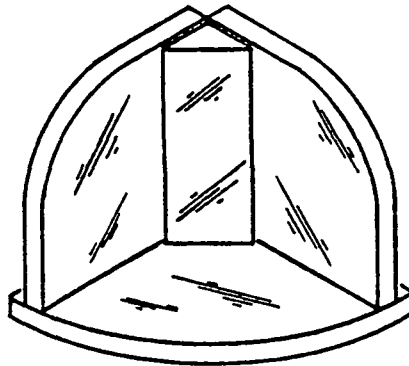
An examination of the numerical comparisons in Table 2-1 would favor this arrangement over almost every other concept. However, from a practical point of view, the probability of success of a truly precision HCR using this arrangement is extremely small. Again, it would be imprudent to rule it out categorically. Perkin-Elmer has experimented with this type of arrangement and concluded that it can be used only to obtain precision in the range of multiples of arc seconds.

#### 2.1.5 Core-Out Solid (Figure 2-5)

This concept is the ultimate in terms of simplicity and hence reliability. However, it has never been executed in real hardware, and it does require very sophisticated optical manufacturing and coating techniques to produce the extremely "concave surfaces" mutually perpendicular and without "turned" edges on the surfaces. If a material such as beryllium were to be used, the raw material and machining costs would be high. Coating such a deeply concave assembly after polishing would also be complex and costly.

INTERNAL STRUCTURE, ALL JOINTS OPTICALLY CONTACTED

CONCEPT 3A



INTERNAL STRUCTURE, STRUCTURE EPOXIED TOGETHER

CONCEPT 3B

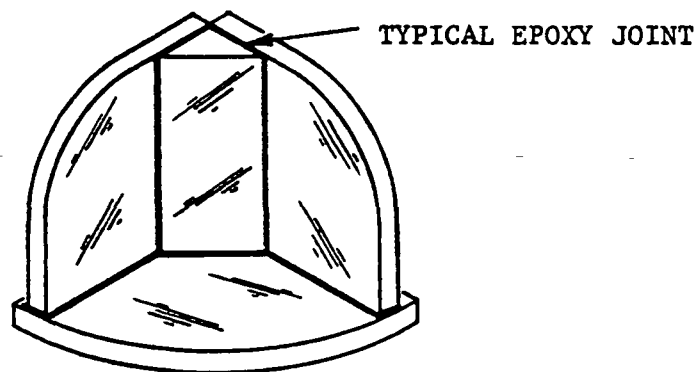


Figure 2-3. Internal Structure

CONCEPT 4

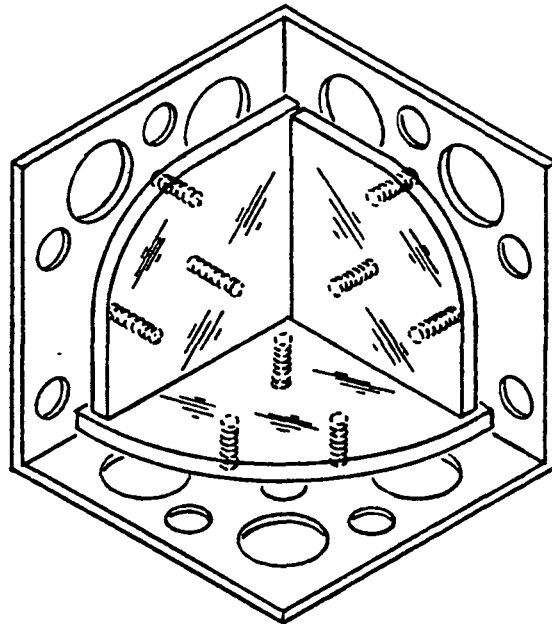


Figure 2-4. External Structure (with Adjustable Attachment to Plates)

CONCEPT 5

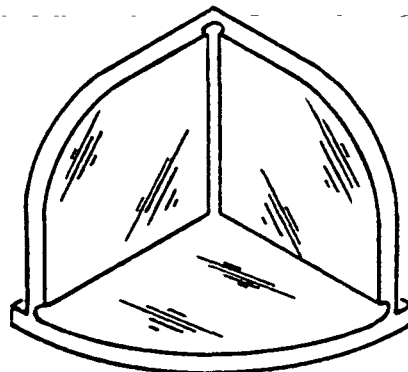


Figure 2-5. Core-Out (with Single Block and then Polish Inside Reflector Surfaces)

### 2.1.6 Epoxy Replication (Figure 2-6)

This concept in which the entire HCR is made of an epoxy or similar material is excellent for approaches in which the driving requirement is low cost with only low to modest requirements for precision. If the HCR were to operate only in the far infrared, the idiosyncrasies of the plastics could perhaps be tolerated. For the present application, it should not be seriously considered. If, and when, new stable plastics are developed and tested, this concept could be resurrected.

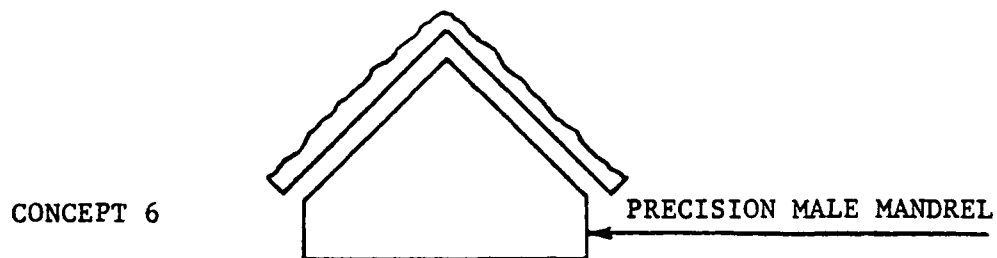


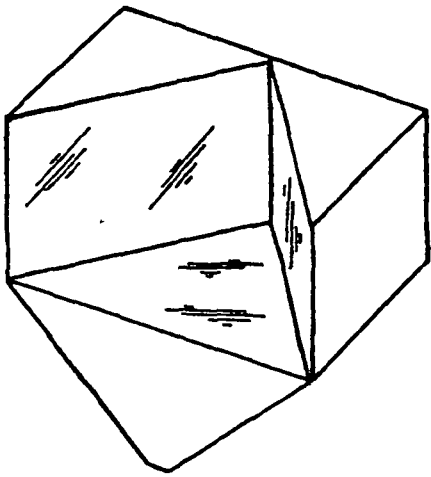
Figure 2-6. Cast Epoxy Replication

### 2.1.7 "Pelkey Prisms" (Figure 2-7)

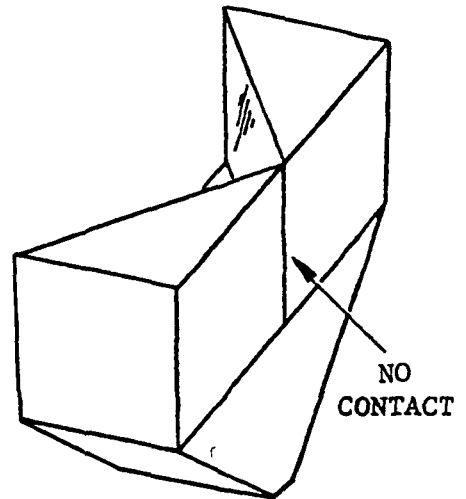
One of the most difficult tasks involved in the assembly of precision hollow corner cubes, the component joint, is eliminated in this HCR configuration. Two right-angle prisms are simply positioned on a third (larger) right-angle prism. There is a natural point for attachment of the HCR to the outside world. This is the apex on the bottom porro-type prism as can be seen in the figure.

The concept is based upon a related device utilized successfully in Perkin-Elmer products. The only problems for the HCR application are in establishing the proper technique for contacting the prisms at the appropriate 90 degree angle and thermal problems caused by nonuniform thickness of the mirror elements.

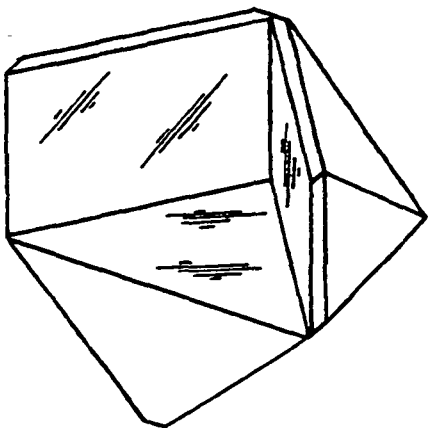
PELKEY HCR PRISMS IN OPTICAL CONTACT



CONCEPT 7A



PELKEY HCR PRISMS (WITH SCULPTURED PRISMS FOR WEIGHT REDUCTION)



CONCEPT 7B

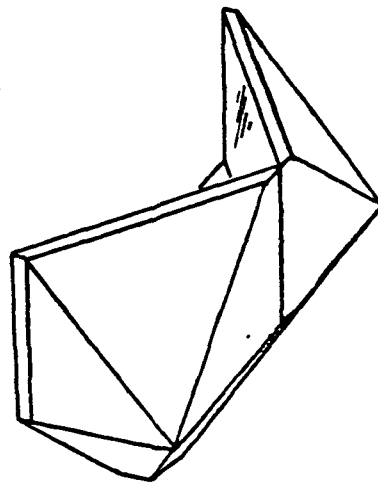


Figure 2-7. The "Pelkey Prism" HCR

### 2.1.8 Exterior Structure with Replicated Surface (Figure 2-8)

This approach might work if the surface can be made exceptionally thin and stress-free and the mechanical structure adequately stiff. Experience with replaced mirrors for space applications and replicated diffraction gratings indicates that few arc-second angular accuracies are possible and  $\lambda/1$  to  $\lambda/2$  surface figures are obtainable. The validity of the concept as a HCR can only be established by experimental work in the optical shop with thermal testing. Since the concept seems quite marginal for the present precision application, Perkin-Elmer recommends no further consideration.

### 2.1.9 "Vrabel HCR" (Figure 2-9)

This configuration is similar to concepts 1 and 7 (refer to Paragraphs 2.1.1 and 2.1.7) with one fundamental exception. The assembly of the concept 1 version requires each plate to have several precise angles and contacting in two meridians. The assembly of the "Pelkey HCR" requires that the two small prisms be contacted to the base prism at precisely 90 degrees to each other. The Vrabel concept eliminates those exacting assembly operations and transfers the difficulty to the precise manufacture of the one mirror plate which serves as the base structure for the assembly. This base structure can be manufactured with adequate precision in the optical shop. Precise, large, open face reflectors like this have been made and tested, and they do work<sup>4</sup>. In the referenced prior development, Cervit substrate assemblies were subjected to extensive thermal testing from  $-2^{\circ}\text{C}$  to  $+68^{\circ}\text{C}$  and the thermally induced change in full aperture wavefront was  $1/4$  wave peak-to-peak at  $6.328 \times 10^{-4}$  mm. Consequently, this concept is considered to be the best of the nine approaches.

Careful sculpturing of the base plate and of the two side plates can reduce the weight to a minimum. The thickness of the base plate is only that amount necessary to insure structural integrity of the HCR and to allow the angles to be measured reliably.

This approach is highly recommended for further development as having a high probability of technical success, a modest cost and a low weight.

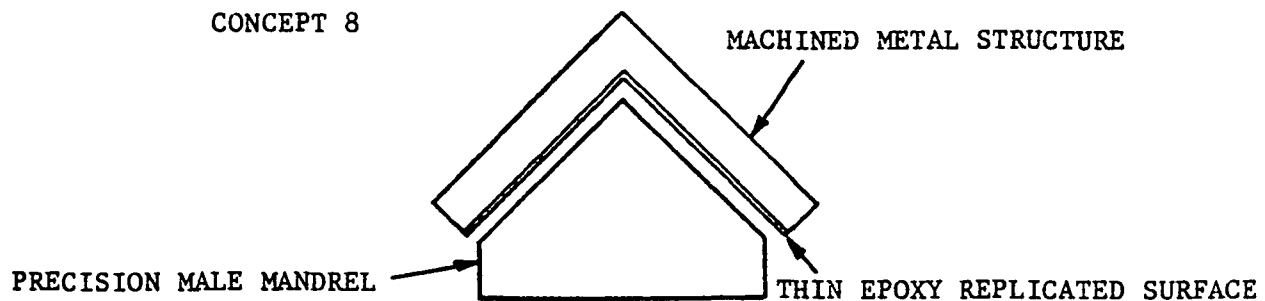


Figure 2-8. Exterior Machined Structure with Replicated Optical Surface

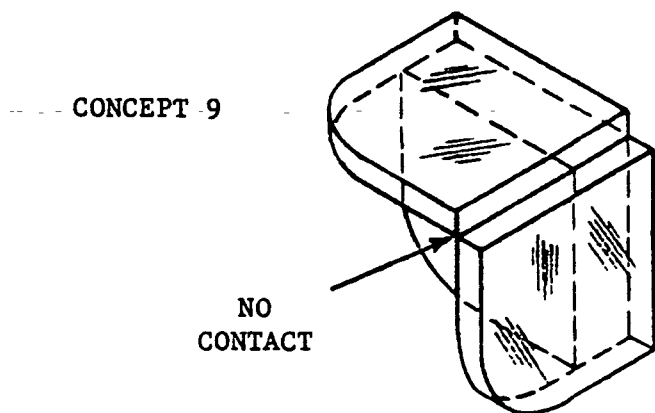


Figure 2-9. "Vrabel HCR" - Plates and Base in Optical Contact

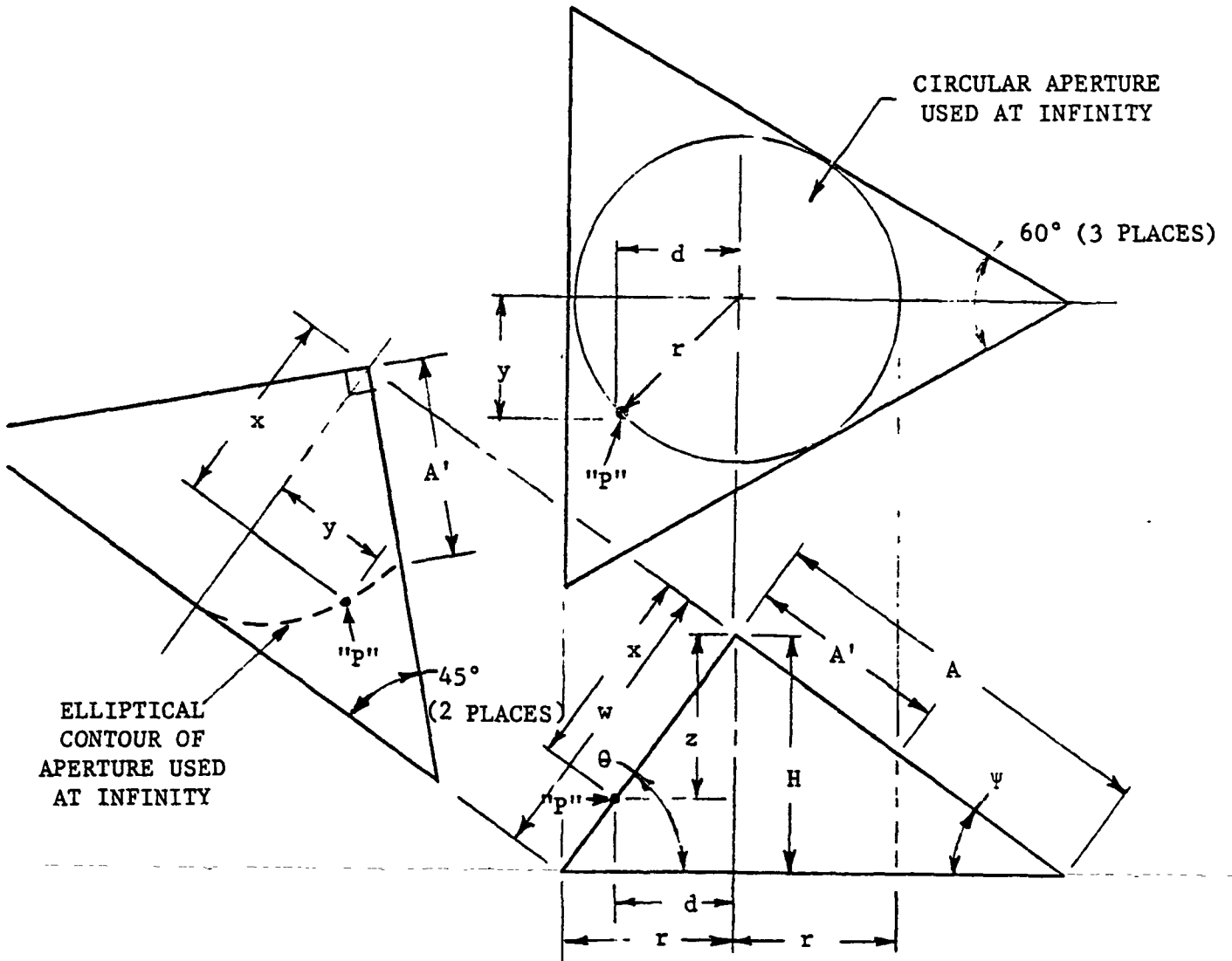
## 2.2 GEOMETRICAL RELATIONSHIPS IN A HCR

In the preceding section, various potential configurations for the HCR were presented. The most favored concepts fall into two basic configurations: flat plates attached to each other or triangular prisms attached to each other. For the intended application, the latter concept is less attractive since it is likely to be heavier and the nonuniform thickness of the mirror elements will tend to accentuate nonuniform thermal gradients through those elements while in orbit. The flat plate configurations therefore are considered preferable for the present application.

This section provides some basic geometrical considerations of the HCR and includes size and mass calculations for "glass" and beryllium components with  $200 \text{ cm}^2$  apertures and constructed either as concept 5 (the core-out solid beryllium discussed in Paragraph 2.1.5) or concept 9 ("Vrabel HCR" discussed in Paragraph 2.1.9). Cervit and ULE are considered the most favorable potential materials for the latter concept.

Figure 2-10 shows the general configuration of a corner reflector while Table 2-2 utilizes the equations of that figure to calculate the dimensions of the  $200 \text{ cm}^2$  HCR.

Figure 2-11 shows the area utilized on the reflector face when the HCR is viewed along its axis of symmetry from an infinite distance. If, in the intended application, the HCR line of sight is very nearly stable with respect to the transmitter on the earth, this is the only aperture which needs to be provided on each mirror. Figure 2-12A shows a full-size wooden mock-up of a HCR with mirrors configured as shown in Figure 2-11. The construction is representative of the Vrabel "optically contacted" HCR. Figure 2-12B shows a variation of that same concept, also in full-size mock-up form, but having mirror faces of quarter-circle shape rather than elliptical ones. Figure 2-12C shows a mock-up similar to that of Figure 2-12A but having mirrors with straight edges approximating the elliptical contour. This concept has a backing plate "cemented" across the opening between mirrors after contacting.



$$\theta = 54.7356^\circ$$

$$\psi = 35.2644^\circ$$

$$H = r \tan \theta = 1.414214r$$

$$w = r / \cos \theta = 1.732050r$$

$$A = H / \sin \psi = H / \cos \theta = r \tan \theta / \cos \theta = 2.449488r$$

$$A' = r / \cos \psi = 1.224744r$$

Location of point "p" on face

$$\left\{ \begin{array}{l} z = x \cos \psi = 0.816496x \\ d = z \tan \psi = 0.707107z \\ y = \sqrt{r^2 - d^2} \end{array} \right.$$

Figure 2-10. Geometrical Relationships

TABLE 2-2

DIMENSIONS FOR A HCR WITH APERTURE AREA = 200 cm<sup>2</sup>

$$\text{Area} = 200 \text{ cm}^2 = \pi r^2$$

$$r = 7.979 \text{ cm} = 3.141 \text{ inches}$$

$$H = (1.414214)(7.979) = 11.284 \text{ cm} = 4.443 \text{ inches}$$

$$W = (1.732050)(7.979) = 13.820 \text{ cm} = 5.441 \text{ inches}$$

$$A = (2.449488)(7.979) = 19.544 \text{ cm} = 7.695 \text{ inches}$$

$$A' = (1.224744)(7.979) = 9.772 \text{ cm} = 3.847 \text{ inches}$$

Recommended plate thickness = 1/6 to 1/8 W = 2.304 to 1.728 cm.

Assume 2 cm for thermal and mass models.

Aperture contour on reflector face (dashed line in Figure 2-10).

x	z	d	y	x	z	d	y
6.91	5.6420	3.9895	6.9100	11.00	8.9815	6.3509	4.8302
7.50	6.1237	4.3301	6.7018	11.50	9.3897	6.6395	4.4251
8.00	6.5320	4.6188	6.5062	12.00	9.7980	6.9282	3.9578
8.50	6.9402	4.9075	6.2914	12.50	10.2062	7.2169	3.4031
9.00	7.3485	5.1962	6.0551	13.00	10.6145	7.5056	2.7075
9.50	7.7567	5.4848	5.7949	13.50	11.0227	7.7942	1.7073
10.00	8.1650	5.7735	5.5074	13.820	11.2840	7.9790	0
10.50	8.5732	6.0622	5.1879	0	0	0	r=7.979

Plotting y vs x provides exact contour of aperture (See Figure 2-11).

NOTE: This is ellipse with eccentricity "e" given by:

$$e = c/a = \sqrt{a^2 - b^2}/a$$

where a = w = 13.820 cm

$$b = r = 7.979 \text{ cm}$$

$$\therefore e = 11.2838/13.82 = 0.816$$

$\xi$  = face angle to tangent @ "P<sub>1</sub>"

$$= \tan^{-1} \frac{B^2 x_1}{a^2 y_1} + 45^\circ$$

$$x_1 = y_1 = 6.91 \text{ cm}, b^2/a^2 = 0.3333$$

$$\xi = \tan^{-1} 0.3333 + 45^\circ = 18.435^\circ + 45^\circ = 63.435^\circ$$

$$\text{Area of face} = \frac{\pi ab}{2} - \left( \frac{13.820}{2} \right)^2 = 173.211 - 47.748 = 125.463 \text{ cm}^2$$

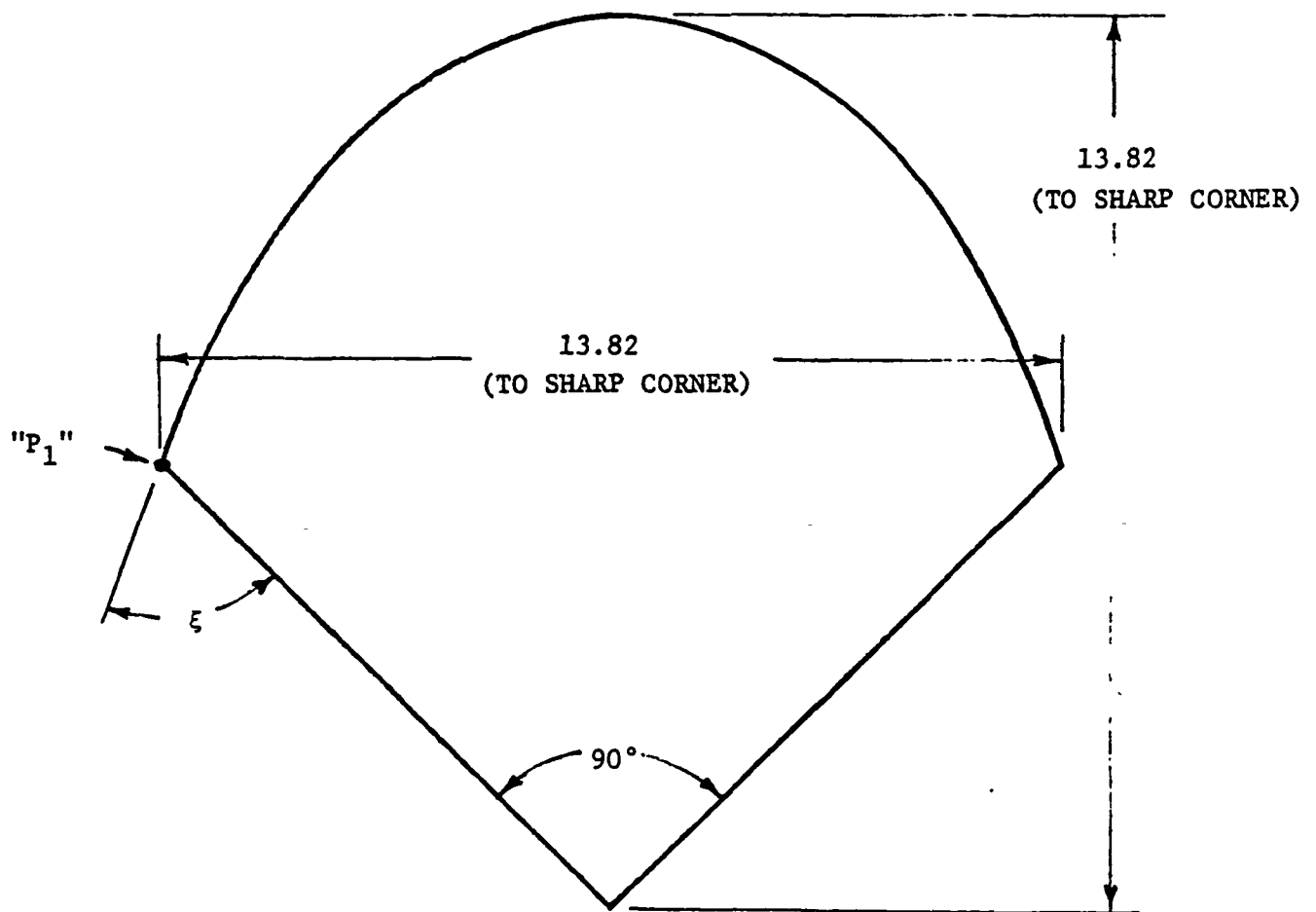
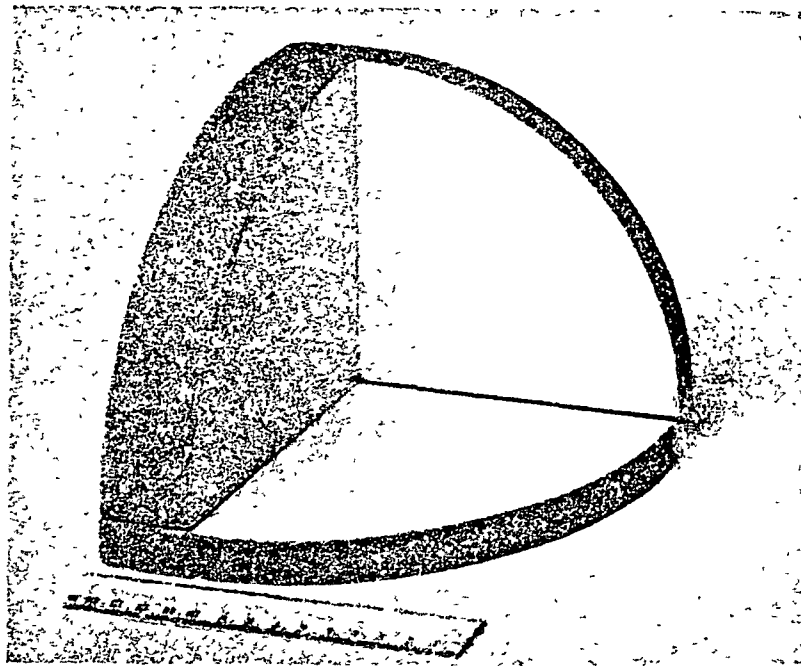
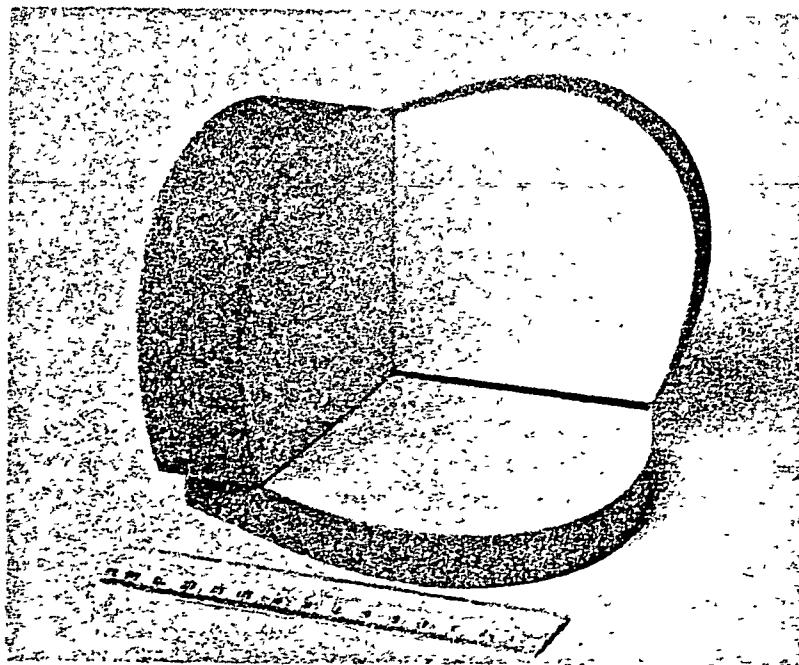


Figure 2-11. Reflector Face Area Utilized at Infinity and Symmetrical Incidence

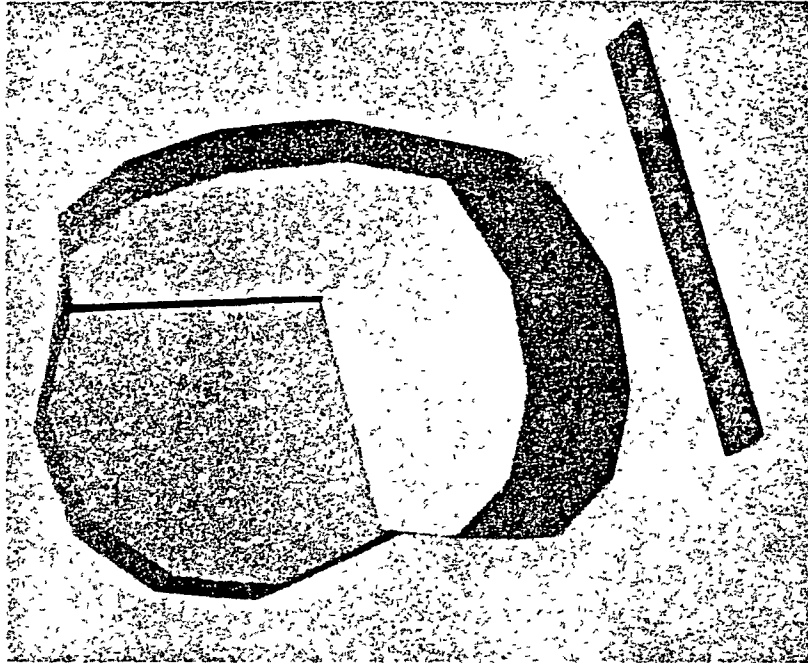


A

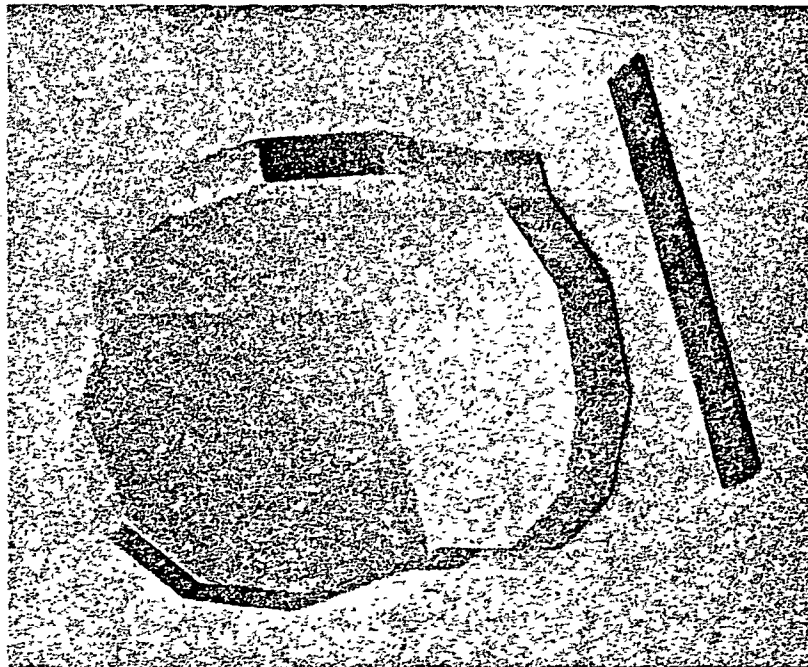


B

Figure 2-12. Photographs of Full-Sized Wooden Mock-Ups of  
Four Types of HCRs (Sheet 1 of 2)



C



D

Figure 2-12. Photographs of Full-Sized Wooden Mock-Ups of Four Types of HCRs (Sheet 2 of 2)

The size and weight advantages of the Figure 2-12A configuration over that shown in Figure 2-12B are indicated in Table 2-3. The assumptions made for parameters such as plate thickness are noted in the table.

Figure 2-12D shows a mock-up of an all-beryllium HCR configuration having straight-line mirror contours. Considerations of the potential problems and cost of fabricating this device to the precision required for the present application have led us to the conclusion that it is not a viable approach.

## 2.3 PROPERTIES OF POTENTIAL HCR MATERIALS

### 2.3.1 Dimensional Stability

In order to perform reliably, the HCR plate materials must be resistant to deformation in deleterious thermal and "g" force environments. Even more important, a diffraction-limited  $200 \text{ cm}^2$  HCR depends upon the existence of materials that exhibit sufficient dimensional stability. If the operating temperature of the HCR is likely to differ from the ambient temperature at which it is fabricated, then a second condition -- that of an isotropic coefficient of expansion -- is necessary. If the latter condition is not met, then nominal changes in the operating temperature will warp the optical surfaces and destroy the optical performance. Present evidence indicates that the stability and isotropy requirements of the  $200 \text{ cm}^2$  area HCR are sufficiently severe that few materials are actually available, particularly in combination with desirable characteristics such as a high elasticity-modulus-to-density ratio and a high thermal-diffusivity-to-coefficient-of-expansion ratio. Table 2-4 lists these and other characteristics of a variety of potential HCR materials.

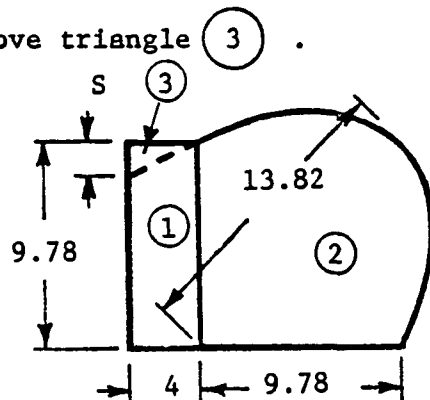
The coefficient of expansion of both fused silica and silicon decreases with temperature and, in both cases, crosses zero and becomes negative. Figure 2-13 shows the variation of coefficient with temperature for a typical sample of fused silica (Englehard Industries, Inc., Hillside, New Jersey) and for a single crystal of silicon. A number of devitrified glass materials, such as Pyroceram (Corning Glass Works, Corning, New York) and Cervit (Owens-Illinois,

TABLE 2-3

## SIZE AND MASS COMPARISONS OF TWO HCR CONFIGURATIONS

CONFIGURATION PER FIGURE 2.12A:A - Using "Glass-Type" Material

Assume two mirror plates 2 cm thick and third plate 5 cm thick. To reduce mass of plate and make "glass" plate more easily fabricated, remove triangle (3).



$$V_1 = (4)(9.78)(2) = 78.24 \text{ cm}^3$$

$$V_2 = (125.46)(2) = 250.92 \text{ cm}^3$$

$$V_3 = (4)(2)(s)$$

where

$$S = 4 \tan (90^\circ - \xi)$$

$$= 4 \tan 26.565^\circ$$

$$= 2 \text{ cm}$$

Hence,

$$V_3 = (4)(2)(2) = 16 \text{ cm}^3$$

$$\begin{aligned} \text{Total volume of HCR} &= (V_1 + V_2 - V_3)(2) + (2.5)(V_2) \\ &= 626.32 + 627.30 = 1253.62 \text{ cm}^3 \end{aligned}$$

Total mass of HCR for:

$$\begin{aligned} \text{ULE } (\rho = 2.21 \text{ g/cm}^3) &= 2.77 \text{ Kg} \\ \text{Cervit } (\rho = 2.50 \text{ g/cm}^3) &= 3.13 \text{ Kg} \end{aligned}$$

B - Using Beryllium Material ( $\rho = 1.82 \text{ g/cm}^3$ ) All plates 2 cm thick.

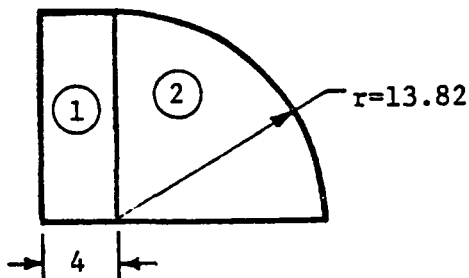
$$\begin{aligned} \text{Total volume of HCR} &= \left( \frac{V_1}{2} + V_2 \right) (2) + V_2 \\ &= (39.12 + 250.92) (2) + 250.92 = 831.00 \text{ cm}^3 \end{aligned}$$

$$\text{Total mass of HCR} = (831.00)(1.82) = 1.51 \text{ Kg}$$

TABLE 2-3 (Continued)

CONFIGURATION PER FIGURE 2.12B:A - Using "Glass-Type" Material

Assume two mirror plates 2 cm thick and third plate 5 cm thick.



$$V_1 = (13.82)(4)(2) = 110.56 \text{ cm}^3$$

$$V_2 = \frac{(\pi)(13.82)^2(2)}{4} = 300.01 \text{ cm}^3$$

$$\text{Total volume of HCR} = (V_1 + V_2)(2) + (V_2)(2.5) = 1571.17 \text{ cm}^3$$

Total mass of HCR for:

$$\text{ULE } (\rho = 2.21 \text{ g/cm}^3) = 3.47 \text{ Kg}$$

$$\text{Cervit } (\rho = 2.50 \text{ g/cm}^3) = 3.93 \text{ Kg}$$

B - Using Beryllium Material ( $\rho = 1.82 \text{ g/cm}^3$ ) All plates 2 cm thick.

$$\text{Total volume of HCR} = \left( \frac{V_1}{2} + V_2 \right) (2) + V_2$$

$$= (55.28 + 300.01)(2) + 300.01$$

$$= 1010.59 \text{ cm}^3$$

$$\text{Total mass of HCR} = (1010.59)(1.82) = 1.84 \text{ Kg}$$

TABLE 2-4

## PUBLISHED PHYSICAL PROPERTIES OF POTENTIAL HOLLOW CORNER CUBE MATERIALS

MATERIAL	DENSITY ( $\rho$ ) gm/cm <sup>3</sup>	MODULUS OF ELASTICITY (E) Newtons/cm <sup>2</sup>	THERMAL CON- DUCTIVITY (K) Cal/cm sec °C	SPECIFIC HEAT (C) Cal/gm °C	COEFFICIENT OF EXPANSION ( $\alpha$ ) °C <sup>-1</sup>	E/ $\rho$	1/Cp $\alpha$	K/Cp $\alpha$	K/Cp.
Fused Silica	2.2	7.0x10 <sup>6</sup>	0.0033	0.188	0.55x10 <sup>-6</sup>	3.18x10 <sup>6</sup>	4400x10 <sup>3</sup>	14.5x10 <sup>3</sup>	0.008
Pyrex -7740	2.35	6.8x10 <sup>6</sup>	0.0027	0.250 <sup>†</sup>	3.20x10 <sup>-6</sup>	2.89x10 <sup>6</sup>	530x10 <sup>3</sup>	1.44x10 <sup>3</sup>	0.0046
Aluminum	2.70	6.9x10 <sup>6</sup>	0.53	0.215	23.9x10 <sup>-6</sup>	2.56x10 <sup>6</sup>	72x10 <sup>3</sup>	38.2x10 <sup>3</sup>	0.92
Beryllium	1.82	28.0x10 <sup>6</sup>	0.38	0.450	12.4x10 <sup>-6</sup>	15.4x10 <sup>6</sup>	99x10 <sup>3</sup>	37.5x10 <sup>3</sup>	0.465
Invar (36% Ni)	8.0	14.8x10 <sup>6</sup>	0.026	0.095	1.30x10 <sup>-6</sup>	1.85x10 <sup>6</sup>	1000x10 <sup>3</sup>	26.3x10 <sup>3</sup>	0.034
Silicon	2.33	13.0x10 <sup>6</sup>	0.39	0.168	2.33x10 <sup>-6</sup>	5.56x10 <sup>6</sup>	1065x10 <sup>3</sup>	427x10 <sup>3</sup>	1.0
ULE	2.21	6.74x10 <sup>6</sup>	0.0031	0.183	0.03x10 <sup>-6</sup>	3.05x10 <sup>6</sup>	8.2x10 <sup>7</sup>	254x10 <sup>3</sup>	0.008
Cervit	2.5	9.23x10 <sup>6</sup>	0.004	0.217	0.1x10 <sup>-6</sup>	3.7x10 <sup>6</sup>	1.8x10 <sup>7</sup>	72x10 <sup>3</sup>	0.007

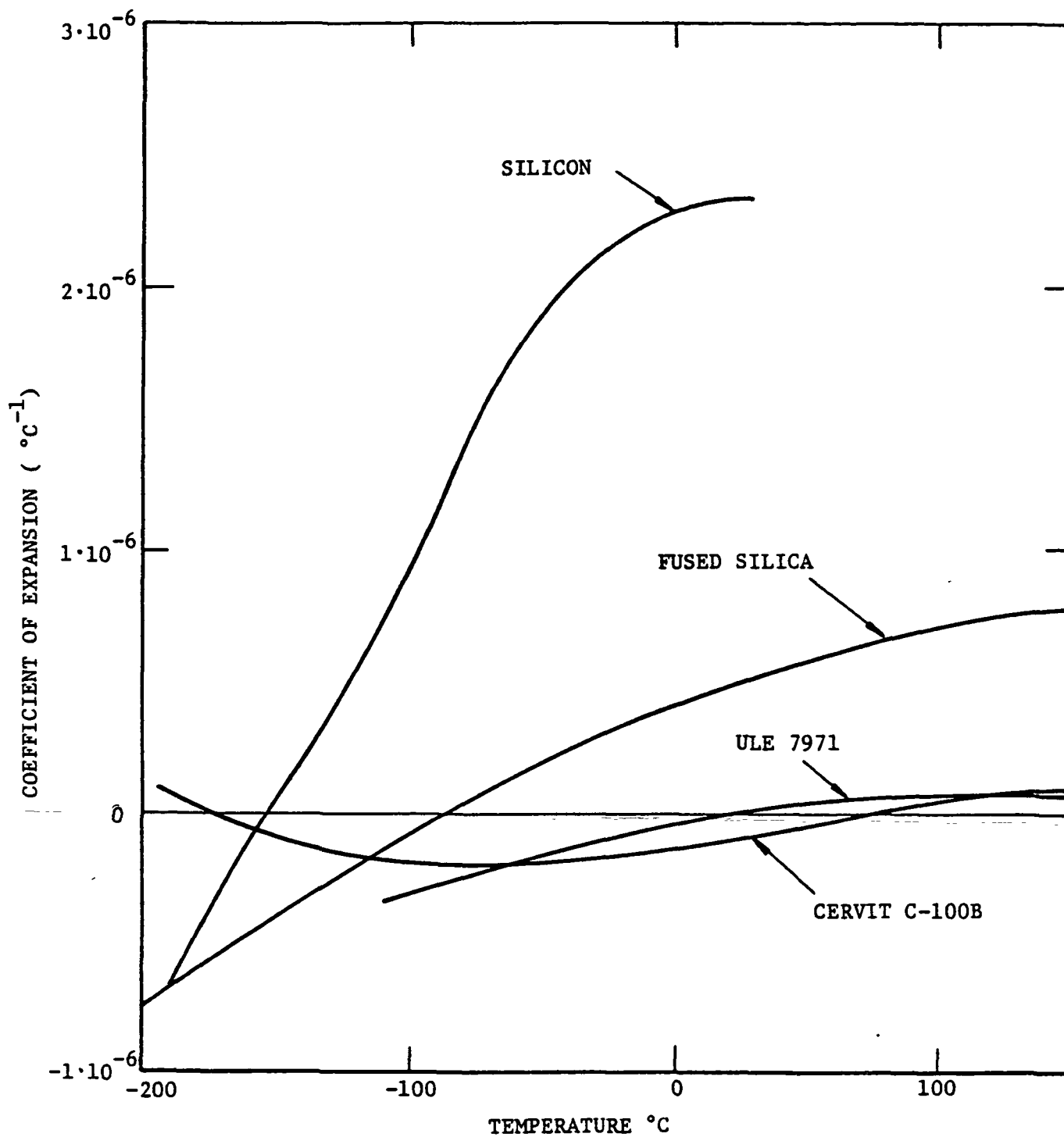


Figure 2-13. Coefficient of Expansion of Typical Materials - Variation with Temperature

Toledo, Ohio), can be tailored to hug the zero coefficient of expansion line over an extended temperature range. These relatively new materials closely resemble true glasses, are polishable, and do not exhibit the severe scattering of earlier materials. Curves for Cervit C100B and ULE are also shown in Figure 2-13.

One method of gauging the stability required in an HCR plate of ~14 cm maximum dimension is to compute the maximum strain in a flat plate which, for some reason, has become bent so as to appear to have optical power. Assuming simple bending, then the maximum strain occurring at the front and back surfaces is given by

$$\epsilon_{\max} = \frac{4d}{D^2} \left( \frac{\lambda}{n} \right)$$

where

$d$  = HCR plate thickness = 2 cm

$D$  = HCR plate maximum dimension = 14 cm

$\frac{\lambda}{n}$  = peak-to-peak mirror surface tolerance =  $\frac{\lambda}{20}$

$\lambda$  =  $5.5 \times 10^{-4}$  mm

Assuming a dimensional instability tolerance equal to the figure error, and taking the plate dimensions as indicated above, then the instability tolerance corresponds to a maximum strain of  $1.1 \times 10^{-7}$ . This is an incredibly small number. It lies at least an order of magnitude below conventional material testing methods and illustrates the interferometric level of dimensional stability required in the HCR plates.

Very little information is available on the dimensional stability of materials subject to low stresses and nominal temperatures. Of the available data, perhaps the most comprehensive is the research done by the Massachusetts Institute of Technology Department of Metallurgy.<sup>5,6</sup> This work included an inves-

tigation of dimensional changes in metals occurring in a constant temperature environment as well as changes induced by cyclic temperature changes. Small changes over long periods of time are typically a few microinches per inch. These changes would not necessarily be detrimental in a HCR if the changes happen symmetrically so that the mirror plates simply change in size and no change occurs in the figure of the corner cube. Directional nonuniformity is inferred by the generally accepted theory that stress relief and intermolecular instabilities are chiefly responsible for dimensional changes, since there is no reason to believe that stresses or concentration gradients are symmetrically arranged in all structures. The Stratoscope II mirror fabricated and tested by Perkin-Elmer provides some data which are directly applicable to the HCR mirror materials problem. These mirror tests were conducted after the mirror had withstood the rigors of an extended (i.e., many years) operational period. This showed the figure to be virtually unaltered and indicates that fused silica is one of the few exceptionally stable mirror materials. Similar results might be expected of selected, high quality Cervit or ULE.

The various mechanisms responsible for material instabilities are not well understood. Impurities or the presence of alloying elements can contribute to spontaneous changes in many different ways. Even if the impurities remain segregated, then stress concentrations around the impurities caused by coefficient of expansion differences can cause plastic deformations. In the unlikely event that impurities are absent, then the relaxation of stresses originating from temperature differences in the casting during its formation in the mold can also cause spontaneous plastic deformation.

No hard and fast rules exist for the selection of dimensionally stable materials. It is known that yield in crystalline materials occurs through the motion of dislocations through the crystal lattice and that the number and mobility of dislocations vary widely, depending on the binding energy between atoms, the lattice structure, the stress distribution, and the type and concentration of impurities.<sup>7,8</sup> Apart from glasses, which have a low thermal conductivity as a result of their amorphous molecular structure<sup>9,10</sup>, the

most promising mirror materials appear to be pure elements or compounds which form light, hard, cubic crystal lattices. A light crystal lattice is most likely to have a high elastic-modulus-to-density ratio and the immobility of the dislocations is exhibited in the bulk lattice as hardness. A cubic lattice ensures that the crystal is isotropic whereas hexagonal lattices are almost always anisotropic as, for example, in the case of beryllium.

Carbon and silicon possess cubic lattice structures but the cubic form of carbon (diamond) has very obvious economic drawbacks. Silicon has found application as an optical material for infrared components such as lenses and domes. Polycrystalline silicon can be ground and polished using conventional curve generators and polishing laps.

The state-of-the-art for silicon optical elements is about a tenth wave over a 12-inch diameter surface. This sort of tolerance is characteristic of the best refractive optical elements, and implies a considerable degree of dimensional stability.

### 2.3.2 Thermal Stability

The amount of thermo-elastic distortion accompanying a given temperature distribution in a HCR is a complex analytical problem for any but the simplest physical configurations and temperature distributions. For the dynamic situation of a HCR moving in and out of sunlight and with conduction as the main heat transport mechanism, the term  $K/C\rho\alpha$  (see Table 2-4) appears to be the most suitable criterion to compare HCR plate materials with each other from the thermal point of view.

In terms of immunity to thermal distortion, silicon and ULE appear to be outstanding, with silicon having a  $K/C\rho\alpha$  value a factor of 10 better than aluminum and beryllium, and a factor of 30 better than fused silica. The coefficient of expansion of the type of invar used in the comparison does not compensate sufficiently for the low heat conductivity to provide any obvious advantage. There are special invar compositions with coefficients of expansion that are smaller than the one chosen as an example, but the coefficient

is small only over a narrow temperature range which detracts from their usefulness. Note that Cervit is better than beryllium but poorer in the  $K/Cp\alpha$  term than ULE or silicon. As will be shown in the detailed thermal analysis of Section 3, ULE is better than Cervit by a 3:1 ratio in terms of mirror distortion due to thermal inputs from the sun in a synchronous orbit.

The thermal diffusivity ( $K/Cp$ ) of the various materials described in Table 2-4 is somewhat analogous to the reciprocal of the time constant in an electrical system so that a large value of  $K/Cp$  indicates a relatively short time to adjust to a new thermal environment. This should be a minor consideration in the selection of plate materials for the orbiting HCR since the environment changes quite slowly during most of the orbit.

### 2.3.3 Compatibility with Optical Fabrication

All of the materials suggested in this report for use in the HCR mirrors are compatible with optical fabrication by more or less conventional techniques. For ease of fabrication and consistency of the end product, fused silica and Cervit rank highest of all those materials considered (see Table 2-4). However, experience with multiple-mirror devices resembling the HCR is limited. The closest comparison is with the optically contacted Cervit penta and penta-roof mirror structures successfully developed by Perkin-Elmer and described in Reference 4. The very low thermal expansion of Cervit facilitates production of flat optical surfaces. As a raw material, it is very homogeneous and predictable in its response to grinding and polishing processes. This leads us to prefer Cervit for the HCR.

The primary reason that ULE does not occupy this position of esteem is that some samples of that material processed in Perkin-Elmer's shops have lacked homogeneity. Careful selection of the raw material would remove this potential objection to use of ULE but would tend to increase cost. Its favorable thermal characteristics and generally good workability would then be expected to lead to a high quality HCR.

From the coating viewpoint, all of the glass-type materials considered here would be equally satisfactory. It would be highly desirable for all coating to be done on the individual mirror plates before they are contacted or bonded together since this allows a more uniform layer to be deposited on the substrate than if the complete HCR were to be coated as an assembly. Cost of the coating operation also would be minimized if the mirrors are handled separately since this reduces the complexity of masking requirements and simplifies the fixturing required.

#### 2.3.4 Optical Coating Considerations

Evaporated thin metallic films, overcoated with protective layers of a dielectric, are conventionally used on the actual reflecting surfaces on optical mirrors. The literature in this field is extensive; excellent summaries may be found in References 11 and 12. Reflectance and durability characteristics of some typical standard coatings are listed in Table 2-5. The "fresh" aluminum and silver listings are interesting but not too pertinent since exposure to the atmosphere tends to reduce these values and their durability is low. Silicon monoxide is a useful protective overcoat for the visible and near-infrared regions. Magnesium fluoride is used primarily in the ultraviolet region. Multiple layer dielectric overcoats can be used to enhance reflectance but their durability is low, and if many layers are used, stress is induced into the coating and the roughness of the optical surface increases.

The coating characteristics of prime interest for the present HCR application are reflectance ( $R_\lambda$ ) in the spectral region of the source used to illuminate the device from the earth, the solar absorptivity ( $\alpha_s$ ) and the infrared emissivity ( $\epsilon$ ). The ratio of  $\alpha_s/\epsilon$  is frequently used as the critical characteristics of a particular coating. Typical (approximate) values of these big parameters for two typical protected coatings at about 300°K are:

	$\alpha_s$	$\epsilon$	$\alpha_s/\epsilon$
Al + MgF <sub>2</sub>	0.1025	0.0115	8.9
Al + SiO	0.10	0.05	2.0

TABLE 2-5

## REFLECTANCE CHARACTERISTICS OF TYPICAL OPTICAL COATINGS

COATING TYPE	PERCENT REFLECTANCE VISIBLE LIGHT ( $\lambda = 5.5 \times 10^{-4} \text{mm}$ )	PERCENT EFFECTIVE TOTAL SOLAR REFLECTANCE OUTSIDE ATMOSPHERE*	DURABILITY	USEFUL SPECTRAL RANGE ( $\mu\text{m}$ )
Al**	91.5	92.4	Low	0.35 to 40
Ag**	98.3	95.0	Low	0.4 to 40
Al + MgF <sub>2</sub>	---	---	Medium	0.2 to 0.4
Al + SiO	90	---	High	0.4 to 5
Ag + SiO	98	---	Medium	0.4 to 5
Ag + Dielectric Multilayer	99	---	Low	0.42 to 10

\* Per Hass, Reference 12

\*\* Freshly evaporated

In order to keep the surface temperatures of the HCR mirror within reasonable bounds when irradiated by the sun, a value of  $\alpha_s/\epsilon$  lower than 2 is desired. Work reported by Hass, et al<sup>13,14</sup> indicates that both parameters for aluminum and silver can be modified by changing the nature and thickness of the overcoat without using excessively thick coatings. For example, surfaces with low ( $\sim 0.11$  to  $0.12$ ) values of  $\alpha_s$  and higher ( $\sim 0.1$  to  $0.65$ ) values of  $\epsilon$  can be produced on aluminum. The overcoat used is a double layer of aluminum oxide ( $Al_2O_3$ ) and silicon dioxide ( $SiO_2$ ) or reactively evaporated silicon oxide ( $SiO_x$ ). The oxide thickness which produces these effects varies from  $6\lambda/4$  to  $30\lambda/4$  ( $\lambda = 0.55 \mu$ ) with the thicker layers giving the higher  $\epsilon$  value.  $\alpha_s$  is essentially independent of oxide thickness.  $\alpha_s/\epsilon$  can therefore be as low as 0.22.

If a similar overcoat is applied to silver, the resulting values of  $\alpha_s$  are in the range of 0.065 to 0.070 while the  $\epsilon$  can be increased to essentially the same values as for aluminum. The resulting  $\alpha_s/\epsilon$  can therefore be as low as 0.10.

It must be recognized that these new coatings were developed for thermal control of spacecraft components and not specifically for optical mirror surfaces. It seems reasonable to conclude, however, that similar results would be obtained on HCR mirrors with modest development effort. Since both types of coatings just described are quite desirable, they would seem ideally suited to the HCR application. Perkin-Elmer therefore believes that values of  $\alpha_s$ ,  $\epsilon$  and  $\alpha_s/\epsilon$  of 0.05, 0.10 and 0.5 are within reach.

Another parameter of the coating of importance in the HCR application is the susceptibility of that coating to elevated temperatures and to the effects of solar ultraviolet irradiation. Hass, et al<sup>14</sup>, has indicated that the latter environment is of no concern. High temperature effects cannot be dismissed so quickly. The coatings of interest here are deposited at temperatures less than  $50^\circ C$  and are subject to slight losses in reflection and possible physical degradation at temperatures approaching  $200^\circ C$ . Only gold is capable of withstanding a temperature of  $250^\circ C$ . If such temperatures are found to be

unavoidable in the orbiting environment, consideration of overcoated gold would probably be appropriate.

## 2.4 ESTABLISHMENT OF PREFERRED HCR CONFIGURATION

In this section, the optical, mechanical and thermal aspects of the HCR design are consolidated in order to define a preferred configuration which can be subjected analytically to the anticipated thermal environment of the synchronous orbit in Section 3 and then the resultant optical performance evaluated in Section 4.

### 2.4.1 Optical Considerations

Since the HCR is fundamentally an optical device, and a high level of operational performance over a long life span is required, the optical parameters of the device must be specified carefully. Although cost considerations must be kept in mind, performance achievement takes first priority for the purposes of the present study. Perkin-Elmer therefore would prefer those HCR configurations which have a high probability of achieving performance goals. From the candidate configurations listed in Table 2-1, concept 9, the "Vrabel HCR" is considered capable of the highest level of performance. It has therefore been selected as the preferred concept.

The choice of material for the individual mirror plates of the HCR was discussed in Section 2.3. ULE and Cervit are the obvious candidates, but the choice between them is not so obvious. For this reason, it is appropriate to consider both materials in the thermal and optical performance analyses. If no distinct preference can then be established, the choice would logically be made on the basis of availability and cost of the raw material.

The optical contact technique of assembling the HCR is inherent in the concept choice. Much experience at Perkin-Elmer in contacting both Cervit and ULE components has indicated that either can be contacted if adequately cleaned and assembled in a controlled (i.e., clean and dry) atmosphere. In order to maximize reliability of the optical contact joint before the HCR reaches the space environment, the entire device should be protected from

moisture or, if that is impossible, the edges of the contacted areas should be covered by a small, continuous, sealant bead. From experience with various sealants used for just this purpose, a nonrigid material must be used. Excellent results have been obtained with RTV-60, a silastic which does not emit acetic acid vapor while curing. The manufacturer (General Electric Company) advertises this compound as not being affected by temperatures between  $-175^{\circ}\text{C}$  and  $+600^{\circ}\text{C}$ . If the HCR temperature in orbit should exceed either of these limits, tests under the more extreme conditions would be appropriate before the sealant is made part of the design.

In order to maximize uniformity of coatings on the mirrors, reduce costs of fixturing and masking operations, and prevent thermally induced failure of the optical contact bonds, all coating should be done on the mirror plates before contacting. Masking of the plates to keep coatings off the areas to be contacted is required. In order to maximize the tolerance on positioning each plate to its mating surface, the masked area should be about 1 mm larger than the area to be contacted. This will result in a narrow, nonreflecting region on each side of the dihedral interfaces between the HCR mirrors. The six resultant radially-oriented, nonreflecting strips will then obscure a small fraction ( $\sim 5$  percent) of the useful aperture. These radial obscurations would cause symmetrical  $120$  degree spikes to appear in the far field diffraction pattern produced by the HCR. This would tend to reduce the central maximum of the diffraction pattern, but this effect is not expected to be large. Since it is virtually unavoidable (no matter how the HCR is fabricated), the small loss of energy must be tolerated.

Since surface figure errors and dihedral angle errors of the HCR each degrade the reflected wavefront, very close tolerances should be placed on these parameters. Turned edges will undoubtedly occur near the edges of the mirror faces so that the clear aperture should be defined at the point where this effect becomes tolerable. The appropriate physical aperture increase of the HCR from the 15.958 cm diameter minimum (which gives a projected aperture of  $200\text{ cm}^2$ ) is 0.462 cm, resulting in a new aperture of 16.420 cm diameter.

The surface figure tolerance should be  $\lambda/20$  peak to peak at  $\lambda = 5.4 \times 10^{-4}$  mm after coating but before contacting. The dihedral angle tolerance should be set at  $\pm 0.030$  arc-second so that the retroreflected beam divergence will not exceed the diffraction limit for the corresponding HCR aperture of 15.958 cm. To obtain this value, the diffraction limit was calculated as (1.22)  $(5.4 \times 10^{-4} \text{ mm})/15.958 \text{ mm} = 4.128 \text{ } \mu\text{rad}$ . This is equivalent to 0.85 arc-second divergence (semi-cove angle) and corresponds to equal angle errors in the HCR of  $0.85/3.26 = 0.26$  arc-second. The 3.26 factor was derived in Reference 2. The 0.26 arc-second tolerance was relaxed to 0.3 arc-second because, statistically, all three dihedral angles are not likely to have the same magnitudes and algebraic signs on the same unit.

The contours of the mirror plates should all be the same and may be circular arcs, elliptical arcs or multiple straight-line segments. From a cost viewpoint, there is no clear advantage of any of these contours; from the weight viewpoint, the elliptical contour gives minimum HCR weight for a given assembly clear aperture. This contour has then been selected for use in the preferred HCR configuration.

The thicknesses of the plates were set at 2 cm for the two side plates and 5 cm for the base plate at the recommendation of optical fabrication experts since these thicknesses are adequate to meet the required surface figure tolerance and to provide adequate area for a reliable optical contact bond. The edges and bevels of the plates should be cloth polished so that they can be cleaned adequately before contacting the HCR assembly.

Figure 2-14 shows the tentative design for the preferred HCR configuration to be analyzed in subsequent sections of this report. This design reflects the various parameters discussed above.

#### 2.4.2 Some Considerations of Mechanical Mounting and Thermal Interface

Mechanical attachment of the HCR to the satellite is an obvious requirement for any operational system. It is not necessary that the HCR be affixed rigidly so that it remains in a predetermined orientation because its

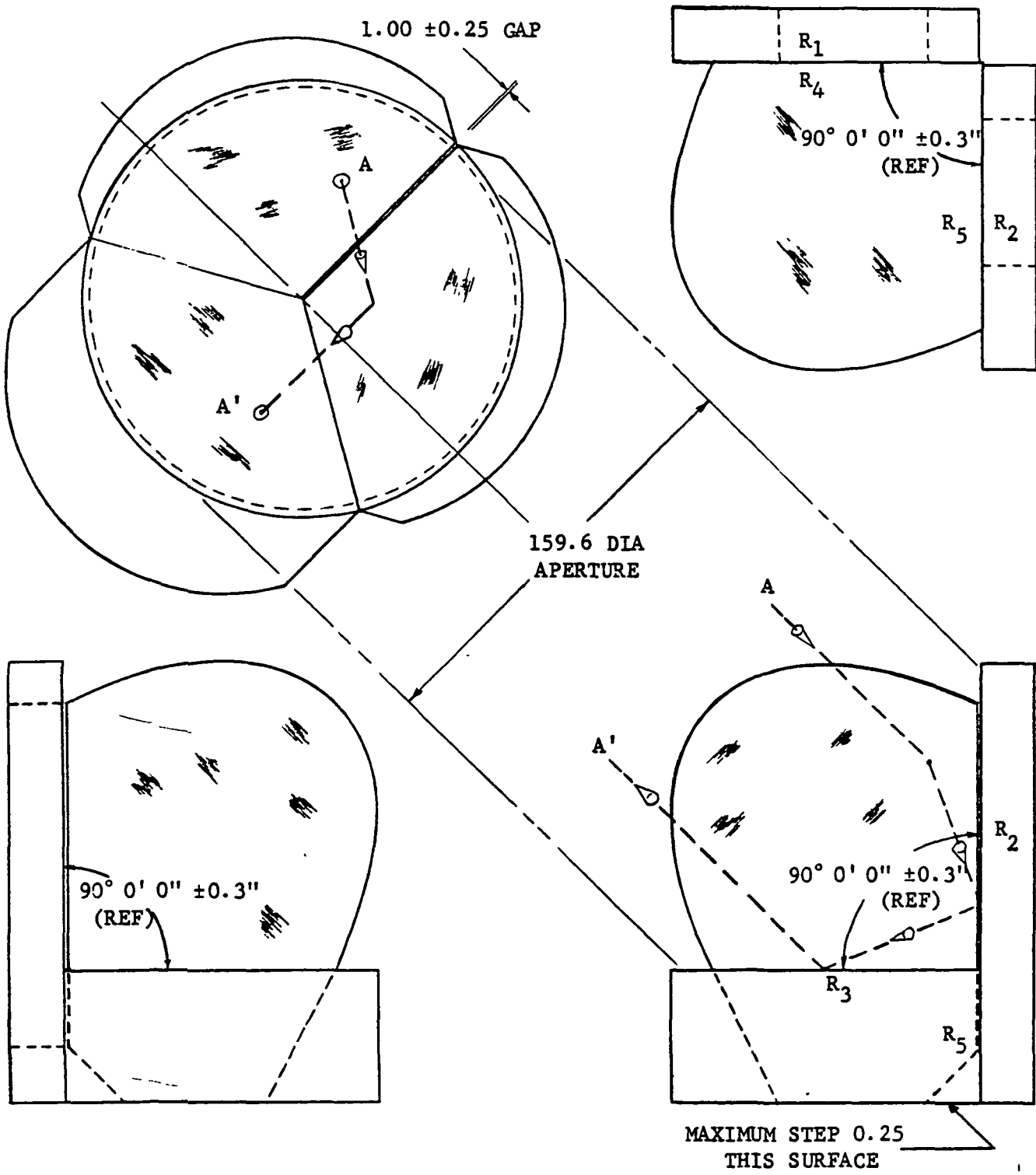


Figure 2-14. Hollow Corner Reflector

instantaneous pointing is not as rigorous a requirement as for most optical payloads. If the HCR moves angularly by several minutes of arc -- or perhaps even a few degrees -- the retroreflected beam will, in general, return to the earth and be usable. This allows the HCR to be held in a rather "soft" mount. Shock and vibration effects of launch, docking, etc. would therefore be diminished in severity.

A typical soft mount for an optical component is obtained by constraining it by a resilient material such as a silastic which bonds the component to a mechanical cell or mount which, in turn, is attached to external hardware structure. Such a mount could be designed so as to minimize mechanical distortion of the mirrors.

In the case of the HCR configuration developed under this study and described in detail from the optical viewpoint in Section 2.4.1, a suggested mechanical support for the optical assembly is shown in Figure 2-15. The thick base plate of the HCR is nonrigidly attached at three points to arms which support the assembly from a base structure. The bond between the arms and the Cervit plate is a silastic, such as one of the RTV compounds which cures at low temperature without emitting acetic acid vapor (which might damage the optical coatings). This mounting should be able to withstand dynamic forces of the space environment without damage to the bond if sufficient contact area is covered at each support point.

The silastic bonds will provide conduction paths for heat flow to or from the HCR plates, depending upon the relative temperatures of the plates and the structure. The thermal conductivity of common silastics is relatively high compared to the materials used in the mirror plates. By locating the support points as far as possible from the optical surface and mounting the HCR by its most structurally rigid component, the surface distortions resulting from heat flow through the supports can probably be kept small. This will need further consideration as part of the detailed design of a specific mounting arrangement.

From the detailed thermal analysis of Section 3, we assume that the rear surfaces of the HCR plates are insulated from the satellite structure. In general, this tends to raise the surface temperature and minimizes the gradient through the plates. If an efficient way were provided for heat to flow from the backs of the plates into the satellite, the gradients would probably double and the resultant surface thermal distortions, due to solar radiation, would significantly increase.

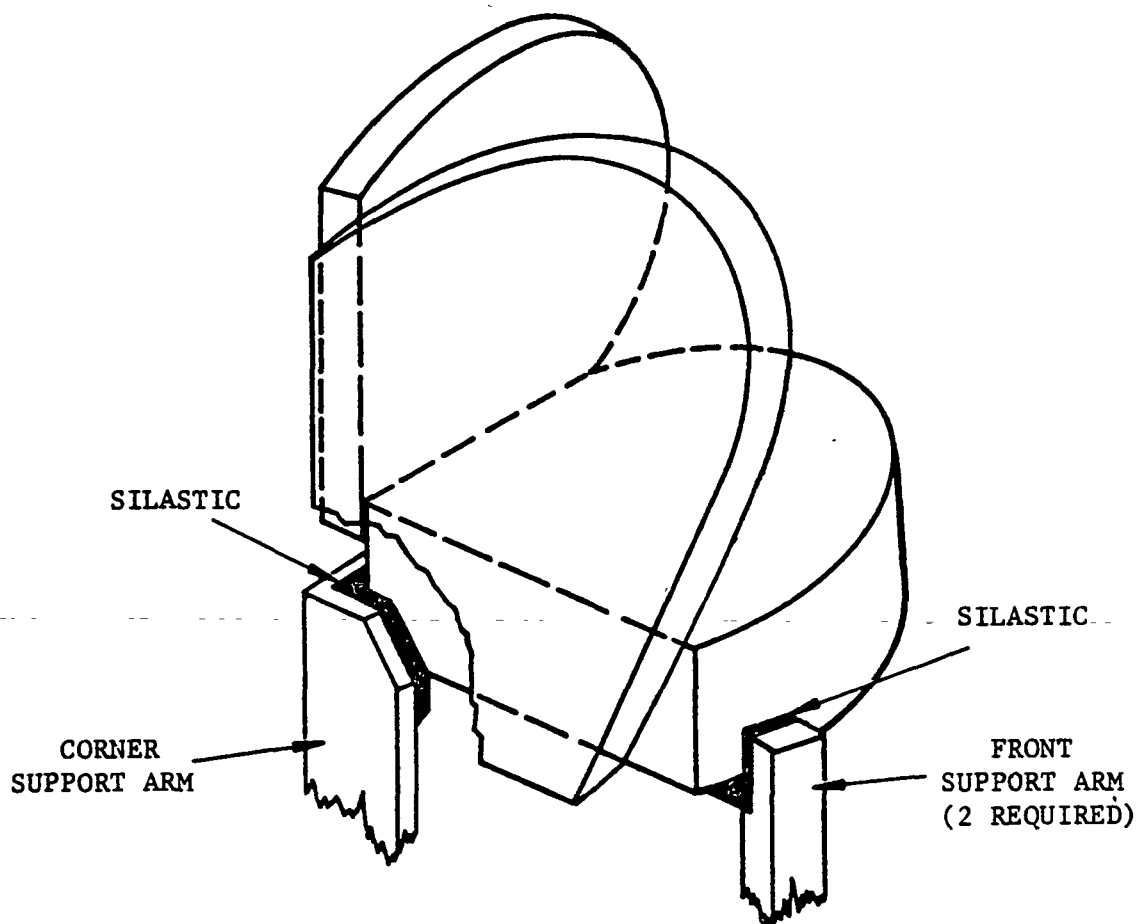


Figure 2-15. A Suggested Mechanical Interface with the HCR Assembly

## SECTION 3

### THERMAL ANALYSIS OF HCR IN GEOSYNCHRONOUS ORBIT

The thermal analysis of the HCR has been directed at solving the following two major problems:

- The calculation of the thermal deformations of the reflecting plates of a corner cube for a uniform unit front-to-rear surface temperature gradient.
- The determination of the transient temperature distributions that the HCR will attain when it is in its specified orbit.

These problems are addressed in the following paragraphs.

#### 3.1 DEFORMATION DUE TO UNIT TEMPERATURE GRADIENT

Calculating thermal deformations requires knowledge of the dimensions, shapes and mechanical constraints of the reflecting plates which make up the HCR, as well as the materials from which those plates are made. For the purpose of the present analysis, the HCR configuration shown in Figure 2-12A has been chosen. To the degree of approximation achieved in this analysis, the results would be essentially the same for the alternate configuration of Figure 2-12B.

The pertinent HCR characteristics and conditions are:

- a. Plates 2 cm thick are optically contacted to the edges of a 4 cm thick plate. All plates are mutually perpendicular.
- b. All plates are made of the same type material -- either ULE or Cervit.

c. Mechanical mounting is assumed to be nondistorting; thermal flow through the mounting is ignored.

d. Input thermal energy is assumed to enter from the front only -- the back of each plate is assumed to be insulated from the surrounding environment.

When heated more or less uniformly from the front, the HCR will tend to distort as indicated in Figure 3-1. The thinner plates (2) and (3) behave as cantilevered plates, distorting approximately to a parabolic contour as indicated in the Views AA' and BB'. Since plate (1) is mechanically constrained along its two straight edges, its deformation pattern, indicated by the control section view of Figure 3-1, is much more complicated. The thermal deformations of the cantilevered plates for unit temperature difference can be determined from the equation:

$$\delta = \frac{1}{2} \alpha \frac{\Delta T}{t} L^2$$

where

$\delta$  = deflection at distance L from the constrained edge

$\alpha$  = coefficient of thermal expansion

$\Delta T$  = front-to-rear temperature difference

t = plate thickness

For the particular case of interest here,

$$\alpha = 3.0 \times 10^{-8} \text{ in/in/}^\circ\text{F (for ULE)}$$

$$t = 2 \text{ cm} = 0.787 \text{ inch}$$

$$L = 4.5 \text{ inches (for elliptically contoured plate edge)}$$

Hence,  $\delta = 3.86 \times 10^{-7}$  inch for  $\Delta T = 1^\circ\text{F}$  for the cantilevered plates.

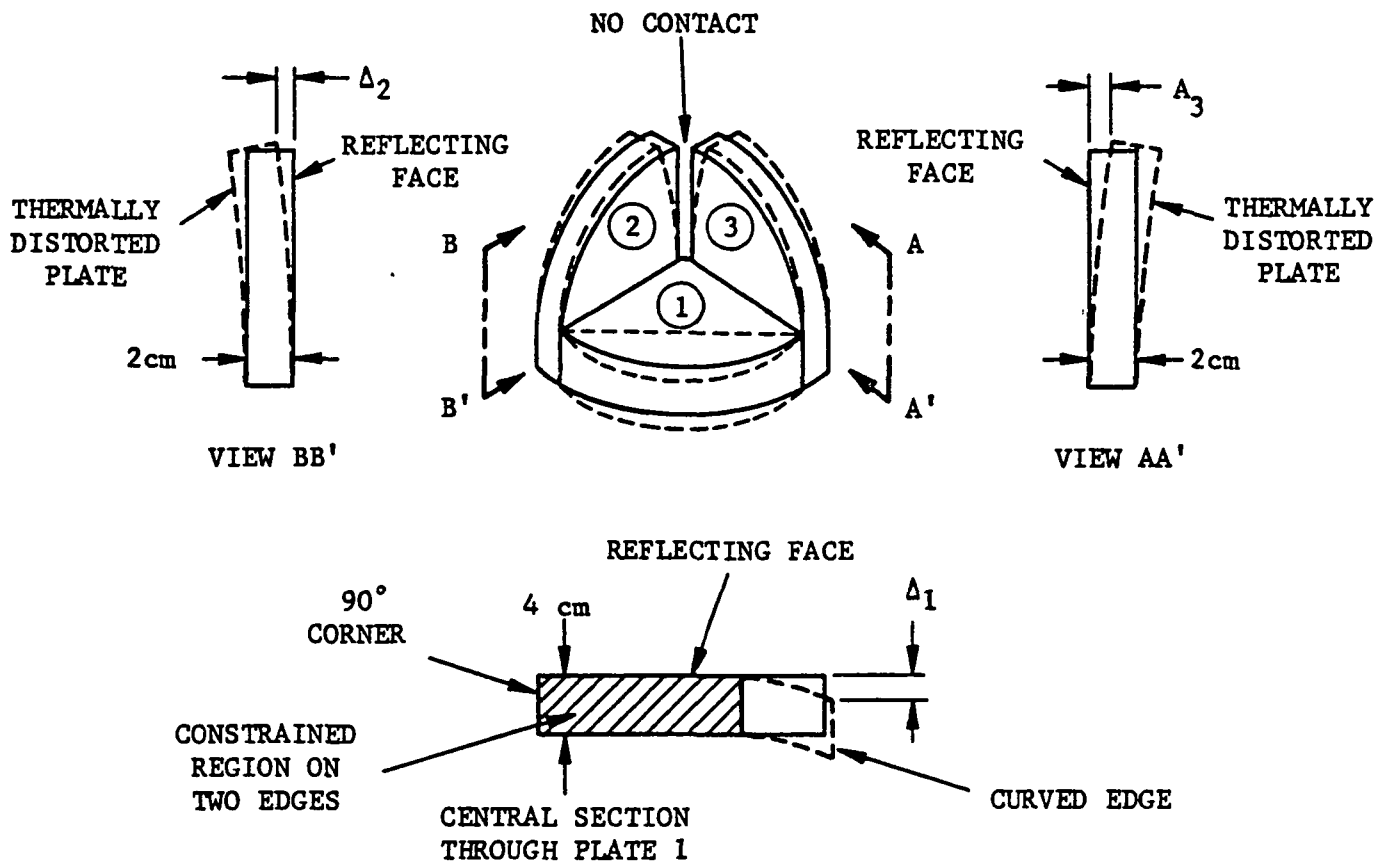


Figure 3-1. Thermal Distortions of a Front-Irradiated HCR

The more complex problem of determining the deformation of the constrained plate for unit temperature difference has been solved by using the NASTRAN, finite element model shown in Figure 3-2 which shows an 83 element, 98 node model of a quarter of a circular plate. The radius is 5.5 inches and the plate thickness 2 or 4 cm. To simulate contact at the dihedral edges with the other plates, the deflections perpendicular to the plate (i.e., in the Z direction) are constrained along each edge for a distance of 3.85 inches. (The contour of the free edge of the plate is immaterial.) Essentially, the same bending results are obtained for the circular arc shown in Figure 3-2 or for the elliptical contour of Figure 2-12A since the distance from the 90 degree corner to the midpoint on the free edge is constant for both configurations.

TABLE 3-1

## MATERIAL PROPERTIES OF ULE USED IN ANALYSES

Young's Modulus	$9.8 \times 10^6$ Lb-Force/In <sup>2</sup>
Coefficient of Thermal Expansion	$3.0 \times 10^{-8}$ In/In/°F
Poisson's Ratio	0.17
Shear Modulus	$4.3 \times 10^6$ Lb-Force/In <sup>2</sup>
Density	138.1 Lb-Mass/Ft <sup>3</sup>
Specific Heat	0.190 Btu/Lb-Mass-°R
Thermal Conductivity	0.77 Btu/Hr-Ft-°R
Thermal Diffusivity	$2.93 \times 10^{-2}$ Ft <sup>2</sup> /Hr

The plate is assumed to be made of ULE with the material properties given in Table 3-1. A 1.0°F front-to-rear linear temperature gradient was imposed on each element and the deflections determined. The results of the analysis are shown in Figures 3-3 and 3-4. Figure 3-3 shows lines of constant Z displacement, while Figure 3-4 shows the variation in Z displacement with radius along the centerline of the plate. It may be seen from these figures that the

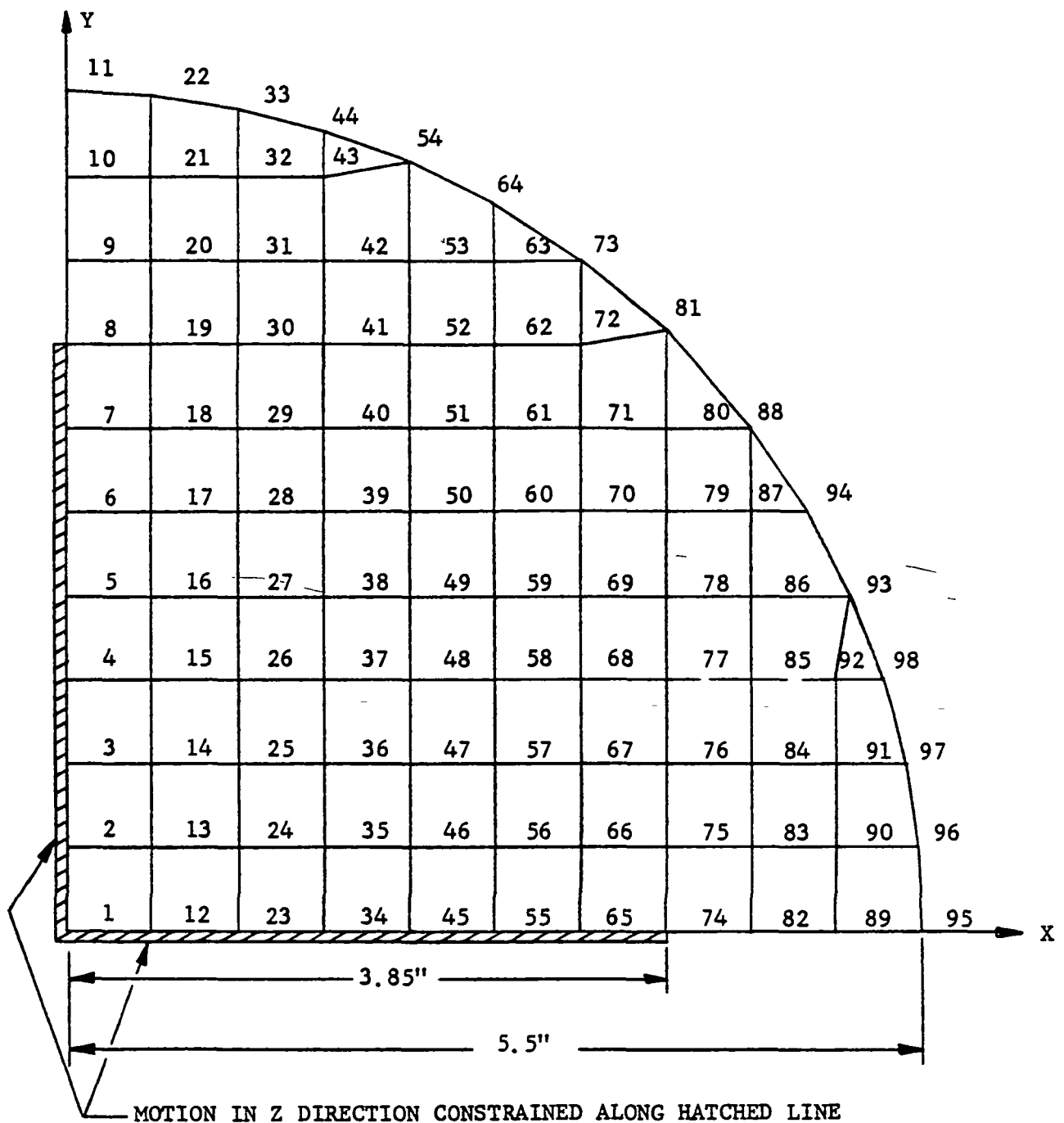


Figure 3-2. Nodal Locations and Element Description for NASTRAN Analysis of HCR Plate Deflections

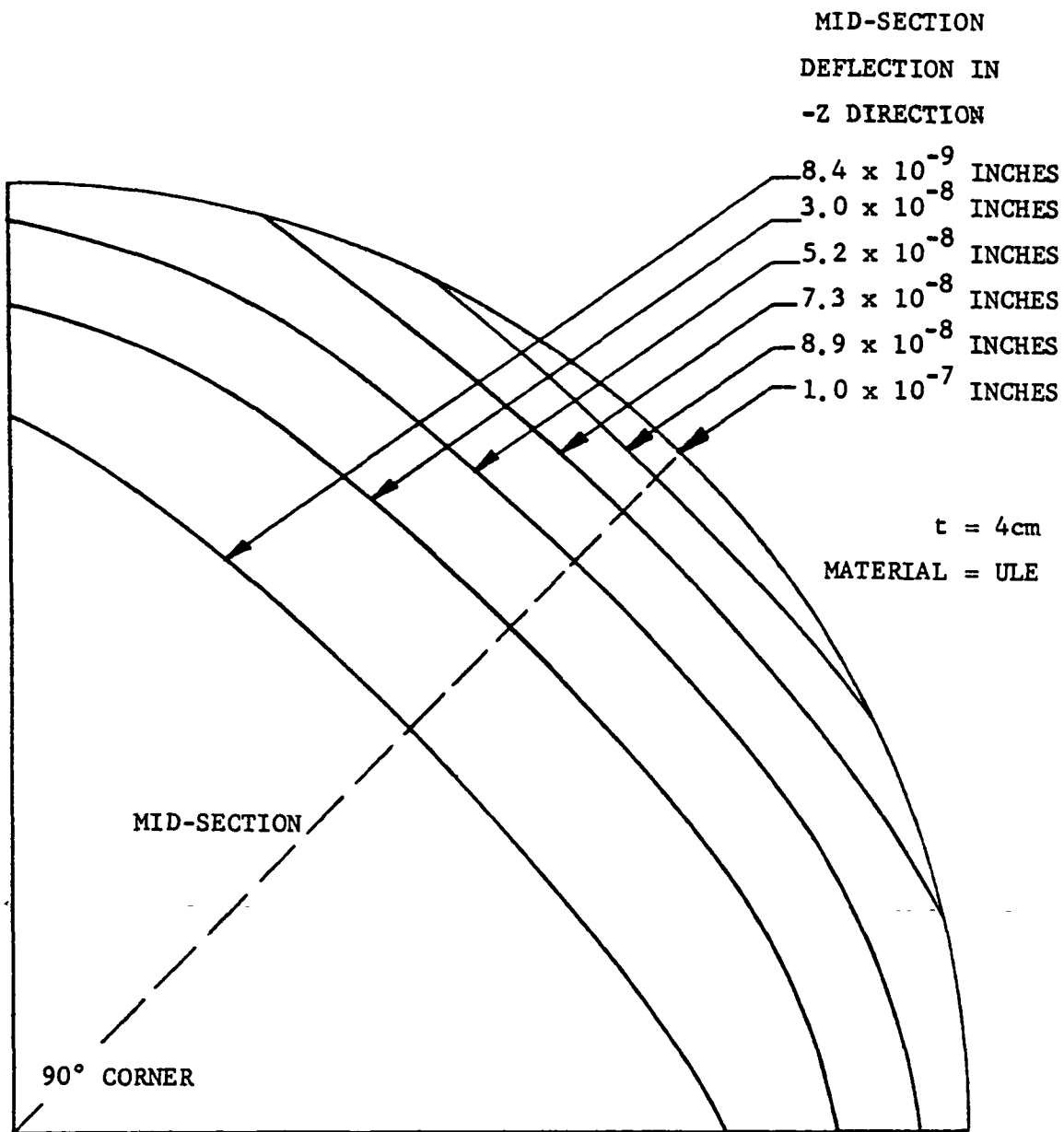


Figure 3-3. Results of Constrained-Plate NASTRAN Analysis: lines of constant deflection in Z direction (perpendicular to plate) for a 1°F front-to-rear temperature difference

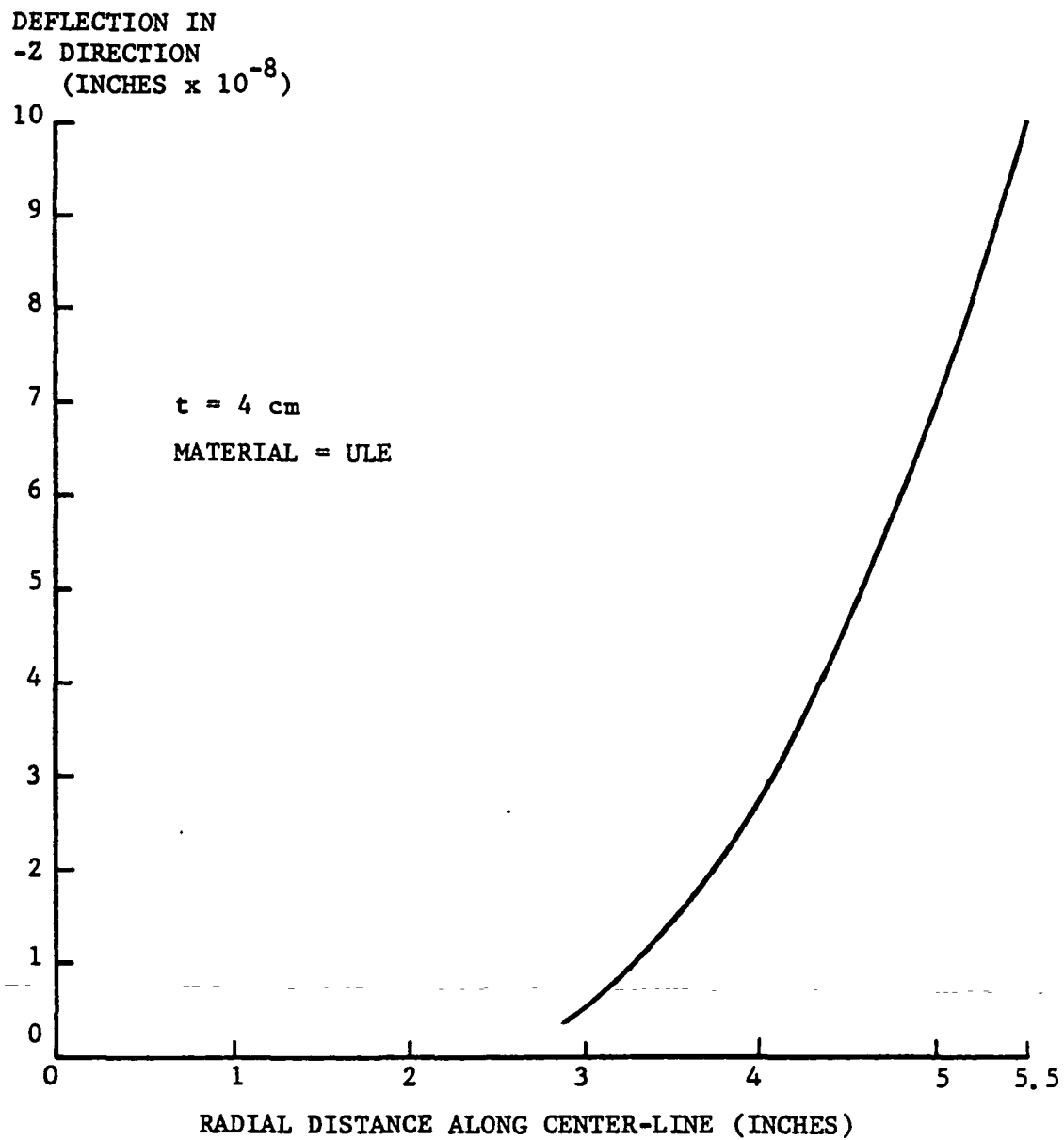


Figure 3-4. Results of Constrained-Plate NASTRAN Analysis: deflection in minus Z direction along center line of plate as a function of distance from  $90^\circ$  corner

maximum displacement of a constrained 4 cm thick plate is about  $1.0 \times 10^{-7}$  inches for the imposed  $1.0^\circ\text{F}$  temperature gradient. A similar analysis for a 2 cm thick plate yielded a maximum deflection of  $1.0 \times 10^{-7}$  inches for the same temperature difference. How this information may be used to estimate the distortions of the actual HCR is explained in Section 3-2, giving due consideration to the expected temperature differences in orbit.

### 3.2 INPUT THERMAL FLUX RECEIVED DURING ORBIT

The determination of the actual temperature distribution that the HCR will achieve in orbit is made difficult by the complexity of the boundary conditions. A precise solution to this problem requires a long running time on the computer because it involves a 24 hour transient cycle. Since the maximum plate deflection for a unit temperature difference is small, an approximate solution to the problem is adequate if the actual front-to-rear temperature difference is sufficiently small. To determine if this can be expected, a simplified solution to the problem was attempted first. The model chosen was a uniform, unshielded, flat plate which orbits earth in a  $\beta = 0$ , synchronous orbit. The energy input to the plate consists of the incident earthshine, albedo, and solar fluxes multiplied by the appropriate spectral absorptivities. For this portion of the study, the values used for  $\alpha_s$  (solar absorptivity) and  $\epsilon$  (infrared emissivity) were 0.1 and 0.05, respectively. The calculated incident solar and albedo fluxes are shown in Figure 3-5 as a function of angular position. To simplify the problem, edge effects were neglected and the heat transfer was assumed to be strictly one-dimensional (through the plate). It was also assumed that the rear of the mirror was insulated.

The first model generated was a 2 cm thick mirror of ULE and had 22 nodes through the thickness of the plate. This required too much computer time to analyze, so a simpler, seven-node model was generated. An additional seven-node model of a 4 cm thick plate was generated and both models were run for three orbits. Figure 3-6 shows the seven-node model in schematic form.

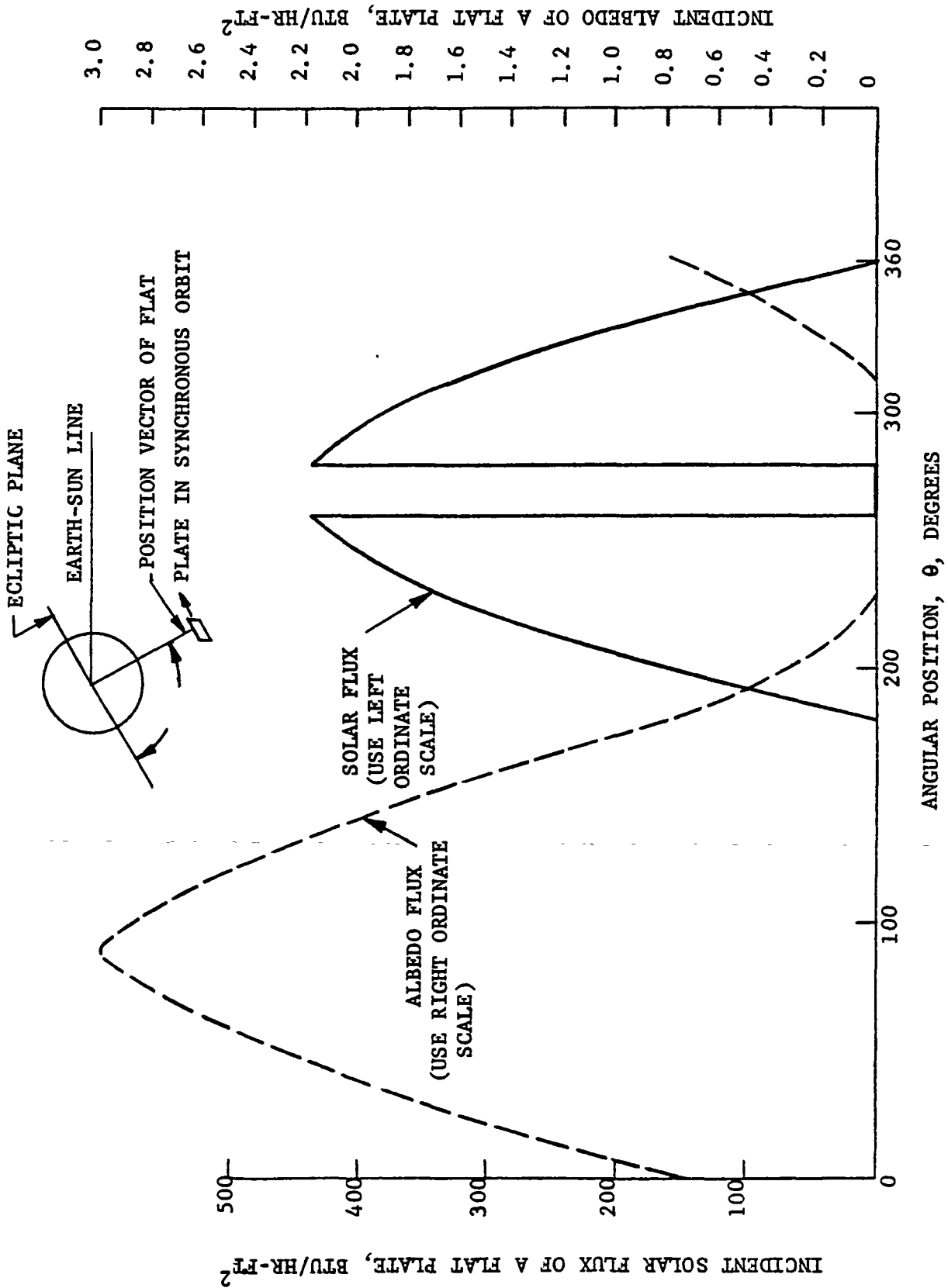


Figure 3-5. Solar and Albedo Fluxes Incident Upon an Earth Oriented Flat Plate in a Synchronous Orbit

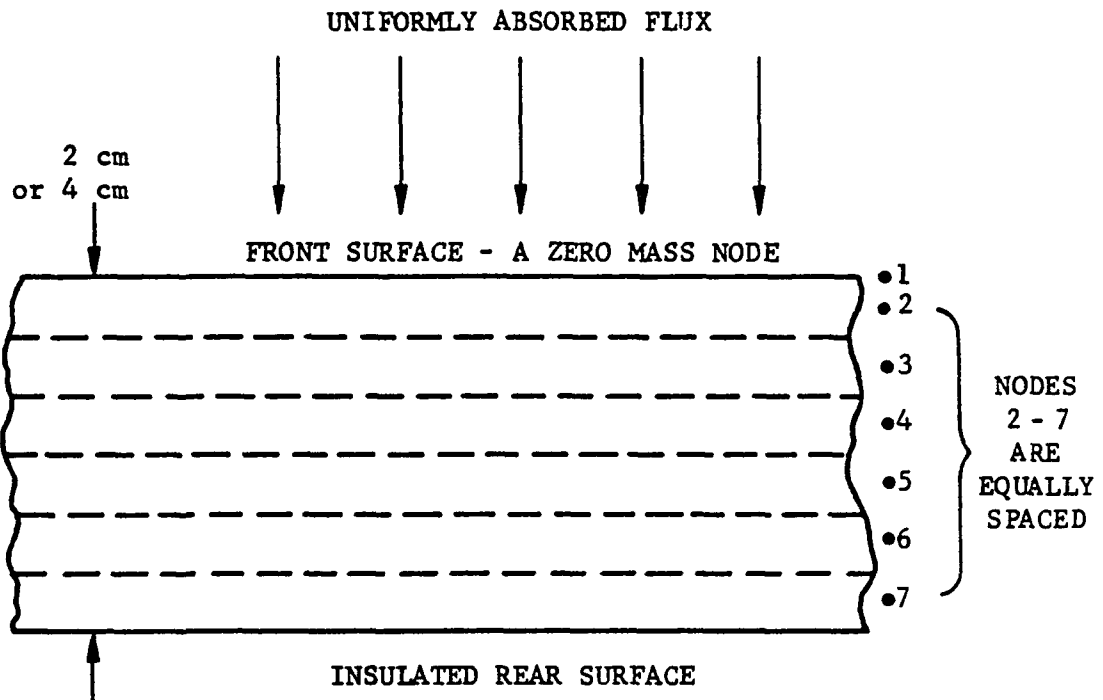


Figure 3-6. Schematic of 7-Node Model used to Estimate Temperature Gradients Through the HCR Plates

Three orbits did not allow enough time to give steady orbital temperatures, but the front-to-rear temperature differences did not change significantly with orbit number and thus are believed to be reasonably accurate. The calculations showed maximum front-to-rear temperature differences of 1.39°F and 2.67°F for the 2 and 4 cm plates, respectively. The corresponding orbital variations in spatial mean temperatures are approximately 45°F and 85°F while the orbital mean temperatures are about 610°R (66°C). This temperature may be reduced by a proper choice of  $\alpha_s/\epsilon$  since, on a mean orbital basis,

$$\overline{\sigma T^4} = \left( \frac{\alpha_s}{\epsilon} \right) (\overline{S} + \overline{A}) + \overline{E}$$

where

T = absolute temperature

$\sigma$  = Stephen-Boltzman constant

$\alpha_s$  = solar absorptivity

$\epsilon$  = infrared emissivity

$\overline{S}$  = mean solar flux

$\overline{A}$  = mean albedo flux

$\overline{E}$  = mean earthshine flux

In general,  $T^4 \neq (\overline{T})^4$  but, if it is assumed that the equality holds, then a value of  $\alpha_s/\epsilon = 1.0$  will yield  $\overline{T} = 515^\circ\text{R}$  ( $10^\circ\text{C}$ ) which would be a more desirable value.

The 2.67°F front-to-rear temperature difference yields a maximum deflection of about  $2.67 \times 10^{-7}$  inches in the 4 cm thick plate. Essentially, the same result is obtained for the 2 cm plate with a 1.39°F front-to-rear  $\Delta T$  since the gradient changes by the same ratio as the deflection.

For visible light ( $\lambda = 0.54 \mu\text{m}$ ), this corresponds to  $\lambda/80$  so, to this approximation, the thermal deformation would not seem to be a serious limitation on the performance of a single mirror in orbit. This is shown below to be the case also for a three mirror HCR.

As a reasonable approximation of the actual situation of interest to NASA, the total flux absorbed by the plates of a three-dimensional HCR was calculated. The ray geometry is shown in Figure 3-7. The coordinate axes lie along the intersections of the surfaces. It is assumed for the moment that the faces of the cube are infinite in extent and that the cube is filled with collimated light whose direction is defined by the angles  $\theta$  and  $\phi$  shown in Figure 3-7. The energy absorbed at every point is comprised of the following components: energy which is directly incident upon the point; energy which has been reflected from one other surface (two possible paths); and energy which has been reflected from two other surfaces.

If it is assumed that the absorptivities of the surfaces are equal and are independent of angle of incidence, then the total energy absorbed at the point "A" is the sum of the four components shown below:

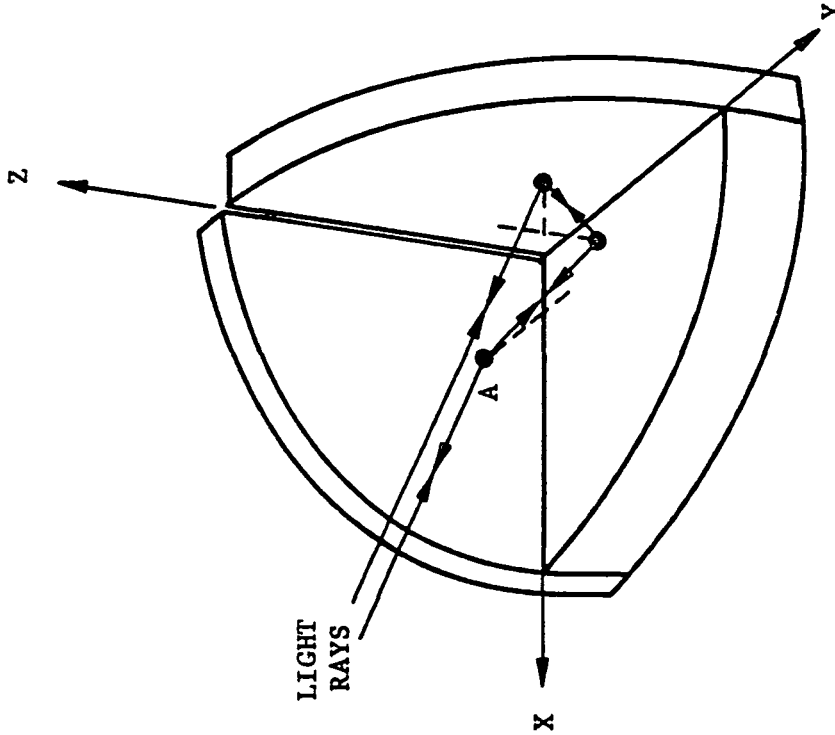
<u>Component</u>	<u>Energy Absorbed</u>
Directly incident ray	$I_o \alpha_s dA_b$
Two rays having one previous reflection	$2I_o \alpha_s (1-\alpha_s) dA_b$
One ray having two previous reflections	$I_o \alpha_s (1-\alpha_s)^2 dA_b$
Total Energy Absorbed	$4I_o \alpha_s (1-\alpha_s + \frac{\alpha_s^2}{4}) dA_b$

where

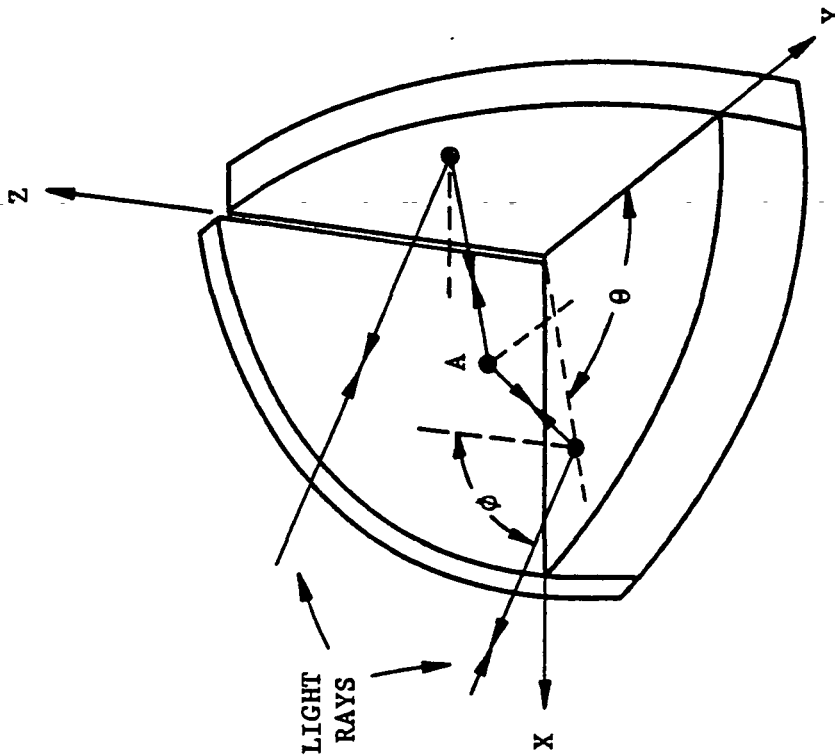
$\alpha_s$  = surface absorptivity

$I_o$  = flux in incoming beam

$dA_b$  = cross section of beam



ONE RAY INCIDENT ON POINT A  
AFTER TWO REFLECTIONS AND  
ONE RAY INCIDENT ON THAT POINT  
DIRECTLY



TWO RAYS INCIDENT ON POINT A  
AFTER ONE REFLECTION

Figure 3-7. Paths of Rays Incident Upon a Single Point A on the Surface of a HCR when all Surfaces are Illuminated

Since the irradiated area,  $dA$ , of the surface on the X-Y plane is given by

$$dA = dA_b / \cos \phi,$$

the flux absorbed by any area on the X-Y plane is given by

$$I_{x-y} = 4I_o \alpha_s (1 - \alpha_s + \frac{\alpha_s^2}{4}) \cos \phi$$

By appropriate application of the trigonometric functions of  $\theta$  and  $\phi$ , the flux absorbed on the YZ and XZ planes can be computed.

There are three special cases of HCR irradiation during the orbit which are of interest. These are:

- a. Beam normal to one face
- b. Beam symmetrically incident on two faces
- c. Beam symmetrically incident on three faces

During the half-orbit in which sunlight enters the HCR (see Figure 3-8), Case "a" occurs at about  $\gamma = 215^\circ$ , Case "c" occurs in the vicinity of the earth's shadow at  $\gamma = 261^\circ$  and  $279^\circ$ , while Case "b" occurs at about  $\gamma = 325^\circ$ . Between these points in the orbit, all three faces are irradiated more or less uniformly, depending upon the HCR's aspect to the incoming sunlight.

The relationships shown in Table 3-2 indicate that in Case "b", when two surfaces with  $\alpha_s = 0.1$  are irradiated symmetrically, each surface absorbs 34 percent more sunlight than if one surface is normal to the beam (Case "a"). Similarly, the Case "c" condition allows 108 percent more energy to be absorbed than in the Case "a" condition. The energy absorbed by the HCR is thus somewhat dependent upon its orientation. In order to be sure of a conservative estimate of thermal effects, the expression for the worse-case irradiation of all three mirrors was considered to apply at all points in the orbit. This expression was used for albedo and earthshine, as well as solar inputs, even though the former fluxes are not collimated. No correction was applied to account for the finite extent of the mirrors despite the fact that this would reduce the flux on some areas of the HCR surfaces.

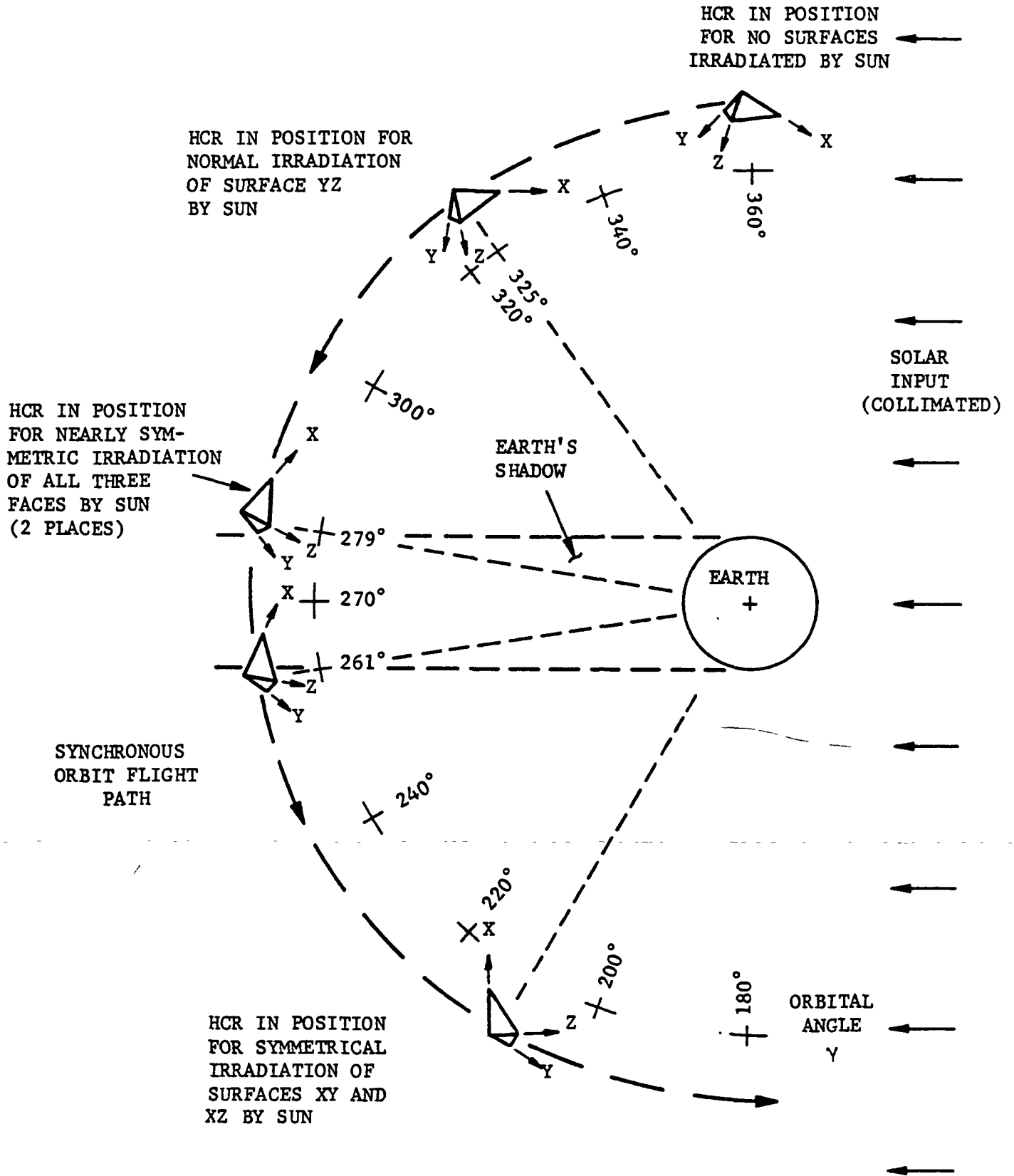


Figure 3-8. Typical Geometry for HCR in Synchronous Orbit

TABLE 3-2

## THREE SPECIAL CASES OF HCR IRRADIATION

CASE I BEAM NORMAL TO ONE FACE	CASE II BEAM SYMMETRICALLY INCIDENT ON TWO FACES	CASE III BEAM SYMMETRICALLY INCIDENT ON THREE FACES
$\psi = 0^\circ$ $\cos \psi = 1$ $I_1 = I_0 \alpha \cos \psi$ $I_1 = I_0 \alpha$	$\psi = 45^\circ$ $\cos \psi = 0.707$ $I_2 = I_0 \alpha \cos \psi$ $+ I_0 \alpha (1-\alpha) \cos \psi$ $I_2 = 0.707 I_0 \alpha (2-\alpha)$	$\psi = 54.73^\circ$ $\cos \psi = 0.577$ $I_3 = 4 I_0 \alpha (1-\alpha + \frac{\alpha^2}{4}) \cos \psi$ $I_3 = 2.308 I_0 \alpha (1-\alpha + \frac{\alpha^2}{4})$

For  $\alpha_s = 0.1$ 

$I_1 = 0.1 I_0$	$I_2 = (0.707 I_0) (0.1) (2-0.1)$ $= 0.134 I_0$ $= 1.34 I_1$	$I_3 = (2.308 I_0) (0.1) (1-0.1 + \frac{0.01}{4})$ $= 0.208 I_0$ $= 2.08 I_1$
-----------------	--	---

For  $\alpha_s = 0.08$ 

$I_1 = 0.08 I_0$	$I_2 = (0.707 I_0) (0.08) (2-0.08)$ $= 0.108 I_0$ $= 1.36 I_1$	$I_3 = (2.308 I_0) (0.08) (1-0.08 + \frac{0.0064}{4})$ $= 0.170 I_0$ $= 2.12 I_1$
------------------	--	---

For  $\alpha_s = 0.05$ 

$I_1 = 0.05 I_0$	$I_2 = (0.707 I_0) (0.05) (2-0.05)$ $= 0.068 I_0$ $= 1.38 I_1$	$I_3 = (2.308 I_0) (0.05) (1-0.05 + \frac{0.0025}{4})$ $= 0.110 I_0$ $= 2.19 I_1$
------------------	--	---

The incident solar, earthshine and albedo flux distributions across the three faces of the cube were next calculated as a function of HCR orbital position. An arbitrary, but fixed, orientation (rotation) of the HCR about its axis of symmetry (passing through the earth's center) was assumed. This orientation differs slightly from that shown in Figure 3-8. The calculated fluxes were multiplied by the factor derived above and used as input (absorbed) fluxes to the seven-node mirror thermal conduction model shown in Figure 3-6. The temperatures at the hottest points on the mirror reflecting surfaces and the corresponding temperature gradients through the mirror thickness were computed. Conduction through the plate was considered, but lateral flow from one point to the next was ignored in this thermal model. Figures 3-9A through 3-9H show the incident solar fluxes while Table 3-3 shows the extremes of those temperatures and the gradients,  $\Delta T_{\max}$ . The three types of coatings listed in the left column of the table have the  $\alpha_s$  and  $\epsilon$  characteristics listed in the next two columns. These represent standard aluminum plus  $\text{SiO}_x$ , a special high emissivity coating characterized as silver plus thick  $\text{SiO}_x$  and a compromise special coating with  $\alpha_s = \epsilon = 0.08$  which lies between these two extremes.

TABLE 3-3

## CALCULATED WORST CASE HCR MIRROR TEMPERATURES

Coating Type	$\alpha_s$	$\epsilon$	$\Delta T_{\max}$ (1) °F (°C)	Temperature in 3rd Cycle (2)		
				Minimum °F (°C)	Maximum °F (°C)	Mean °F (°C)
1	0.1	0.05	4.56 (2.53)	197 (90)	462 (239)	311 (155)
2	0.05	0.10	2.45 (1.36)	34 (1)	176 (80)	96 (36)
3	0.08	0.08	3.76 (2.09)	100 (38)	317 (159)	194 (90)

(1) Maximum front-to-rear temperature difference for 2 cm thick plate.

(2) Based on properties of ULE.









Table 3-4 lists the extreme surface deformations which would be expected to result from the  $\Delta T_{\max}$  values listed in Table 3-3. For ULE, the constrained 4 cm thick mirror deflections were obtained by multiplying the  $1.0 \times 10^{-7}$  inches per  $^{\circ}\text{F} \Delta T$  from the NASTRAN analysis described earlier by twice the appropriate  $\Delta T_{\max}$  for 2 cm thickness from Table 3-2. The deflections for Cervit were obtained from those for ULE by multiplying by the ratio of coefficients of thermal expansion ( $1 \times 10^{-7}/0.3 \times 10^{-7}$ ) and dividing by the ratio of thermal diffusivities ( $3.1 \times 10^{-2}/2.9 \times 10^{-2}$ ). The results for Cervit are, therefore, 3.1 times those for ULE.

For the cantilevered plates, the deflections were calculated by multiplying the  $3.86 \times 10^{-7}$  inches per  $^{\circ}\text{F} \Delta T$  by the appropriate value of  $\Delta T_{\max}$  for ULE. This value was then multiplied by 3.1 to give the corresponding values for Cervit.

TABLE 3-4

## CALCULATED WORST CASE DEPARTURE FROM PLANE OF HCR MIRRORS

Coating Type *	ULE Mirrors		Cervit Mirrors	
	Cantilevered ( $\mu\text{m}$ )	Constrained ( $\mu\text{m}$ )	Cantilevered ( $\mu\text{m}$ )	Constrained ( $\mu\text{m}$ )
1	$4.5 \times 10^{-2}$ ( $\lambda/12$ ) See Note	$2.3 \times 10^{-2}$ ( $\lambda/23$ )	$1.4 \times 10^{-1}$ ( $\lambda/4$ )	$7.1 \times 10^{-2}$ ( $\lambda/8$ )
2	$2.4 \times 10^{-2}$ ( $\lambda/22$ )	$1.2 \times 10^{-2}$ ( $\lambda/45$ )	$7.4 \times 10^{-2}$ ( $\lambda/7$ )	$3.7 \times 10^{-2}$ ( $\lambda/15$ )
3	$3.7 \times 10^{-2}$ ( $\lambda/15$ )	$1.9 \times 10^{-2}$ ( $\lambda/28$ )	$1.1 \times 10^{-1}$ ( $\lambda/5$ )	$5.9 \times 10^{-2}$ ( $\lambda/9$ )

\*Types defined in Table 3-3.

Note: Sag of Surface expressed in wavelengths for  $\lambda = 0.54 \mu\text{m}$ .

When expressed in wavelengths of visible light, the HCR surface deformations start to have meaning in an optical sense. The numbers in parentheses in Table 3-4 provide this data and represent the maximum sags of the surfaces from the nominal planes. The sags of points on the surfaces closer to the surface intersections are progressively smaller, so the RMS departure from the plane is smaller than the peak values listed. Since each light ray from the earth will intercept all three HCR surfaces before it returns to the earth, the combined effects of all three surfaces must be considered. This topic is discussed in Section 4 of this report.

### 3.3 TEMPERATURE PROFILE ANALYSIS

The analyses discussed above considered the feasibility of the HCR application within the time and money constraints of the contract. They did not, however, provide a detailed prediction of the transient temperature distribution within the plates after steady orbital conditions had been reached. Such a determination would require a larger expenditure of computer funds than was available for the project. A method of analysis that would be used to obtain the temperature profiles was outlined, however, and it is described in Appendix C since it contains several interesting features. The method is based on use of a 58 node computer model. The more detailed thermal analysis recommended in Section 5 would use this model.

### 3.4 LITERATURE SEARCH

While the nature of this study did not require that a thorough literature search should be made for references pertinent to the thermal analysis of HCR's, Reference 15 was found and it deserves comments. That prior report was concerned with the design of corner cubes to be used on the lunar surface and contains a section on the calculation of the transient temperature of a HCR. The prior analysis differed from the present analysis in that it assumed that the HCR was oriented so that the incoming sunlight was parallel to one of the faces; thus, the maximum incident energy flux was  $(2 - \alpha) S \cos \theta$  instead of the  $4 [1 - \alpha + (\alpha^2/4)] S \cos \theta$  derived in the present analysis ( $S$  is the solar constant). It was not noted that this factor only applies for an infinite

cube and no attempt was made to derive the correct fluxes for the finite cube. For the calculation of the temperature distribution in the corner cube, the analysis in Reference 15 assumed that each face was an isothermal node and that equilibrium conditions occurred at all times. These assumptions are appropriate to that analysis based on the length of the lunar day. The assumptions, however, are not valid at dusk or dawn, and they do not permit the calculation of thermal distortions. This was noted in the report, and it was pointed out that thermal deformations at lunar dusk and dawn would cause an HCR to deform excessively at these times. The prior report, therefore, does not provide any basis for analysis of the orbiting HCR of interest in the present study.

## SECTION 4

### OPTICAL EFFECTS OF THERMAL DISTORTIONS

The geometrical deformations of a thermally irradiated HCR in a geosynchronous orbit are discussed in Section 3. The worst case changes in mirror shape from the nominal planes are best described by reference to Figure 3-1 and Table 3-4 which show the nature and conservative estimates of the magnitudes, respectively, of the surface distortions. In this analysis, the corresponding deformation of a plane input wave, when retroreflected by the HCR, is calculated and then the effects upon the far field diffraction pattern are estimated.

As the first step of this computation, the geometric shapes of the mirrors were expressed mathematically for ray tracing. The two cantilevered surfaces were designated as parabolic toric cylinders while the constrained surface was designated as a generalized aspheric of the form:

$$x = \frac{CY^2}{1 + \sqrt{1 - EC^2Y^2}} + AY^4 + BY^6 + CY^8 + DY^{10}$$

Because the calculations of the precise deformations to be expected of the surfaces in orbit had not yet been completed at the time that the computer facilities and the services of a qualified optical designer were available to this project, the inputs to the ray traces were estimated in terms of the maximum surface sags from the respective planes for the following two hypothetical cases:

	<u>Case 1</u>	<u>Case 2</u>
Sags of Cantilevered Surfaces	$\lambda/10$	$\lambda/4$
Sags of Constrained Surface*	$\lambda/25$	$\lambda/10$

---

\*The surface has a contour which is shown in Figure 3-4 of Section 3.

Where  $\lambda$  was the wavelength of green light, 0.54  $\mu\text{m}$ . The corresponding values of the constants for the mathematical expressions for the surfaces were then:

	<u>Case 1</u>	<u>Case 2</u>
Toric Curvature (reciprocal radius in mm)	$-5.124 \times 10^{-9}$	$-1.28 \times 10^{-8}$
Aspheric Eccentricity "E"	1.0	1.0
Aspheric Curvature "C"	0	0
Aspheric Coefficient "A"	0	0
Aspheric Coefficient "B"	$-3.3515 \times 10^{-18}$	$-8.3788 \times 10^{-18}$
Aspheric Coefficient "C"	$-3.4632 \times 10^{-22}$	$-8.6580 \times 10^{-22}$
Aspheric Coefficient "D"	$1.9464 \times 10^{-26}$	$4.8660 \times 10^{-26}$

The ray trace program was then instructed to arrange the surfaces at the appropriate angles to the input optical axis which was also the axis of symmetry of the HCR. The paths of 156 rays, arranged in the form of a 19 x 19 square grid and lying within one-half the circular aperture of the HCR, were then traced through the three reflections and the optical path differences (OPD's) of each ray from a plane wavefront exiting the HCR aperture were computed. Tables 4-1 and 4-2 list these OPD's for the two hypothetical distorted HCR cases. The columns of interest are the ray number, the "Y" and "Z" coordinates of the entering rays (where the axes and point numbering system are defined as indicated in Figure 4-1) and the OPD's which are expressed in mm. The OPD's for all 293 rays entering the full circular aperture may be derived from the 156 rays shown since all but the 19 rays crossing the aperture in the  $Z = 0$  meridian are duplicated in the minus Z-direction.

Figures 4-2A and 4-2B show the values of the OPD's in wavelengths of green light for the lower right quadrants of the apertures of the two HCR cases. Analysis of the data of Tables 4-1 and 4-2 indicates that the wavefront profiles across any diameter of either HCR aperture are symmetrical with respect to the axis of symmetry. The shape of each reflected wavefront is generally

TABLE 4-1

RAY TRACE PRINTOUT OF THERMALLY DISTORTED HCR - HYPOTHETICAL CASE 1

CUBE  
CYCLE 0  
CULOW J

09:22:50-----01/17/75

I	MAY	CLM	Y	Z	N		F.P.		DIST	YS	DEL Y
					0.0	0.0	0.0	0.0			
10	3	0.0	0.0	0.0	-1.76540-13	-1.43600-06	1.43600-06	-5.06720-07	-1.01140-06		
					0.0	0.0					
					0.0	0.0					
1	3	0.95	0.0		-1.369140-06	3.489280-13	0.0		-8.140270-05		
					-8.100000 01	1.990030-05					
2	3	0.84	0.0		-2.251720-06	-1.347930-12	0.0		-6.349140-05		
					-7.199490 01	1.768920-05					
3	3	0.74	0.0		-1.905490-06	-9.424990-13	0.0		-4.440180-05		
					-6.300000 01	1.547800-05					
4	3	0.63	0.0		-1.374120-06	-3.666660-13	0.0		-2.965690-05		
					-5.400000 01	1.326690-05					
5	3	0.53	0.0		-9.696240-07	-3.797030-14	0.0		-1.920000-05		
					-4.500000 01	1.105570-05					
6	3	0.42	0.0		-6.916970-07	8.509830-14	0.0		-1.180370-05		
					-3.600000 01	8.844600-06					
7	3	0.32	0.0		-4.406610-07	1.052910-13	0.0		-6.520370-06		
					-2.700000 01	6.633440-06					
8	3	0.21	0.0		-3.209350-07	8.518180-14	0.0		-2.880340-06		
					-1.400000 01	4.422290-06					
9	3	0.11	0.0		-1.598420-07	4.794770-14	0.0		-7.191150-07		
					-8.499990 00	2.211150-06					
10	3	0.0	0.0		0.0	0.0	0.0		0.0		
					0.0	0.0					
11	3	-0.11	0.0		1.598420-07	-5.845330-14	0.0		-7.191150-07		
					8.999990 00	-2.211150-06					
12	3	-0.21	0.0		3.209350-07	-1.277030-13	0.0		-2.880340-06		
					1.400000 01	-4.422290-06					
13	3	-0.32	0.0		4.406610-07	-2.105540-13	0.0		-6.520370-06		
					2.700000 01	-6.633440-06					
14	3	-0.42	0.0		6.916970-07	-3.229230-13	0.0		-1.180370-05		
					3.600000 01	-8.844610-06					
15	3	-0.53	0.0		9.696230-07	-5.110780-13	0.0		-1.920000-05		
					4.500000 01	-1.105580-05					
16	3	-0.63	0.0		1.379120-06	-8.591610-13	0.0		-2.965690-05		
					5.400000 01	-1.326690-05					
17	3	-0.74	0.0		1.905490-06	-1.413400-12	0.0		-4.440180-05		
					6.300000 01	-1.547810-05					
18	3	-0.84	0.0		2.251730-06	-1.860420-12	0.0		-6.349150-05		
					7.200000 01	-1.768920-05					
19	3	-0.95	0.0		1.369200-06	-6.344520-13	0.0		-8.140260-05		
					8.099990 01	-1.990030-05					
20	3	0.95	0.11		-1.325230-06	-4.914730-08	0.0		-8.162750-05		
					-8.100010 01	-8.999470 00					
21	3	0.84	0.11		-2.245710-06	-9.369670-08	0.0		-6.391360-05		
					-7.199490 01	-8.999970 00					
22	3	0.74	0.11		-1.912010-06	-9.117020-08	0.0		-4.481140-05		
					-6.300000 01	-8.999970 00					
23	3	0.63	0.11		-1.386190-06	-7.711340-08	0.0		-3.000300-05		
					-5.400000 01	-8.999470 00					
24	3	0.53	0.11		-9.743970-07	-6.504620-08	0.0		-1.949200-05		
					-4.500000 01	-8.999980 00					
25	3	0.42	0.11		-6.941070-07	-5.791900-08	0.0		-1.206390-05		
					-3.600000 01	-8.999980 00					
26	3	0.32	0.11		-4.915840-07	-5.469310-08	0.0		-6.766260-06		
					-2.700000 01	-8.999980 00					
27	3	0.21	0.11		-3.211740-07	-5.360110-08	0.0		-3.121450-06		
					-1.400000 01	-8.999980 00					
28	3	0.11	0.11		-1.598720-07	-5.336160-08	0.0		-9.591390-07		
					-4.999990 00	-8.999980 00					
29	3	0.0	0.11		-5.495400-15	-5.334020-08	0.0		-2.400240-07		
					-3.059250-06	-8.999990 00					
30	3	-0.11	0.11		1.598720-07	-5.336180-08	0.0		-9.591390-07		
					4.999980 00	-8.999990 00					
31	3	-0.21	0.11		3.211740-07	-5.360130-08	0.0		-3.121450-06		
					1.400000 01	-8.999990 00					
32	3	-0.32	0.11		4.915840-07	-5.469350-08	0.0		-6.766260-06		
					2.700000 01	-8.999990 00					
33	3	-0.42	0.11		6.941070-07	-5.791960-08	0.0		-1.206390-05		
					3.600000 01	-8.999990 00					
34	3	-0.53	0.11		9.743960-07	-6.504680-08	0.0		-1.949200-05		
					4.500000 01	-9.000000 00					
35	3	-0.63	0.11		1.386190-06	-7.711400-08	0.0		-3.000310-05		
					5.400000 01	-4.000000 00					

(31)

TABLE 4-1 (Continued)

36	3	-0.74	0.11	1.412010-06	-4.117000-08	0.0	-4.481150-05
				5.300000 01	-4.000000 00		
37	3	-0.84	0.11	2.245710-06	-4.364810-08	0.0	-6.391370-05
				7.200000 01	-4.000010 00		
38	3	-0.95	0.11	1.325290-06	-4.915100-08	0.0	-8.162740-05
				8.099990 01	-4.000000 00		
39	3	0.95	0.21	-1.187490-06	-8.807820-08	0.0	-8.225700-05
				-8.100010 01	-1.400000 01		
40	3	0.84	0.21	-2.224980-06	-1.856820-07	0.0	-6.517290-05
				-7.199990 01	-1.400000 01		
41	3	0.74	0.21	-1.929230-06	-1.839810-07	0.0	-4.604780-05
				-6.300000 01	-1.800000 01		
42	3	0.63	0.21	-1.407430-06	-1.565890-07	0.0	-3.105210-05
				-5.400000 01	-1.400000 01		
43	3	0.53	0.21	-9.890480-07	-1.320480-07	0.0	-2.037670-05
				-4.500000 01	-1.400000 01		
44	3	0.42	0.21	-7.016760-07	-1.171010-07	0.0	-1.285000-05
				-3.600000 01	-1.800000 01		
45	3	0.32	0.21	-4.946000-07	-1.100570-07	0.0	-7.506830-06
				-2.700000 01	-1.800000 01		
46	3	0.21	0.21	-3.220480-07	-1.074920-07	0.0	-3.846000-06
				-1.400000 01	-1.400000 01		
47	3	0.11	0.21	-1.600200-07	-1.068220-07	0.0	-1.679210-06
				-4.999990 00	-1.400000 01		
48	3	0.0	0.21	-2.400860-14	-1.067230-07	0.0	-9.600970-07
				-7.814720-06	-1.800000 01		
49	3	-0.11	0.21	1.600200-07	-1.068220-07	0.0	-1.679210-06
				8.999980 00	-1.400000 01		
50	3	-0.21	0.21	3.220480-07	-1.074930-07	0.0	-3.846000-06
				1.400000 01	-1.400000 01		
51	3	-0.32	0.21	4.946000-07	-1.100580-07	0.0	-7.506830-06
				2.699990 01	-1.800000 01		
52	3	-0.42	0.21	7.016760-07	-1.171020-07	0.0	-1.285000-05
				3.600000 01	-1.400000 01		
53	3	-0.53	0.21	9.890440-07	-1.320490-07	0.0	-2.037670-05
				4.500000 01	-1.400000 01		
54	3	-0.63	0.21	1.407430-06	-1.565900-07	0.0	-3.105210-05
				5.400000 01	-1.400000 01		
55	3	-0.74	0.21	1.929220-06	-1.839820-07	0.0	-4.604790-05
				6.300000 01	-1.400000 01		
56	3	-0.84	0.21	2.224990-06	-1.856850-07	0.0	-6.517300-05
				7.200000 01	-1.400000 01		
57	3	-0.95	0.21	1.187560-06	-8.808810-08	0.0	-8.225680-05
				8.099990 01	-1.400000 01		
58	3	0.95	0.32	-9.371570-07	-1.042660-07	0.0	-8.314530-05
				-8.100010 01	-2.700000 01		
59	3	0.84	0.32	-2.181060-06	-2.729950-07	0.0	-6.724190-05
				-7.200000 01	-2.699990 01		
60	3	0.74	0.32	-1.954840-06	-2.796350-07	0.0	-4.813170-05
				-6.300000 01	-2.699990 01		
61	3	0.63	0.32	-1.442770-06	-2.407810-07	0.0	-3.283580-05
				-5.400000 01	-2.699990 01		
62	3	0.53	0.32	-1.014490-06	-2.031670-07	0.0	-2.188120-05
				-4.500000 01	-2.700000 01		
63	3	0.42	0.32	-7.154130-07	-1.790910-07	0.0	-1.418010-05
				-3.600010 01	-2.700000 01		
64	3	0.32	0.32	-5.004520-07	-1.670390-07	0.0	-8.752090-06
				-2.700000 01	-2.700000 01		
65	3	0.21	0.32	-3.239740-07	-1.622020-07	0.0	-5.058720-06
				-1.800000 01	-2.700000 01		
66	3	0.11	0.32	-1.504690-07	-1.606830-07	0.0	-2.883220-06
				-9.000000 00	-2.700000 01		
67	3	0.0	0.32	-5.620500-14	-1.603820-07	0.0	-2.160220-06
				-1.426640-05	-2.700000 01		
68	3	-0.11	0.32	1.604690-07	-1.606830-07	0.0	-2.883220-06
				8.999970 00	-2.700000 01		
69	3	-0.21	0.32	3.239740-07	-1.622030-07	0.0	-5.058720-06
				1.400000 01	-2.700000 01		
70	3	-0.32	0.32	5.004520-07	-1.670400-07	0.0	-8.752080-06
				2.699990 01	-2.700000 01		
71	3	-0.42	0.32	7.154130-07	-1.790920-07	0.0	-1.418010-05
				3.600000 01	-2.700000 01		
72	3	-0.53	0.32	1.014490-06	-2.031680-07	0.0	-2.188120-05
				4.500000 01	-2.700000 01		
73	3	-0.63	0.32	1.442760-06	-2.407820-07	0.0	-3.283580-05
				5.400000 01	-2.700000 01		
74	3	-0.74	0.32	1.954840-06	-2.796370-07	0.0	-4.813180-05
				6.300000 01	-2.700000 01		
75	3	-0.84	0.32	2.181070-06	-2.729990-07	0.0	-6.724200-05
				7.200000 01	-2.700000 01		
76	3	-0.95	0.32	9.372430-07	-1.042770-07	0.0	-8.314520-05
				8.099980 01	-2.700000 01		

(32)

TABLE 4-1 (Continued)

77	3	0.84	0.42	-2.094250-06	-3.501750-07	0.0	-7.005690-05
				-7.200000 01	-3.400000 01		
78	3	0.74	0.42	-1.943230-06	-3.782620-07	0.0	-5.109040-05
				-4.300000 01	-3.600000 01		
79	3	.53	0.42	-1.491550-06	-3.314980-07	0.0	-3.540700-05
				-5.400000 01	-3.600000 01		
80	3	0.53	0.42	-1.052010-06	-2.404100-07	0.0	-2.405360-05
				-4.500000 01	-3.400000 01		
81	3	0.42	0.42	-7.369410-07	-2.459740-07	0.0	-1.608830-05
				-3.500010 01	-3.500000 01		
82	3	0.32	0.42	-5.104200-07	-2.271560-07	0.0	-1.052290-05
				-2.700000 01	-3.400000 01		
83	3	0.21	0.42	-3.277360-07	-2.187820-07	0.0	-6.771140-06
				-1.500000 01	-3.400000 01		
84	3	0.11	0.42	-1.615670-07	-2.157100-07	0.0	-4.575680-06
				-3.000010 00	-3.400000 01		
85	3	0.0	0.42	-1.042080-13	-2.149890-07	0.0	-3.849880-06
				-2.242780-05	-3.600000 01		
86	3	-0.11	0.42	1.615670-07	-2.157110-07	0.0	-4.575680-06
				8.999960 00	-3.600000 01		
87	3	-0.21	0.42	3.277360-07	-2.187820-07	0.0	-6.771180-06
				1.799990 01	-3.600000 01		
88	3	-0.32	0.42	5.104200-07	-2.271560-07	0.0	-1.052290-05
				2.699990 01	-3.600000 01		
89	3	-0.42	0.42	7.369400-07	-2.459740-07	0.0	-1.608830-05
				3.600000 01	-3.600000 01		
90	3	-0.53	0.42	1.052010-06	-2.409110-07	0.0	-2.405350-05
				4.500000 01	-3.600000 01		
91	3	-0.63	0.42	1.491550-06	-3.318990-07	0.0	-3.540700-05
				5.400000 01	-3.600000 01		
92	3	-0.74	0.42	1.943230-06	-3.782640-07	0.0	-5.109050-05
				6.300000 01	-3.600010 01		
93	3	-0.84	0.42	2.098270-06	-3.501810-07	0.0	-7.005690-05
				7.200000 01	-3.600010 01		
94	3	0.84	0.53	-1.951180-06	-4.070360-07	0.0	-7.348500-05
				-7.200000 01	-4.500000 01		
95	3	0.74	0.53	-2.004340-06	-4.778600-07	0.0	-5.494380-05
				-6.300000 01	-4.500000 01		
96	3	0.63	0.53	-1.551640-06	-4.315840-07	0.0	-3.883590-05
				-5.400000 01	-4.500000 01		
97	3	0.53	0.53	-1.102820-06	-3.480970-07	0.0	-2.696590-05
				-4.500000 01	-4.500000 01		
98	3	0.42	0.53	-7.683320-07	-3.205640-07	0.0	-1.863070-05
				-3.600010 01	-4.500000 01		
99	3	0.32	0.53	-5.263110-07	-2.927840-07	0.0	-1.285730-05
				-2.700000 01	-4.500000 01		
100	3	0.21	0.53	-3.345170-07	-2.791360-07	0.0	-9.008010-06
				-1.400000 01	-4.500000 01		
101	3	0.11	0.53	-1.638720-07	-2.734840-07	0.0	-6.774140-06
				-4.000020 00	-4.500000 01		
102	3	0.0	0.53	-1.710300-13	-2.720880-07	0.0	-6.038750-06
				-3.231240-05	-4.500000 01		
103	3	-0.11	0.53	1.638710-07	-2.734840-07	0.0	-6.774140-06
				8.999950 00	-4.500000 01		
104	3	-0.21	0.53	3.345170-07	-2.791360-07	0.0	-9.008000-06
				1.799990 01	-4.500000 01		
105	3	-0.32	0.53	5.263100-07	-2.927850-07	0.0	-1.285730-05
				2.699990 01	-4.500000 01		
106	3	-0.42	0.53	7.683310-07	-3.205650-07	0.0	-1.863060-05
				3.600000 01	-4.500000 01		
107	3	-0.53	0.53	1.102820-06	-3.480980-07	0.0	-2.696590-05
				4.500000 01	-4.500000 01		
108	3	-0.63	0.53	1.551630-06	-4.315850-07	0.0	-3.883580-05
				5.400000 01	-4.500000 01		
109	3	-0.74	0.53	2.004340-06	-4.778620-07	0.0	-5.494380-05
				6.300000 01	-4.500000 01		
110	3	-0.84	0.53	1.951200-06	-4.070450-07	0.0	-7.348500-05
				7.200000 01	-4.500000 01		
111	3	0.74	0.63	-2.001240-06	-5.725430-07	0.0	-5.967780-05
				-5.300000 01	-5.400000 01		
112	3	0.63	0.63	-1.617860-06	-5.400050-07	0.0	-4.320200-05
				-5.400000 01	-5.400000 01		
113	3	0.53	0.63	-1.167220-06	-4.675080-07	0.0	-3.071610-05
				-4.500010 01	-5.400000 01		
114	3	0.42	0.63	-8.117410-07	-4.064100-07	0.0	-2.189220-05
				-3.600010 01	-5.400000 01		
115	3	0.32	0.63	-5.503450-07	-3.673850-07	0.0	-1.581980-05
				-2.700000 01	-5.400000 01		
116	3	0.21	0.63	-3.459050-07	-3.463660-07	0.0	-1.181610-05
				-1.400000 01	-5.400000 01		
117	3	0.11	0.63	-1.681720-07	-3.367910-07	0.0	-9.514830-06
				-9.000030 00	-5.400000 01		

(33)

TABLE 4-1 (Continued)

118	3	0.0	0.63	-7.654680-13	-1.341100-07	0.0	-8.761110-06
				-6.346370-05	-7.400000 01		
119	3	-0.11	0.73	1.281710-07	-1.367910-07	0.0	-9.514820-06
				1.449440 00	-7.400000 01		
120	3	-0.21	0.83	3.454030-07	-3.463660-07	0.0	-1.181610-05
				1.799900 01	-5.400000 01		
121	3	-0.32	0.63	5.503440-07	-3.673860-07	0.0	-1.561980-05
				2.499440 01	-7.400000 01		
122	3	-0.42	0.63	4.117390-07	-4.064110-07	0.0	-2.189210-05
				1.500000 01	-5.400000 01		
123	3	-0.53	0.63	1.167210-06	-4.675090-07	0.0	-3.071600-05
				4.500000 01	-7.400000 01		
124	3	-0.63	0.63	1.617860-06	-7.400000-07	0.0	-4.320200-05
				5.400000 01	-7.400000 01		
125	3	-0.74	0.63	2.001240-06	-5.725470-07	0.0	-5.967780-05
				6.300000 01	-5.400000 01		
126	3	0.63	0.74	-1.679740-06	-6.541020-07	0.0	-4.857360-05
				-5.400000 01	-6.300000 01		
127	3	0.53	0.74	-1.243210-06	-5.809380-07	0.0	-3.542340-05
				-4.500000 01	-7.300000 01		
128	3	0.42	0.74	-3.686650-07	-5.073950-07	0.0	-2.599150-05
				-3.600010 01	-6.300000 01		
129	3	0.32	0.74	-5.848220-07	-4.554670-07	0.0	-1.951070-05
				-2.700000 01	-6.300000 01		
130	3	0.21	0.74	-3.537700-07	-4.249630-07	0.0	-1.527660-05
				-1.800000 01	-6.300000 01		
131	3	0.11	0.74	-1.754580-07	-4.099470-07	0.0	-1.286580-05
				-4.000040 00	-7.300000 01		
132	3	0.0	0.74	-4.021510-13	-4.055250-07	0.0	-1.208050-05
				-5.748650-05	-6.300000 01		
133	3	-0.11	0.74	1.754570-07	-4.099470-07	0.0	-1.286570-05
				4.999430 00	-6.300000 01		
134	3	-0.21	0.74	3.637690-07	-4.249640-07	0.0	-1.527660-05
				1.749990 01	-6.300000 01		
135	3	-0.32	0.74	5.848200-07	-4.554670-07	0.0	-1.951060-05
				2.699990 01	-6.300000 01		
136	3	-0.42	0.74	8.686620-07	-5.073950-07	0.0	-2.599150-05
				3.800000 01	-6.300000 01		
137	3	-0.53	0.74	1.243210-06	-5.809380-07	0.0	-3.542330-05
				4.500000 01	-6.300000 01		
138	3	-0.63	0.74	1.679740-06	-6.541040-07	0.0	-4.857350-05
				5.400000 01	-6.300000 01		
139	3	0.53	0.84	-1.324390-06	-7.072790-07	0.0	-4.121230-05
				-4.500010 01	-7.200000 01		
140	3	0.42	0.84	-9.386660-07	-6.266080-07	0.0	-3.108020-05
				-3.600010 01	-7.200000 01		
141	3	0.32	0.84	-5.314170-07	-5.620060-07	0.0	-2.407370-05
				-2.700000 01	-7.200000 01		
142	3	0.21	0.84	-3.899200-07	-5.205850-07	0.0	-1.951650-05
				-1.800000 01	-7.200000 01		
143	3	0.11	0.84	-1.867400-07	-4.987690-07	0.0	-1.644080-05
				-4.000060 00	-7.200000 01		
144	3	0.0	0.84	-6.050540-13	-4.920860-07	0.0	-1.610590-05
				-7.301470-05	-7.200000 01		
145	3	-0.11	0.84	1.467840-07	-4.987690-07	0.0	-1.644080-05
				4.999410 00	-7.200000 01		
146	3	-0.21	0.84	3.899180-07	-5.205850-07	0.0	-1.951650-05
				1.799440 01	-7.200000 01		
147	3	-0.32	0.84	6.314150-07	-5.620070-07	0.0	-2.407360-05
				2.699990 01	-7.200000 01		
148	3	-0.42	0.84	9.386620-07	-6.266090-07	0.0	-3.108020-05
				3.500000 01	-7.200000 01		
149	3	-0.53	0.84	1.324380-06	-7.072800-07	0.0	-4.121220-05
				4.500000 01	-7.200000 01		
150	3	0.32	0.95	-6.899430-07	-6.948600-07	0.0	-2.969410-05
				-2.700000 01	-8.100000 01		
151	3	0.21	0.95	-4.254210-07	-6.369790-07	0.0	-2.471560-05
				-1.800010 01	-8.100000 01		
152	3	0.11	0.95	-2.029480-07	-6.098020-07	0.0	-2.191030-05
				-9.000080 00	-8.100000 01		
153	3	0.0	0.95	-9.095500-13	-5.005450-07	0.0	-2.100380-05
				-9.040360-05	-8.100000 01		
154	3	-0.11	0.95	2.029460-07	-6.098020-07	0.0	-2.191030-05
				4.499400 00	-8.100000 01		
155	3	-0.21	0.95	4.254180-07	-6.369800-07	0.0	(34) -2.471560-05
				1.799440 01	-8.100000 01		
156	3	-0.32	0.95	6.849340-07	-6.948600-07	0.0	-2.969410-05
				2.499440 01	-8.100000 01		

TABLE 4-2

RAY TRACE PRINTOUT OF THERMALLY DISTORTED HCR - HYPOTHETICAL CASE 2

CUHF  
CYCLE 0  
CULO 0

10:12:56-----01/17/75

1	MAY CLP	U.U	Z	0.0	0.0	U.IST	YS	DEL Y
10	3	0.0	0.0	-1.76540-13	-1.43600-06	1.43600-06	-1.26680-06	-2.52850-06
				U.U	0.0			
				Y*	Z*		DEL	UPD
1	3	0.95	0.0	-3.422720-06	3.377080-13	0.0		-2.035070-04
				-8.100020 01	1.990000-05			
2	3	0.84	0.0	-5.629300-06	-4.385290-12	0.0		-1.587280-04
				-7.199990 01	1.768920-05			
3	3	0.74	0.0	-4.764990-06	-6.773760-12	0.0		-1.110040-04
				-6.299990 01	1.547800-05			
4	3	0.63	0.0	-3.447810-06	-3.214270-12	0.0		-7.414230-05
				-5.400000 01	1.326690-05			
5	3	0.53	0.0	-2.424060-06	-1.123480-12	0.0		-4.800000-05
				-4.500000 01	1.105570-05			
6	3	0.42	0.0	-1.729240-06	-2.331910-13	0.0		-2.950930-05
				-3.800000 01	8.844590-06			
7	3	0.32	0.0	-1.226650-06	6.586290-14	0.0		-1.630090-05
				-2.700000 01	6.633430-06			
8	3	0.21	0.0	-8.023370-07	1.325990-13	0.0		-7.200850-06
				-1.800000 01	4.427290-06			
9	3	0.11	0.0	-3.996040-07	1.005720-13	0.0		-1.797790-06
				-4.999990 00	2.211150-06			
10	3	0.0	0.0	0.0	0.0	0.0		0.0
				0.0	0.0			
11	3	-0.11	0.0	3.996040-07	-1.654780-13	0.0		-1.797790-06
				8.999990 00	-2.211150-06			
12	3	-0.21	0.0	8.023370-07	-3.991260-13	0.0		-7.200840-06
				1.800000 01	-4.427290-06			
13	3	-0.32	0.0	1.226650-06	-7.236170-13	0.0		-1.630090-05
				2.899990 01	-6.633440-06			
14	3	-0.42	0.0	1.729240-06	-1.257060-12	0.0		-2.950920-05
				3.600000 01	-4.844610-06			
15	3	-0.53	0.0	2.424060-06	-2.307300-12	0.0		-4.800000-05
				4.500000 01	-1.105570-05			
16	3	-0.63	0.0	3.447810-06	-4.445880-12	0.0		-7.414230-05
				5.400000 01	-1.326690-05			
17	3	-0.74	0.0	4.764990-06	-7.950990-12	0.0		-1.110050-04
				6.300010 01	-1.747810-05			
18	3	-0.84	0.0	5.629300-06	-1.064080-11	0.0		-1.587290-04
				7.200010 01	-1.768920-05			
19	3	-0.95	0.0	3.423110-06	-2.122200-12	0.0		-2.035060-04
				8.099980 01	-1.490010-05			
20	3	0.95	0.11	-3.312930-06	-1.228630-07	0.0		-2.040690-04
				-4.100020 01	-4.999980 00			
21	3	0.84	0.11	-5.614250-06	-2.342460-07	0.0		-1.597840-04
				-7.199990 01	-8.999970 00			
22	3	0.74	0.11	-4.780040-06	-2.279290-07	0.0		-1.120280-04
				-6.299990 01	-8.999970 00			
23	3	0.63	0.11	-3.465490-06	-1.927860-07	0.0		-7.500760-05
				-5.400000 01	-4.999970 00			
24	3	0.53	0.11	-2.436000-06	-1.626160-07	0.0		-4.873000-05
				-4.500000 01	-8.999980 00			
25	3	0.42	0.11	-1.735270-06	-1.447980-07	0.0		-3.015970-05
				-3.800010 01	-8.999980 00			
26	3	0.32	0.11	-1.228960-06	-1.367330-07	0.0		-1.691560-05
				-2.700000 01	-4.999980 00			
27	3	0.21	0.11	-8.029480-07	-1.340030-07	0.0		-7.803630-06
				-1.800000 01	-4.999980 00			
28	3	0.11	0.11	-3.996040-07	-1.334040-07	0.0		-2.397850-06
				-4.999990 00	-4.999990 00			
29	3	0.0	0.11	-3.831860-14	-1.333510-07	0.0		-6.000610-07
				-4.331410-06	-4.999990 00			
30	3	-0.11	0.11	3.996040-07	-1.334040-07	0.0		-2.397850-06
				8.999980 00	8.999990 00			
31	3	-0.21	0.11	8.029480-07	-1.340030-07	0.0		-7.803620-06
				1.800000 01	-4.999990 00			
32	3	-0.32	0.11	1.228960-06	-1.367340-07	0.0		-1.691560-05
				2.899990 01	-4.999990 00			
33	3	-0.42	0.11	1.735270-06	-1.448000-07	0.0		-3.015970-05
				3.800000 01	-4.999990 00			
34	3	-0.53	0.11	2.435990-06	-1.626180-07	0.0		-4.873000-05
				4.500000 01	-4.000000 00			
35	3	-0.63	0.11	3.465470-06	-1.927880-07	0.0		-7.500770-05
				5.400000 01	-4.000000 00			

(36)

TABLE 4-2 (Continued)

36	3	-0.74	0.11	4.700020-06 4.000010 01	-2.279320-07 -4.000000 00	0.0	-1.120290-04
37	1	-0.44	0.11	5.414290-06 7.000010 01	-2.342530-07 -4.000010 00	0.0	-1.597850-04
38	1	-0.95	0.11	3.313340-06 8.099970 01	-1.228820-07 -9.000000 00	0.0	-2.040680-04
39	1	0.95	0.21	-2.468560-06 -4.100020 01	-2.201820-07 -1.400000 01	0.0	-2.056430-04
40	3	0.84	0.21	-5.562430-06 -7.149990 01	-4.641580-07 -1.799990 01	0.0	-1.629320-04
41	3	0.74	0.21	-4.423080-06 -6.799990 01	-4.549560-07 -1.400000 01	0.0	-1.151200-04
42	3	0.63	0.21	-3.518580-06 -5.400000 01	-3.914750-07 -1.400000 01	0.0	-7.763020-05
43	3	0.53	0.21	-2.472620-06 -4.500000 01	-3.301210-07 -1.400000 01	0.0	-5.094170-05
44	3	0.42	0.21	-1.754190-06 -3.600010 01	-2.427530-07 -1.400000 01	0.0	-3.212500-05
45	3	0.32	0.21	-1.736500-06 -2.700000 01	-2.751430-07 -1.400000 01	0.0	-1.876710-05
46	3	0.21	0.21	-8.051210-07 -1.400000 01	-2.687300-07 -1.400000 01	0.0	-9.615020-06
47	3	0.11	0.21	-4.000500-07 -9.000000 00	-2.670550-07 -1.400000 01	0.0	-4.198030-06
48	3	0.0	0.21	-1.543870-13 -1.240340-05	-2.668090-07 -1.400000 01	0.0	-2.400240-06
49	3	-0.11	0.21	4.000500-07 4.999970 00	-2.670550-07 -1.400000 01	0.0	-4.198030-06
50	3	-0.21	0.21	8.051200-07 1.400000 01	-2.687320-07 -1.400000 01	0.0	-9.615010-06
51	3	-0.32	0.21	1.236500-06 2.499990 01	-2.751450-07 -1.400000 01	0.0	-1.876710-05
52	3	-0.42	0.21	1.754190-06 3.600000 01	-2.427560-07 -1.400000 01	0.0	-3.212500-05
53	3	-0.53	0.21	2.472610-06 4.500000 01	-3.301230-07 -1.400000 01	0.0	-5.094170-05
54	3	-0.63	0.21	3.518560-06 5.400000 01	-3.914780-07 -1.400000 01	0.0	-7.763020-05
55	3	-0.74	0.21	4.423060-06 4.300010 01	-4.549610-07 -1.400000 01	0.0	-1.151200-04
56	3	-0.84	0.21	5.562480-06 7.200010 01	-4.641700-07 -1.400000 01	0.0	-1.629330-04
57	3	-0.95	0.21	2.964000-06 4.099970 01	-2.202200-07 -1.400000 01	0.0	-2.056420-04
58	3	0.95	0.32	-2.342690-06 -4.100030 01	-2.403340-07 -2.700000 01	0.0	-2.078030-04
59	3	0.84	0.32	-3.452620-06 -7.149990 01	-6.424840-07 -2.544440 01	0.0	-1.681050-04
60	3	0.74	0.32	-4.427120-06 -6.244440 01	-6.990910-07 -2.699990 01	0.0	-1.203240-04
61	3	0.63	0.32	-3.406920-06 -5.400000 01	-6.019540-07 -2.699990 01	0.0	-8.208460-05
62	3	0.53	0.32	-2.536220-06 -4.500000 01	-5.079190-07 -2.700000 01	0.0	-5.470300-05
63	3	0.42	0.32	-1.788530-06 -3.600010 01	-4.477270-07 -2.700000 01	0.0	-3.545020-05
64	3	0.32	0.32	-1.251130-06 -2.700000 01	-4.175980-07 -2.700000 01	0.0	-2.188020-05
65	3	0.21	0.32	-8.099350-07 -1.400000 01	-4.055060-07 -2.700000 01	0.0	-1.264680-05
66	3	0.11	0.32	-4.011730-07 -9.000010 00	-4.017060-07 -2.700000 01	0.0	-7.208060-06
67	3	0.0	0.32	-3.623070-13 -2.572150-05	-4.009540-07 -2.700000 01	0.0	-5.404370-06
68	3	-0.11	0.32	4.011720-07 8.999960 00	-4.017070-07 -2.700000 01	0.0	-7.208060-06
69	3	-0.21	0.32	4.099340-07 1.799990 01	-4.055070-07 -2.700000 01	0.0	-1.264680-05
70	3	-0.32	0.32	1.251130-06 2.499990 01	-4.176010-07 -2.700000 01	0.0	-2.188020-05
71	3	-0.42	0.32	1.788530-06 3.600000 01	-4.477300-07 -2.700000 01	0.0	-3.545020-05
72	3	-0.53	0.32	2.536210-06 4.500000 01	-5.079220-07 -2.700000 01	0.0	-5.470290-05
73	3	-0.63	0.32	3.506400-06 5.400000 01	-6.019580-07 -2.700000 01	0.0	-8.208460-05
74	3	-0.74	0.32	4.427100-06 4.300010 01	-4.549980-07 -2.700000 01	0.0	-1.203300-04
75	3	-0.84	0.32	5.562490-06 7.200000 01	-4.642080-07 -2.700000 01	0.0	-1.681050-04
76	3	-0.95	0.32	2.963200-06 4.099960 01	-2.407020-07 -2.499990 01	0.0	-2.078030-04

(37)

TABLE 4-2 (Continued)

77	3	0.84	0.42	-5.245000-06	-4.754320-07	0.0	-1.751420-04
				-7.200000 01	-4.400000 01		
78	3	1.74	0.42	-4.458000-06	-4.436570-07	0.0	-1.277260-04
				-5.249000 01	-4.400000 01		
79	3	0.63	0.42	-3.728400-06	-4.247460-07	0.0	-6.851750-05
				-5.400000 01	-4.400000 01		
80	3	0.53	0.42	-2.430040-06	-7.022760-07	0.0	-6.013400-05
				-4.500010 01	-3.400000 01		
81	3	0.42	0.42	-1.442350-06	-6.144340-07	0.0	-4.022070-05
				-3.500010 01	-3.400000 01		
82	3	0.32	0.42	-1.276050-06	-5.678840-07	0.0	-2.630720-05
				-2.700000 01	-3.600000 01		
83	3	0.21	0.42	-8.143400-07	-5.469540-07	0.0	-1.692800-05
				-1.400000 01	-3.400000 01		
84	3	0.11	0.42	-4.039190-07	-5.392760-07	0.0	-1.143920-05
				-4.000030 00	-3.600000 01		
85	3	0.0	0.42	-6.560170-13	-5.374720-07	0.0	-9.624710-06
				-4.280250-05	-3.600000 01		
86	3	-0.11	0.42	4.039180-07	-5.392770-07	0.0	-1.143920-05
				8.999440 00	-3.500000 01		
87	3	-0.21	0.42	8.193390-07	-5.469560-07	0.0	-1.692800-05
				1.799990 01	-3.600000 01		
88	3	-0.32	0.42	1.276050-06	-5.673920-07	0.0	-2.630720-05
				2.699990 01	-3.400000 01		
89	3	-0.42	0.42	1.442350-06	-6.149370-07	0.0	-4.022060-05
				3.400000 01	-3.600000 01		
90	3	-0.53	0.42	2.630030-06	-7.022800-07	0.0	-6.013390-05
				4.500000 01	-3.600000 01		
91	3	-0.63	0.42	3.728870-06	-4.247510-07	0.0	-6.851750-05
				5.400000 01	-3.600000 01		
92	3	-0.74	0.42	4.458070-06	-4.436670-07	0.0	-1.277260-04
				6.300000 01	-3.600010 01		
93	3	-0.84	0.42	5.245700-06	-4.754630-07	0.0	-1.751420-04
				7.200000 01	-3.600010 01		
94	3	0.84	0.53	-4.877680-06	-1.017580-06	0.0	-1.837130-04
				-7.200000 01	-4.400000 01		
95	3	0.74	0.53	-5.010870-06	-1.194650-06	0.0	-1.373600-04
				-5.400000 01	-4.500000 01		
96	3	0.63	0.53	-3.879110-06	-1.078960-06	0.0	-9.708980-05
				-5.400000 01	-4.500000 01		
97	3	0.53	0.53	-2.757070-06	-4.202430-07	0.0	-6.741490-05
				-4.500010 01	-4.500000 01		
98	3	0.42	0.53	-1.920640-06	-4.014100-07	0.0	-4.657670-05
				-3.400010 01	-4.500000 01		
99	3	0.32	0.53	-1.317780-06	-7.114660-07	0.0	-3.214340-05
				-2.700000 01	-4.400000 01		
100	3	0.21	0.53	-4.367460-07	-7.476380-07	0.0	-2.252000-05
				-1.400000 01	-4.500000 01		
101	3	0.11	0.53	-4.046400-07	-6.837080-07	0.0	-1.693530-05
				-4.000050 00	-4.500000 01		
102	3	0.0	0.53	-1.057060-12	-4.400200-07	0.0	-1.509690-05
				-6.414720-05	-4.500000 01		
103	3	-0.11	0.53	4.046780-07	-6.837090-07	0.0	-1.693530-05
				4.499420 00	-4.500000 01		
104	3	-0.21	0.53	8.362410-07	-5.978400-07	0.0	-2.252000-05
				1.799990 01	-4.500000 01		
105	3	-0.32	0.53	1.315780-06	-7.319630-07	0.0	-3.214330-05
				2.699990 01	-4.500000 01		
106	3	-0.42	0.53	1.442350-06	-6.144140-07	0.0	-4.657660-05
				3.600000 01	-4.500000 01		
107	3	-0.53	0.53	2.757050-06	-4.202470-07	0.0	-6.741470-05
				4.500010 01	-4.500000 01		
108	3	-0.63	0.53	3.879090-06	-1.078970-06	0.0	-9.708970-05
				5.400000 01	-4.500000 01		
109	3	-0.74	0.53	5.010850-06	-1.194660-06	0.0	-1.373600-04
				6.300000 01	-4.500010 01		
110	3	-0.84	0.53	4.878030-06	-1.017620-06	0.0	-1.837130-04
				7.199990 01	-4.500000 01		
111	3	0.74	0.63	-5.003090-06	-1.431350-06	0.0	-1.491950-04
				-6.400000 01	-5.400000 01		
112	3	0.63	0.63	-4.044680-06	-1.330010-06	0.0	-1.080050-04
				-5.400000 01	-5.400000 01		
113	3	0.53	0.63	-2.718660-06	-1.163770-06	0.0	-7.679030-05
				-4.500010 01	-4.400000 01		
114	3	0.42	0.63	-2.024360-06	-1.014620-06	0.0	-5.473050-05
				-3.400010 01	-4.400000 01		
115	3	0.32	0.63	-1.375870-06	-7.184620-07	0.0	(38) -3.954960-05
				-2.700010 01	-5.400000 01		
116	3	0.21	0.63	-8.647650-07	-4.659140-07	0.0	-2.954030-05
				-1.400010 01	-5.400000 01		
117	3	0.11	0.63	-4.204300-07	-4.414760-07	0.0	-2.378710-05
				-9.000080 00	-5.400000 01		

TABLE 4-2 (Continued)

118	3	0.0	0.63	-1.601020-12	-8.352750-07	0.0	-2.190280-05
				-3.002130-05	-5.400000 01		
119	3	-0.11	0.63	4.204270-07	-2.414770-07	0.0	-2.378700-05
				4.399900 00	-7.400000 01		
120	3	-0.21	0.63	4.447010-07	-7.554100-07	0.0	-2.454420-05
				1.799990 01	-5.400000 01		
121	3	-0.32	0.63	1.375860-06	-7.184650-07	0.0	-3.954440-05
				2.699990 01	-5.400000 01		
122	3	-0.42	0.63	2.029350-06	-1.016030-06	0.0	-5.473030-05
				3.599990 01	-5.400000 01		
123	3	-0.53	0.63	2.918040-06	-1.164780-06	0.0	-7.679010-05
				4.499990 01	-5.400000 01		
124	3	-0.63	0.63	4.044650-06	-1.350020-06	0.0	-1.080050-04
				5.400000 01	-7.400000 01		
125	3	-0.74	0.63	5.003100-06	-1.431380-06	0.0	-1.491950-04
				6.300000 01	-5.400000 01		
126	3	0.63	0.74	-4.199380-06	-1.634260-06	0.0	-1.214340-04
				-5.400010 01	-5.300000 01		
127	3	0.53	0.74	-3.108050-06	-1.452340-06	0.0	-8.855670-05
				-4.500010 01	-6.300000 01		
128	3	0.42	0.74	-2.171670-06	-1.268490-06	0.0	-6.497900-05
				-3.600020 01	-6.300000 01		
129	3	0.32	0.74	-1.462060-06	-1.138670-06	0.0	-4.877670-05
				-2.700010 01	-6.300000 01		
130	3	0.21	0.74	-9.044290-07	-1.062410-06	0.0	-3.819140-05
				-1.400010 01	-6.300000 01		
131	3	0.11	0.74	-4.386470-07	-1.024870-06	0.0	-3.216440-05
				-9.000110 00	-6.300000 01		
132	3	0.0	0.74	-2.358630-12	-1.013810-06	0.0	-3.020120-05
				-1.204990-04	-6.300000 01		
133	3	-0.11	0.74	4.386420-07	-1.024870-06	0.0	-3.216430-05
				8.999860 00	-6.300000 01		
134	3	-0.21	0.74	9.094220-07	-1.062410-06	0.0	-3.819130-05
				1.799980 01	-5.300000 01		
135	3	-0.32	0.74	1.462050-06	-1.138670-06	0.0	-4.877650-05
				2.699980 01	-6.300000 01		
136	3	-0.42	0.74	2.171660-06	-1.268490-06	0.0	-6.497870-05
				3.599990 01	-6.300000 01		
137	3	-0.53	0.74	3.108020-06	-1.452350-06	0.0	-8.855640-05
				4.499990 01	-6.300000 01		
138	3	-0.63	0.74	4.199350-06	-1.635270-06	0.0	-1.214340-04
				5.399990 01	-6.300000 01		
139	3	0.53	0.84	-3.310990-06	-1.768200-06	0.0	-1.030310-04
				-4.500010 01	-7.200000 01		
140	3	0.42	0.84	-2.346680-06	-1.566520-06	0.0	-7.770080-05
				-3.400020 01	-7.200000 01		
141	3	0.32	0.84	-1.578550-06	-1.405020-06	0.0	-6.018430-05
				-2.700010 01	-7.200000 01		
142	3	0.21	0.84	-9.748040-07	-1.301460-06	0.0	-4.879130-05
				-1.400010 01	-7.200000 01		
143	3	0.11	0.84	-4.669780-07	-1.246920-06	0.0	-4.235190-05
				-9.000140 00	-7.200000 01		
144	3	0.0	0.84	-3.445190-12	-1.230210-06	0.0	-4.026470-05
				-1.560150-04	-7.200000 01		
145	3	-0.11	0.84	4.669710-07	-1.246920-06	0.0	-4.235190-05
				8.999830 00	-7.200000 01		
146	3	-0.21	0.84	9.747950-07	-1.301460-06	0.0	-4.879110-05
				1.799980 01	-7.200000 01		
147	3	-0.32	0.84	1.578540-06	-1.405020-06	0.0	-6.018400-05
				2.699980 01	-7.200000 01		
148	3	-0.42	0.84	2.346660-06	-1.566520-06	0.0	-7.770040-05
				3.599990 01	-7.200000 01		
149	3	-0.53	0.84	3.310960-06	-1.768200-06	0.0	-1.030310-04
				4.499990 01	-7.200000 01		
150	3	0.32	0.95	-1.724870-06	-1.727150-06	0.0	-7.423540-05
				-2.700020 01	-8.100000 01		
151	3	0.21	0.95	-1.063560-06	-1.597450-06	0.0	-6.178910-05
				-1.400020 01	-7.100000 01		
152	3	0.11	0.95	-5.074980-07	-1.524500-06	0.0	-5.477580-05
				-9.000180 00	-7.100000 01		
153	3	0.0	0.95	-5.035940-12	-1.501360-06	0.0	-5.250950-05
				-1.971580-04	-7.100000 01		
154	3	-0.11	0.95	5.074880-07	-1.524500-06	0.0	-5.477570-05
				8.499790 00	-7.100000 01		
155	3	-0.21	0.95	1.063540-06	-1.597450-06	0.0	-6.178690-05
				1.799980 01	-7.100000 01		
156	3	-0.32	0.95	1.724850-06	-1.727150-06	0.0	-7.423510-05
				2.699980 01	-8.100000 01		

(39)

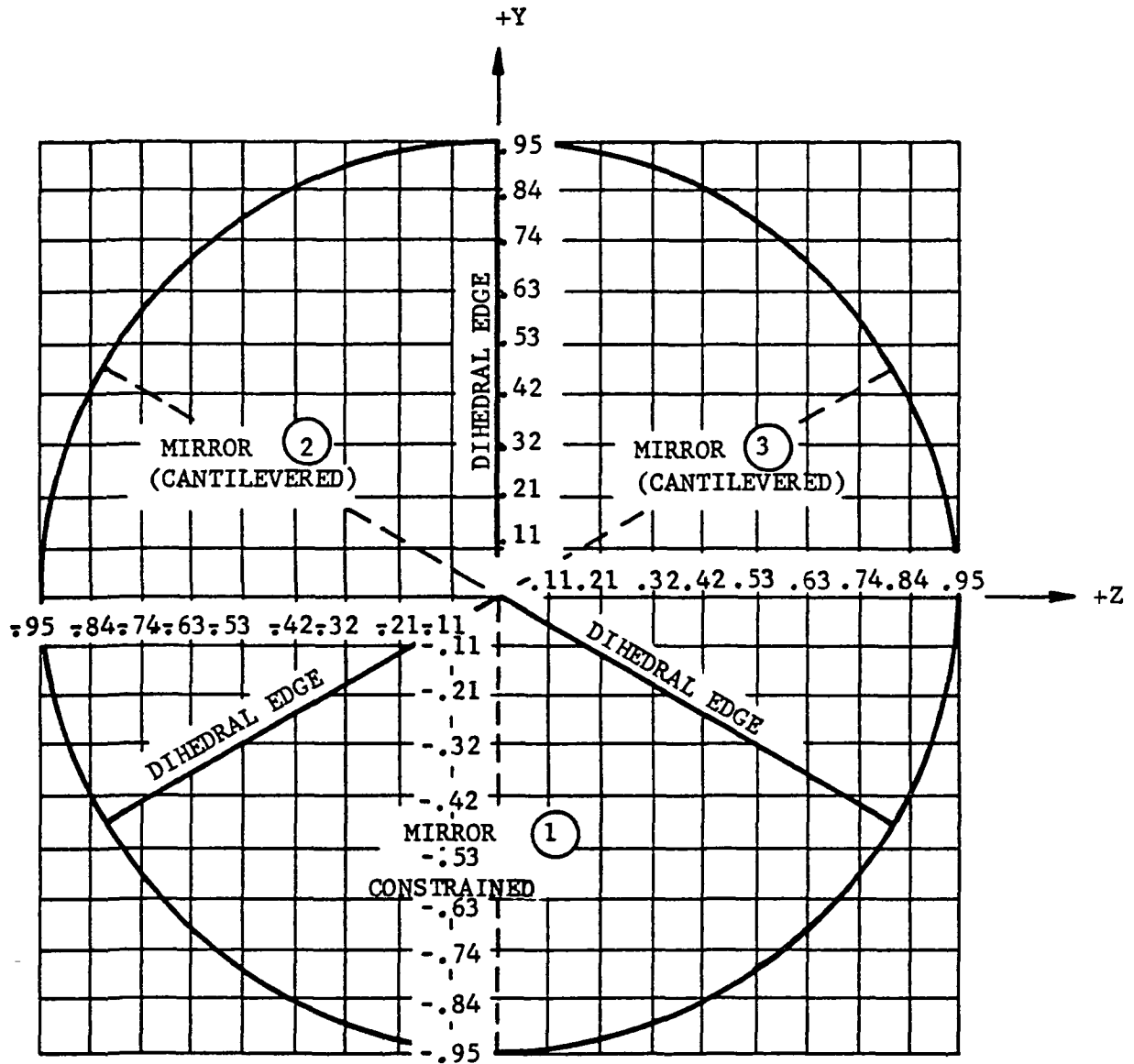


Figure 4-1. Coordinate System for HCR Wavefront Distortion Analysis

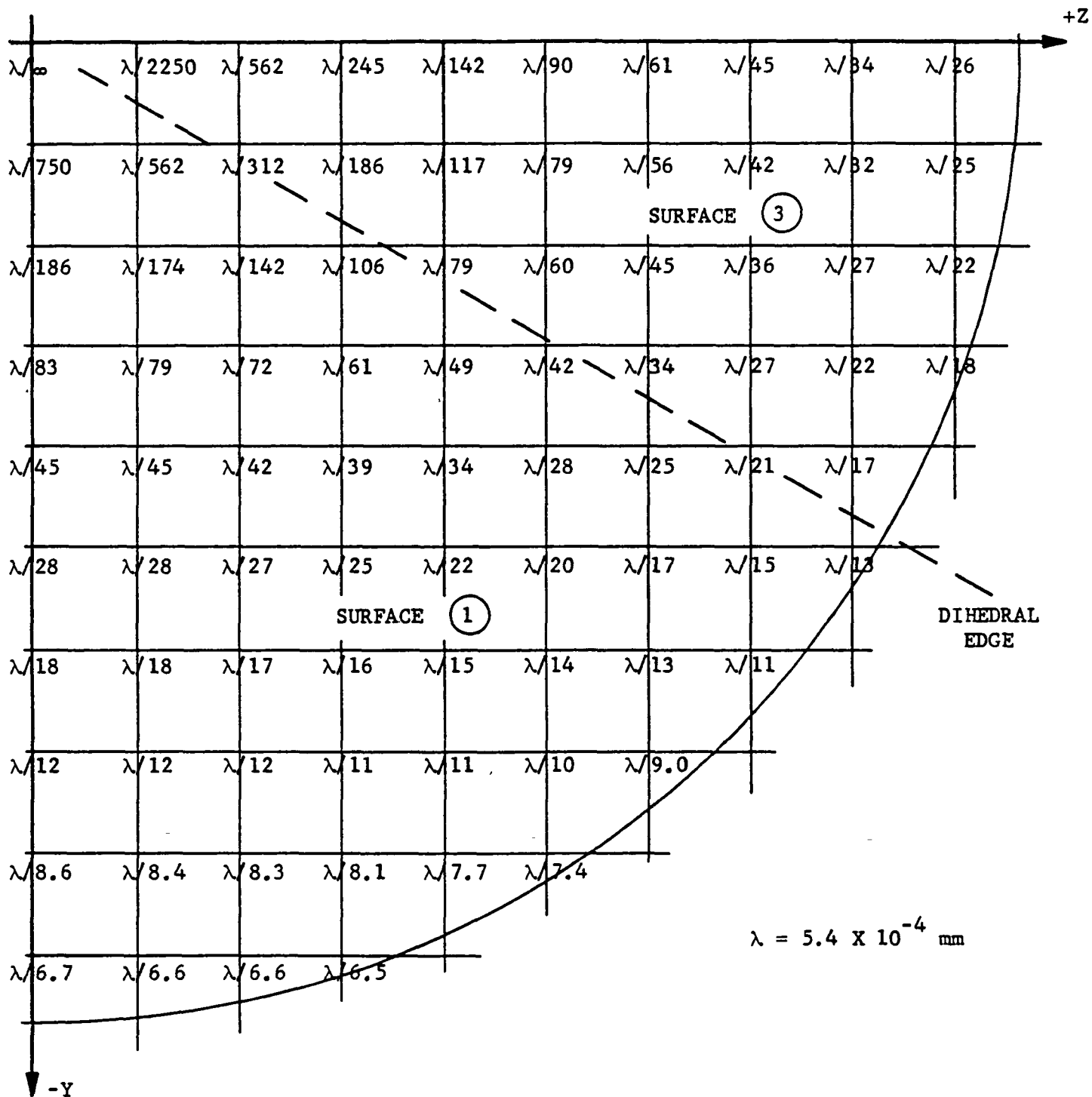


Figure 4-2A. OPD Map of Lower Right Quadrant of HCR Aperture - Hypothetical Case 1

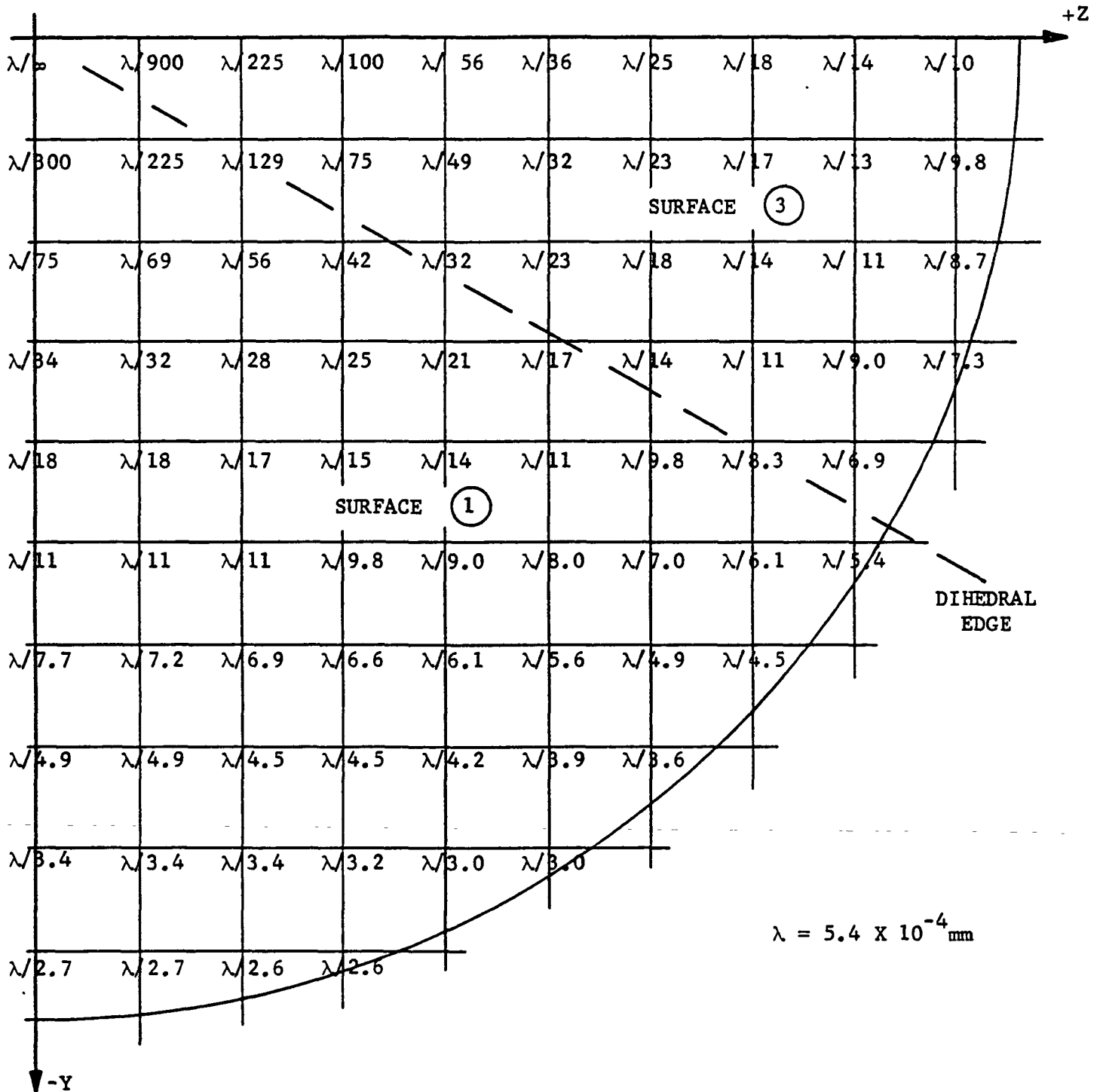


Figure 4-2B. OPD Map of Lower Right Quadrant of HCR Aperture - Hypothetical Case 2

concave toward the source on earth and is astigmatic, i.e., has different curvatures in any two orthogonal meridians. The semiprofiles in the extreme meridians and along the diagonal meridian are plotted to scale in Figures 4-3A and 4-3B for the two HCR cases. The axes are oriented as indicated in Figure 4-1. Any rotation of the HCR about the axis of symmetry would equally rotate the reflected astigmatic wavefront.

Two calculations were made with the OPD's tabulated in Tables 4-1 and 4-2. The first was to derive the RMS wavefront error corresponding to each set of OPD's. These values are  $\lambda/15.3$  for Case 1 and  $\lambda/6.1$  for Case 2, respectively ( $\lambda = 5.4 \times 10^{-4}$  mm). The second calculation gave the intensity of the central maximum of the far field diffraction pattern relative to that of a perfect reflector. The mathematical basis for this calculation is as follows:

The central maximum intensity I is:

$$I = |U|^2$$

where

$$U = \int_0^R \int_0^{2\pi} e^{i\phi(r,\theta)} r dr d\theta$$

In this expression, r and  $\theta$  are polar coordinates of a specific point in the pupil of radius R. To a close approximation, the 293 OPD's for the wavefront in question can be combined in a summation instead of in a double integral and normalized by the expressions:

$$U = \sum_{\rho} e^{i\phi}$$

$$I = \left| \frac{u}{N} \right|^2$$

where N is the number of points and  $\phi$  is the individual OPD at one of the N points. For the two cases of interest here, the values of the central intensity are 73 percent and 33 percent for Cases 1 and 2, respectively, compared to the theoretical values for a perfect HCR.

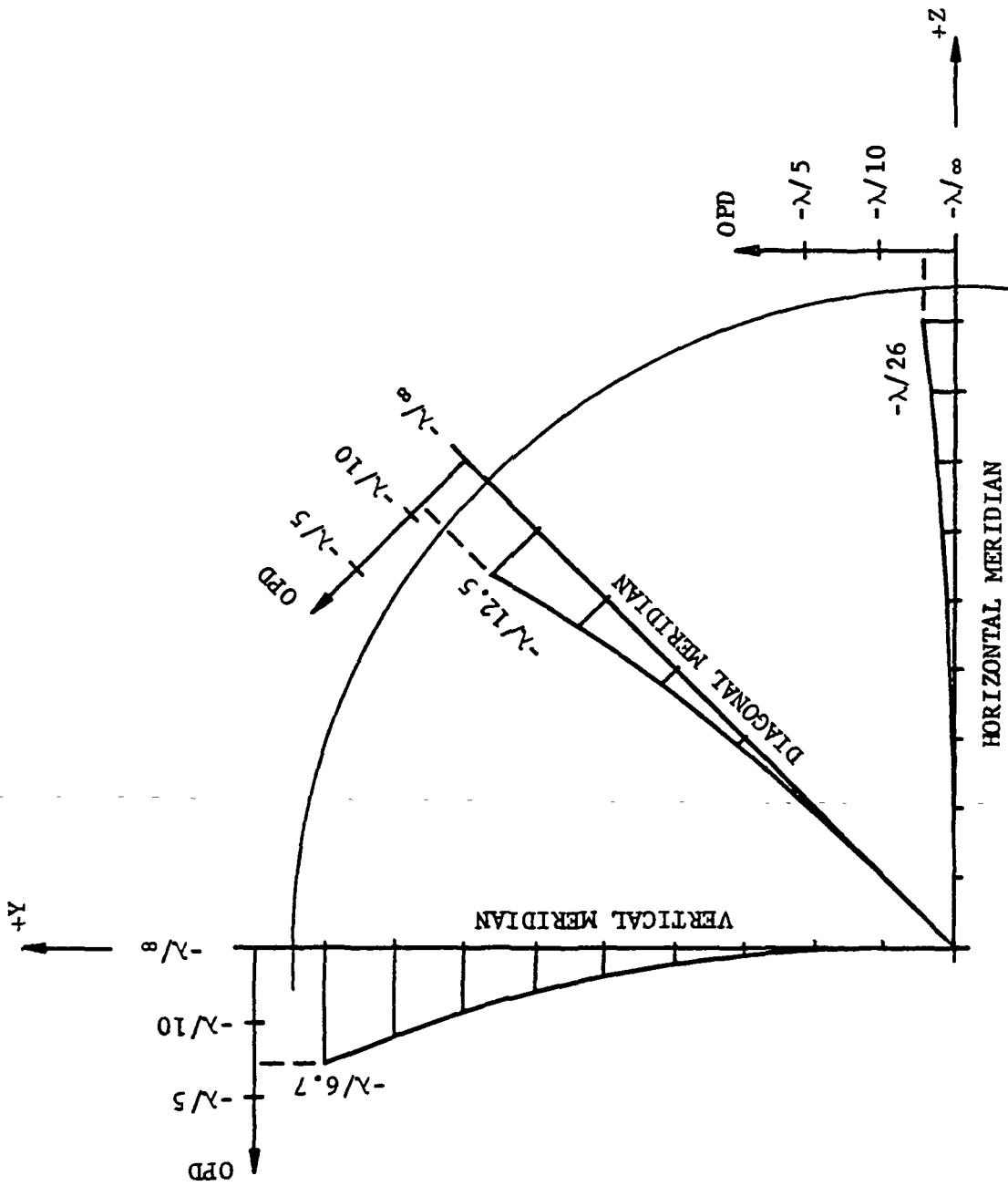


Figure 4-3A. Semi-Profiles of Concave Wavefront Reflected from Thermally Distorted HCR - Hypothetical Case 1

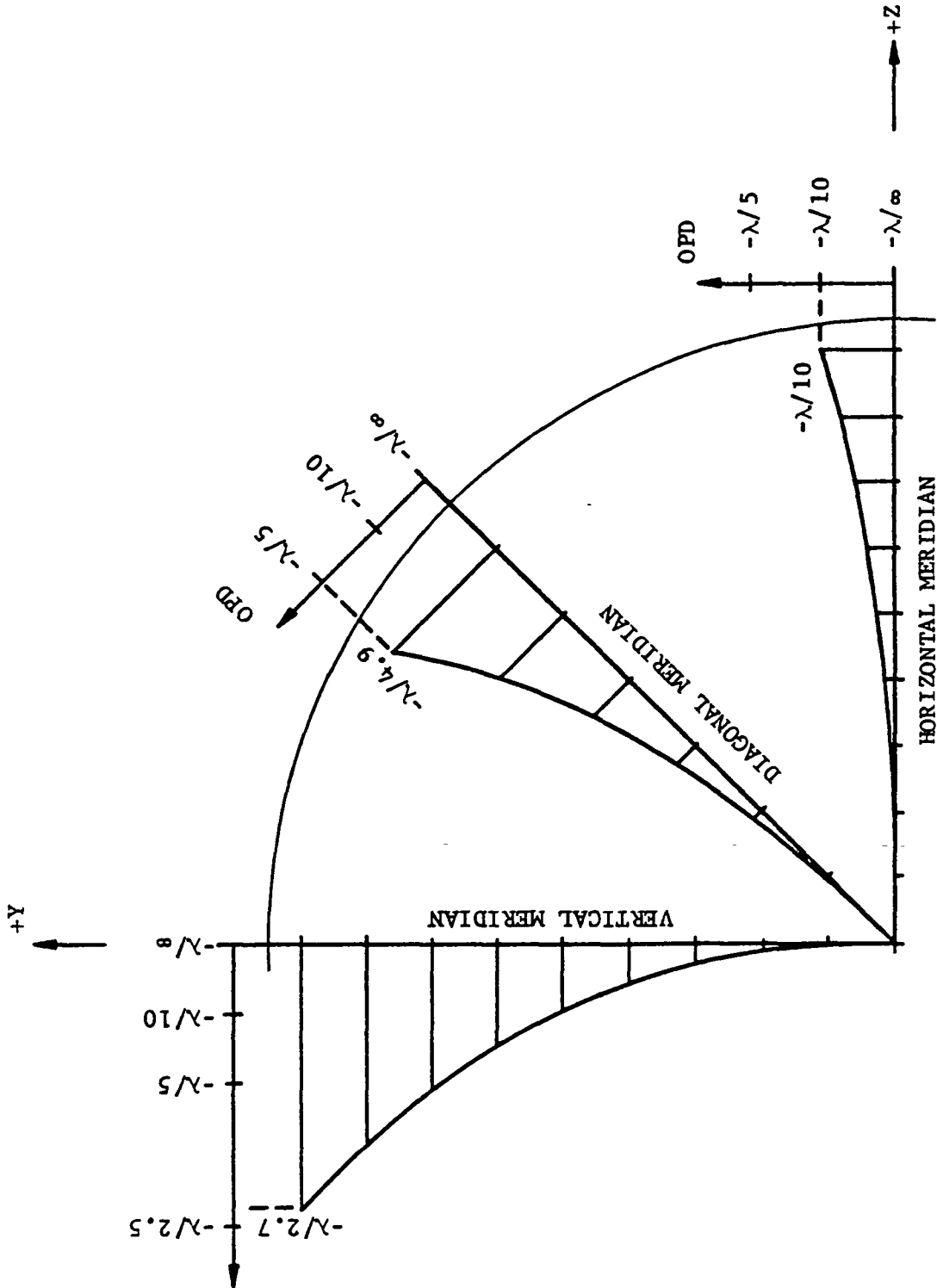


Figure 4-3B. Semi-Profiles of Concave Wavefront Reflected from Thermally Distorted HCR - Hypothetical Case 2

It is of interest to compare these calculated intensities to the values given by Marechal's equation for this parameter as defined on page 468 of Born and Wolf "Principles of Optics"<sup>17</sup> which is

$$I_{\text{peak}} = 1 - \left(\frac{2\pi}{\lambda}\right)^2 (\Delta\phi_p)^2$$

where  $\Delta\phi_p$  is the RMS departure of the wavefront from the sphere centered at the diffraction focus (i.e., in the far field). For the abovementioned RMS error of the Case 1 hypothetical HCR, the value of  $I_{\text{peak}}$  computed by this expression is 83 percent. The variation between this value and the 73 percent value calculated by numerical integration of the OPD map is believed to result from the nonrandom distribution of OPD's in the real case as compared to the assumed random distribution for the Marechal type calculation. In either case, this distorted HCR would be considered to provide excellent imagery. Since the Marechal equation is valid only for wavefronts with relatively small RMS deformation and "small" generally means  $\lambda/10$  or smaller, it cannot be used to confirm the numerically integrated intensity value for the Case 2 deformed HCR. The 33 percent calculated value of the latter intensity is considered accurate within the degree of approximation of our thermal analysis of the orbiting HCR. It may, therefore, be used as the basis for evaluating the thermal results.

Table 3-4 gives the maximum calculated sags of the mirror plates for HCR's made of ULE and Cervit and having three types of reflecting coatings at that point in the synchronous orbit where solar irradiation causes the maximum surface distortions. Selected values are reproduced in Table 4-3 for reference along with the corresponding data for the two hypothetical HCR's just discussed. The basis for the estimations in the "RMS Wavefront" and "Relative Intensity" columns are explained in the footnotes on the table.

Figure 4-4 shows the variation of the diffraction pattern central maximum intensity with RMS wavefront error in two ways. The computed values for the two hypothetical cases were plotted at the points marked (X). The straight dashed line through these points provides a means of estimating the inten-

TABLE 4-3  
SUMMARY OF SURFACE DISTORTIONS AND OPTICAL EFFECTS

HCR DESCRIPTION	COATING CHARACTERISTICS		MAXIMUM SURFACE SAG		RMS WAVE-FRONT DEFORMATION	RELATIVE INTENSITY OF CENTRAL MAXIMUM (PERCENT)
	$\alpha_s$	$\epsilon$	CONSTRAINED SURFACE	CANTILEVERED SURFACES		
Best Case Cervit	0.05	0.10	$\lambda/15$ *	$\lambda/7$	$\lambda/11$ ** (Estimated)	63 (Estimated)
Worst Case Cervit	0.10	0.05	$\lambda/8$	$\lambda/4$	$\lambda/6$ (Estimated)	32 (Estimated)
Best Case ULE	0.05	0.10	$\lambda/45$	$\lambda/22$	$\lambda/34$ (Estimated)	88 (Estimated)
Worst Case ULE	0.10	0.05	$\lambda/23$	$\lambda/12$	$\lambda/18$ Est. (Estimated)	77 (Estimated)
Hypothetical Case 1	--	--	$\lambda/25$	$\lambda/10$	$\lambda/15.3$ (Computed)	73 (Computed)
Hypothetical Case 2	--	--	$\lambda/10$	$\lambda/4$	$\lambda/6.1$ (Computed)	33 (Computed)

\*  $\lambda = 5.4 \times 10^{-4}$  mm (green)

\*\* Estimated RMS values are  $1.53 \times$  denominator from cantilevered surface column.

\*\*\* Estimated intensity values are from Figure 4-4.

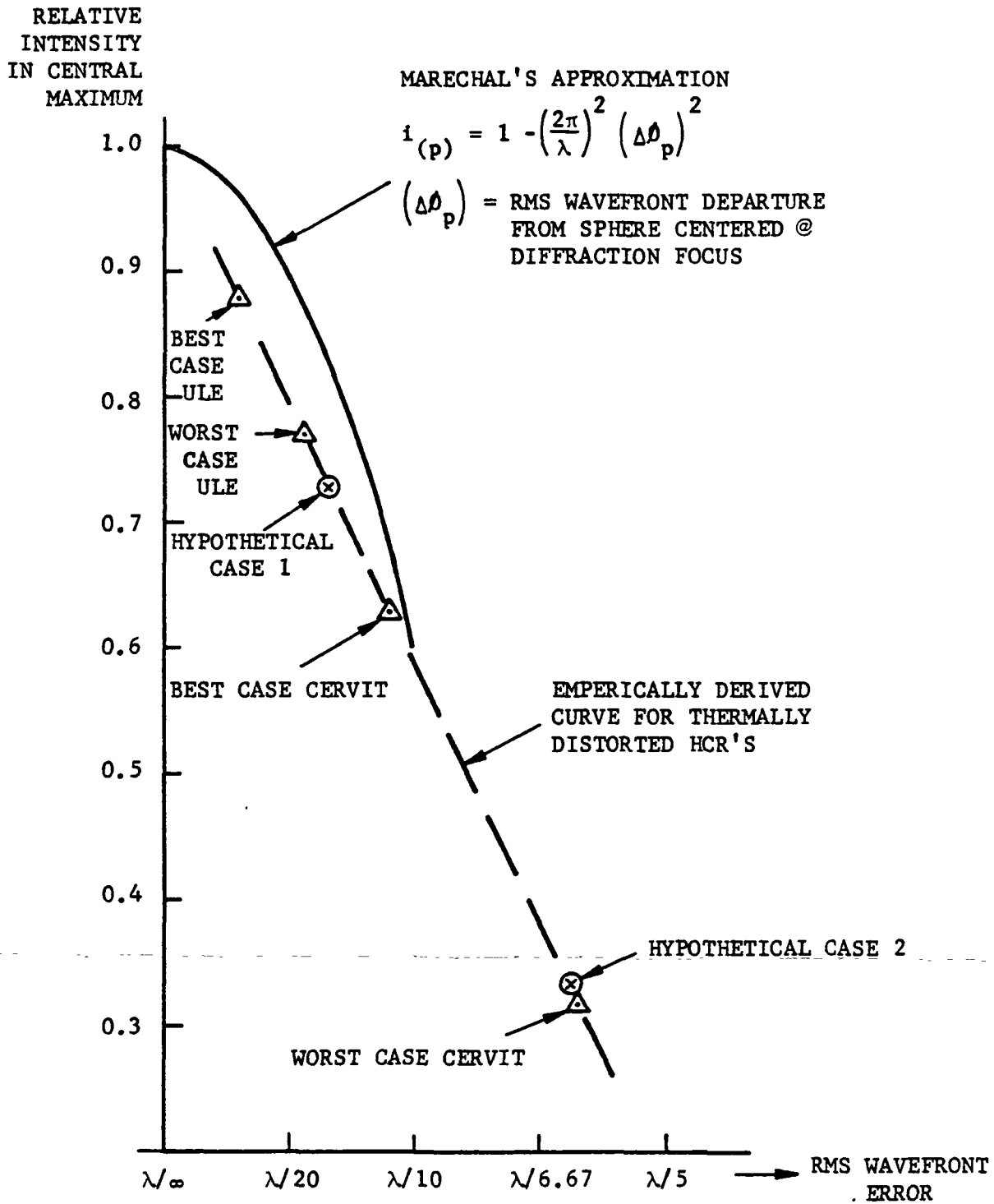


Figure 4-4. Variation of Central Maximum Intensity with RMS Wavefront Error ( $\lambda = 5.4 \times 10^{-4}$  mm)

sities for the various HCR designs indicated by  $\Delta$  symbols. The solid curve represents the Marechal approximation for random wavefront errors which, as was explained earlier, does not fully apply to these deformed HCR's.

It may be noted that HCR's made of ULE with any of the coatings considered here would be considered excellent. Cervit would perform quite well if the "best" coating can be applied. Its performance with the standard coating is not as good. From the optical performance viewpoint, therefore, it would seem that ULE is the preferred material for use in the thermally distorted HCR operating in a synchronous orbit.

## SECTION 5

### CONCLUSIONS AND RECOMMENDATIONS

The results of this study indicate that a HCR constructed of two suitably coated, flat ULE mirrors 2 cm thick (optically contacted to a similar mirror, 5 cm thick, so as to form three mutually perpendicular surfaces within  $\pm 0.30$  arc-second) could retroreflect a beam from the earth with a high degree of optical fidelity even though the HCR is subjected to the solar input characteristics of a satellite in a synchronous orbit. The performance of this HCR, expressed in terms of the relative energy in the central maximum of the far-field diffraction pattern, should exceed 80 percent of that expected from an ideal, undistorted HCR in visible light.

While the preliminary design of such a HCR, having an aperture of 200 square centimeters, has been established under this study (see Section 2.4), more detailed considerations should be given to certain aspects of that design in a future related effort. Those aspects include:

- Theoretical and experimental verification of the suitability of the recommended overcoated metallic coating having special thermal characteristics discussed in Section 2.3.4. Included in this would be considerations of polarization effects, durability, and ease of application to the HCR mirrors.
- Detailed design of a suitable mechanical mount for the HCR and establishment of a suitable mechanical and thermal interface with a typical satellite.
- Complete thermal analysis using a more detailed computer model than could be utilized under the limited scope of the present study. This analysis would be expected to confirm the approximate (but conservative) evaluation summarized in Section 3 of this report and would use the 58 node model discussed in Section 3.3.

Following these detailed design considerations, several prototype HCR models should be fabricated and evaluated in a simulated environment typical of that expected in the synchronous orbit. The shock and vibration (including acoustic) effects of launch, staging, docking, etc. should be evaluated as well as thermal inputs. Optical performance should be evaluated by interferometric techniques while the prototypes are thermally distorted to confirm predictions made in Section 4 of this report. In order to provide a reasonable statistical evaluation and to maximize confidence in the test results, Perkin-Elmer recommends that a minimum of 20 units be fabricated and tested.

The Perkin-Elmer Corporation is well-qualified and eager to continue to assist NASA in this development program. We have the expertise required to complete the design, fabrication and experimental tasks as well as the computer programs and scientific skills needed to complete the detailed thermal analysis of the final design. Through application of these talents, NASA is assured of the high caliber product and definitive experimental results which would then lead to a successful application of the HCR to a variety of operational systems.

## SECTION 6

## REFERENCES

1. R. F. Chang, et. al., "Far-Field Diffraction Pattern for Corner Reflectors with Complex Reflection Coefficients", J. Opt. Soc. Am. 61, 431 (1971).
2. P. R. Yoder, Jr., "Study of Light Deviation Errors in Triple Mirrors and Tetrahedral Prisms", J. Opt. Soc. Am. 48, 496 (1958).
3. K. N. Chandler, "On the Effects of Small Errors in the Angles of Corner Cube Reflectors", J. Opt. Soc. Am. 50, 203 (1960).
4. P. R. Yoder, Jr., "High Precision 10-cm Aperture Penta and Roof-Penta Mirror Assemblies", Applied Optics 10, 2231 (1971).
5. J. J. Jarosh, "The Dimensional Stability of Metals", Instrumentation Laboratory, Massachusetts Institute of Technology, August 1950.
6. B. S. Lement and B. L. Averbach, "Measurement and Control of the Dimensional Behavior of Metals", Instrumentation Laboratory, Massachusetts Institute of Technology, December 1955.
7. Hume-Rothery and Raynor, The Structure of Metals and Alloys, The Institute of Metals, No. 1, 1956.
8. Barrett, Structure of Metals (McGraw-Hill, 1952).
9. Stanworth, Physical Properties of Glass (Oxford Clarendon Press, 1950).
10. G. W. Morey, The Properties of Glass (Reinhold Publishing Corporation, 1938).
11. L. F. Drummeter and G. Hass, Physics of Thin Films, Vol. 2 (Academic Press, 1964).
12. G. Hass, "Mirror Coatings", Applied Optics and Optical Engineering III, R. Kingslake, Ed. (Academic Press, 1965).
13. G. Hass and J. B. Ramsey, et. al., Applied Optics 10, 1296 (1971).
14. G. Hass, J. B. Heaney, et. al., Optics Communications 8, 183 (1973).

15. W. M. Meyers, "Design and Analysis of Solid and Hollow Cube Corner Reflectors and Holders", G.E. Co. Document No. 66SD4431, AFCRL 66-563, (July 1966).
16. R. H. MacNeal, "An Asymmetrical Finite Difference Network", Quarterly of Applied Mathematics, XI, 295-310, (Oct. 1953).
17. M. Born and E. Wolf, Principles of Optics (The MacMillan Company, 1964).

#### BIBLIOGRAPHY

ER-166, "Manual of Computer Programs for Thermal Analysis of Orbiting Vehicles", dated 6 May 1971, The Perkin-Elmer Corporation, Optical Technology Division.

APPENDIX A

SOME CONSIDERATIONS OF BONDED HCR AS MANUFACTURED  
BY PRECISION LAPPING & OPTICAL CO., INC.

## APPENDIX A

### SOME CONSIDERATIONS OF BONDED HCR AS MANUFACTURED BY PRECISION LAPPING & OPTICAL CO., INC.

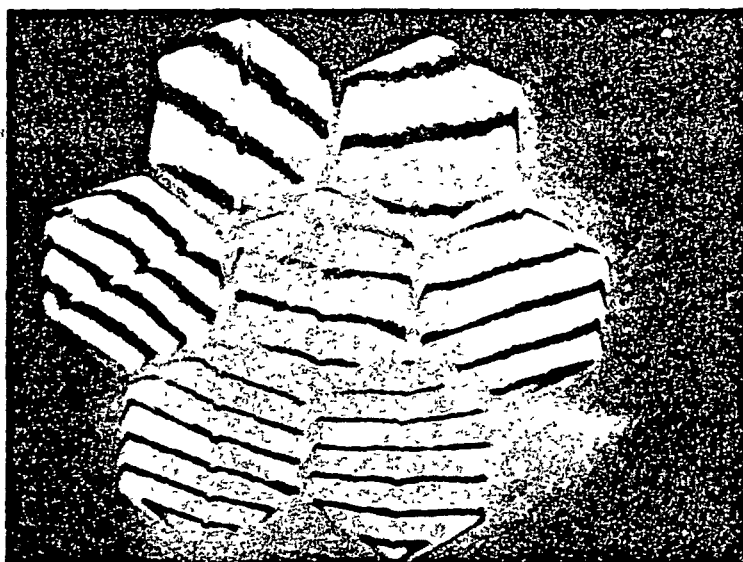
Concept No. 2 for the HCR (Hollow Corner Retroreflector), as defined in Section 2 of this report, consists of three mirror plates held at right angles to each other by an epoxy or similar bonding material. Perkin-Elmer's experience with this type of construction for other optical components indicates that there may be potential problems in achieving adequate long-term stability for the present application of the HCR as contemplated by GSFC.

Devices of this general type are currently being manufactured by Precision Lapping & Optical Co., Inc., of Valley Stream, N.Y. The attached data sheet describes a 5 inch aperture HCR offered by this firm. In order to seek more information concerning the device, Perkin-Elmer's Project Engineer discussed the design with Mr. Morton Lipkins of Precision Lapping on 26 December 1974. Mr. Lipkins holds a basic patent (No. 3,663,084 -- see attached copy) on bonded HCRs and has filed applications for four related patents.

Precision Lapping manufactures single and multiple HCRs in the 1/4 to 24 inch aperture range and is under contract to Johnson Space Flight Center for units to be flown on the Apollo-Soyuz Space Mission. While these devices are generally intended for commercial applications, the performance claimed by Precision Lapping leads to the conclusion that such devices should be suitable for military and space applications.

Due to the proprietary nature of the processes and materials used in the construction of these HCRs, details regarding their design have not been revealed to Perkin-Elmer. Interferograms (see below) and typical hardware examined by our representative indicate a high quality product. No specific test data indicating environmental resistance or long-term reliability was

provided by Mr. Lipkins. Nevertheless, he indicated willingness to provide sample HCRs with hexagonal  $200 \text{ cm}^2$  apertures made by their best state-of-the-art construction techniques and materials for evaluation by Perkin-Elmer and/or GSFC in the future. No estimate of the cost of these units was requested nor volunteered.



Typical Interferogram of HCR Cluster Manufactured by Precision Lapping and Optical Co. (Photo furnished by Mr. M. Lipkins)

APPENDIX

OUTLINE OF 58 NODE COMPUTER MODEL PROPOSED  
FOR MORE DETAILED THERMAL ANALYSIS OF THE HCR

## APPENDIX C

OUTLINE OF 58 NODE COMPUTER MODEL PROPOSED  
FOR MORE DETAILED THERMAL ANALYSIS OF THE HCR

The proposed 58 node model contains 16 nodes in each of the three faces of the HCR. The location of the nodal points and the allowable conduction paths between them are shown in Figure C-1 for the X - Y plane. The nodal arrangements in the other planes are similar. The nodal areas associated with each node are indicated in the figure. These areas were determined with the Perkin-Elmer computer program TRIANGLE, which is based on the theory of the irregular triangular grid presented in Reference 16.

The model would also contain one node for space, one node for an isothermal rear environment, and eight additional nodes on the 5 cm thick base plate of the HCR where it is joined to the 2 cm thick plates.

The aspects of the 58 node model, which is different from most multinode heat transfer analyses, are in the calculations of the radiation interchange and the total incident fluxes. Both these calculations involve the properties of specular surfaces. The method for calculating the radiation interchanges is considered first.

Figure C-2 shows the path of two reflected rays from point 1 on the X - Z plane, surface B, to point 2 on the X - Y plane, surface A. One ray goes directly to 2 and the other is partially reflected at point 3 on surface B, i.e., the fraction  $(1-\alpha)$  of it is reflected; the rest is absorbed. Both rays are reflected in a specular fashion from point 2. The direct ray may next be incident upon surface C, but the reflected ray must leave the corner cube. Neither

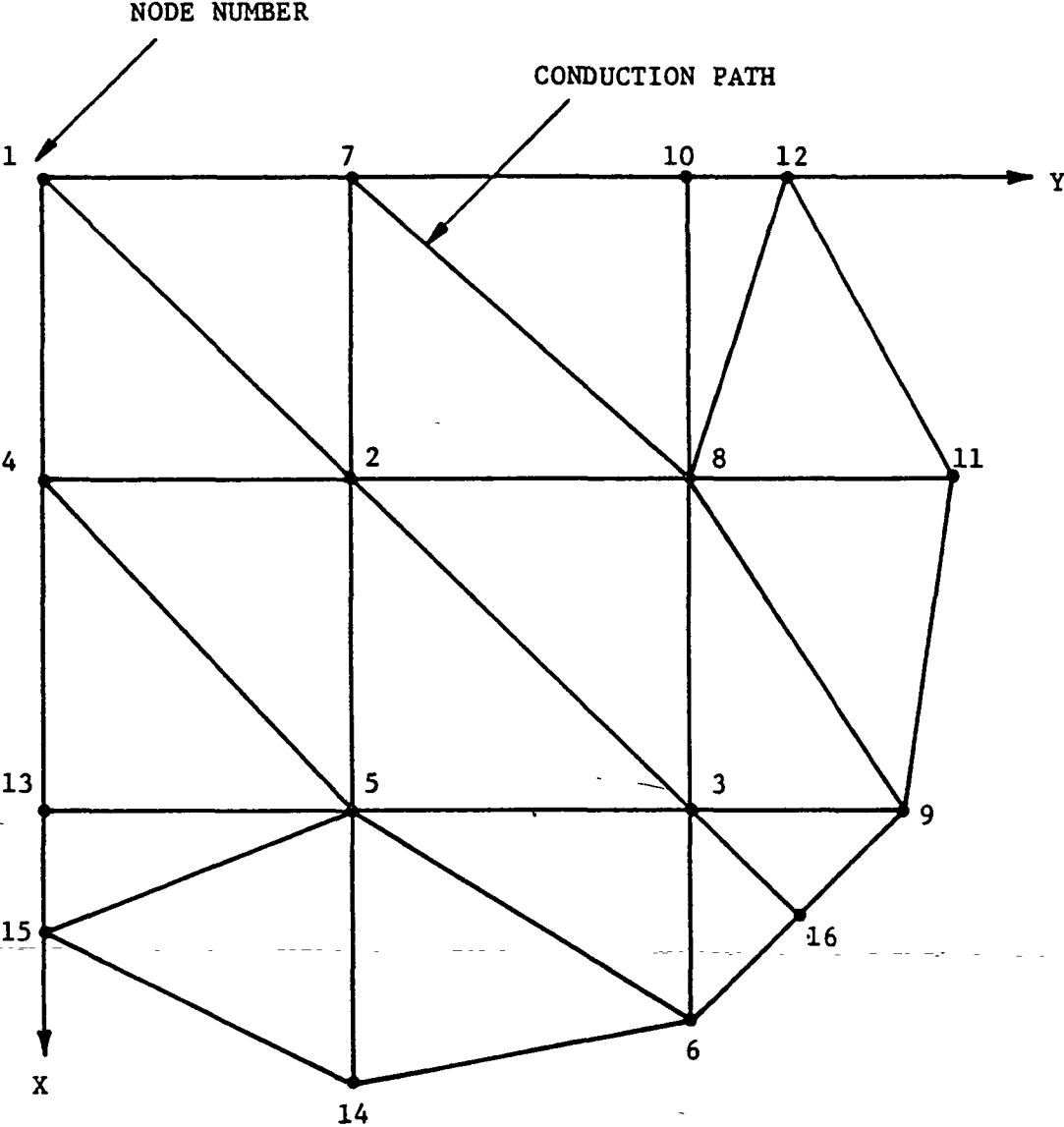


Figure C-1. Nodal Locations and Allowable Conduction Paths in X - Y Plane of 58 Node Model

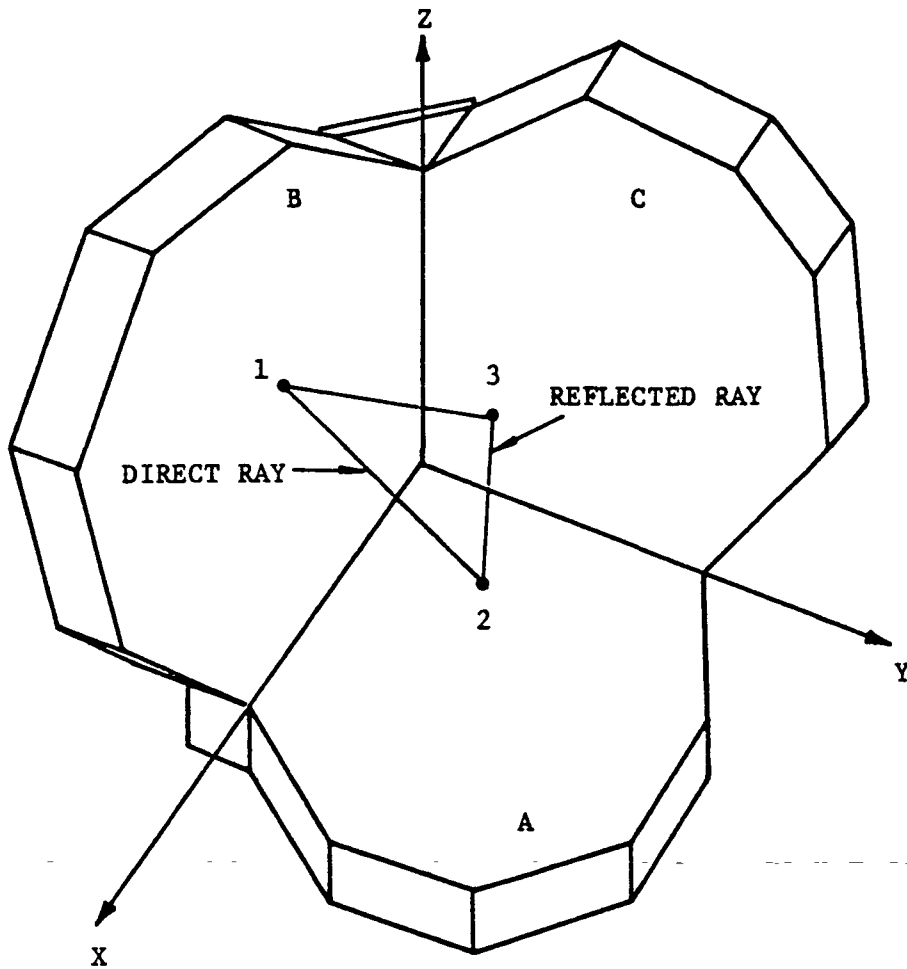


Figure C-2. Alternate Paths of Emitted Energy from Point 1 to Point 2

ray can return to surface B. The radiation shape factor from an infinitesimal area at point 1 to an infinitesimal area at point 2 may be found by using the structural equations or standard computer programs such as CONFAC. The radiation shape factor for the reflected ray is found in a similar fashion except that the mirror image of point 2 is used. This is illustrated in Figure C-3. The equivalent shape factor for radiation heat transfer between surfaces 1 and 2 is thus  $(F_{1-2} + \rho F_{1-2})$ . Similar analyses apply between the other two pairs of surfaces, i.e., (B,C) and (A,C). Shadowing or blockage is not a factor in this analysis because the plates are all the same size and because the plates are flat.

Blockage, however, becomes important in the calculation of the incident fluxes from external sources, i.e., the solar, earthshine, and albedo fluxes. Five parallel incoming rays that strike surface A are shown in Figure C-4. These rays are representative of the incoming solar, albedo and earthshine. One ray is directly incident upon the surface. (The directly incident fluxes may be calculated by standard computer programs. At Perkin-Elmer, this is done with the program called FLUXES, which is fully described in ER-166\*.) The second incoming ray strikes surface C and is reflected onto surface D. The energy flux corresponding to this ray is  $\rho$  times the flux that passes through a port equivalent to surface C and is incident upon the mirror image of surface A (see Figure C-5). If the computer program equivalent to FLUXES does not contain a "PORT" option, then an equivalent port must be generated by blockage surfaces. One means of accomplishing this is shown in Figure C-6. In a similar fashion, the flux which is reflected off B onto A is equal to  $\rho$  times the flux which passes through a port equivalent to surface B and is incident upon the mirror image of surface A in mirror B. The last two rays shown in Figure C-4 are those that are incident upon surface D after reflections off two surfaces. The ray that strikes surfaces C and B in that order is shown in Figure C-7. The incoming ray strikes surface C at point R, is reflected to point Q on surface B, and then is incident upon surface A at

---

\*ER-166, "Manual of Computer Programs for Thermal Analysis of Orbiting Vehicles", dated 6 May 1971, The Perkin-Elmer Corporation, Optical Technology Division.

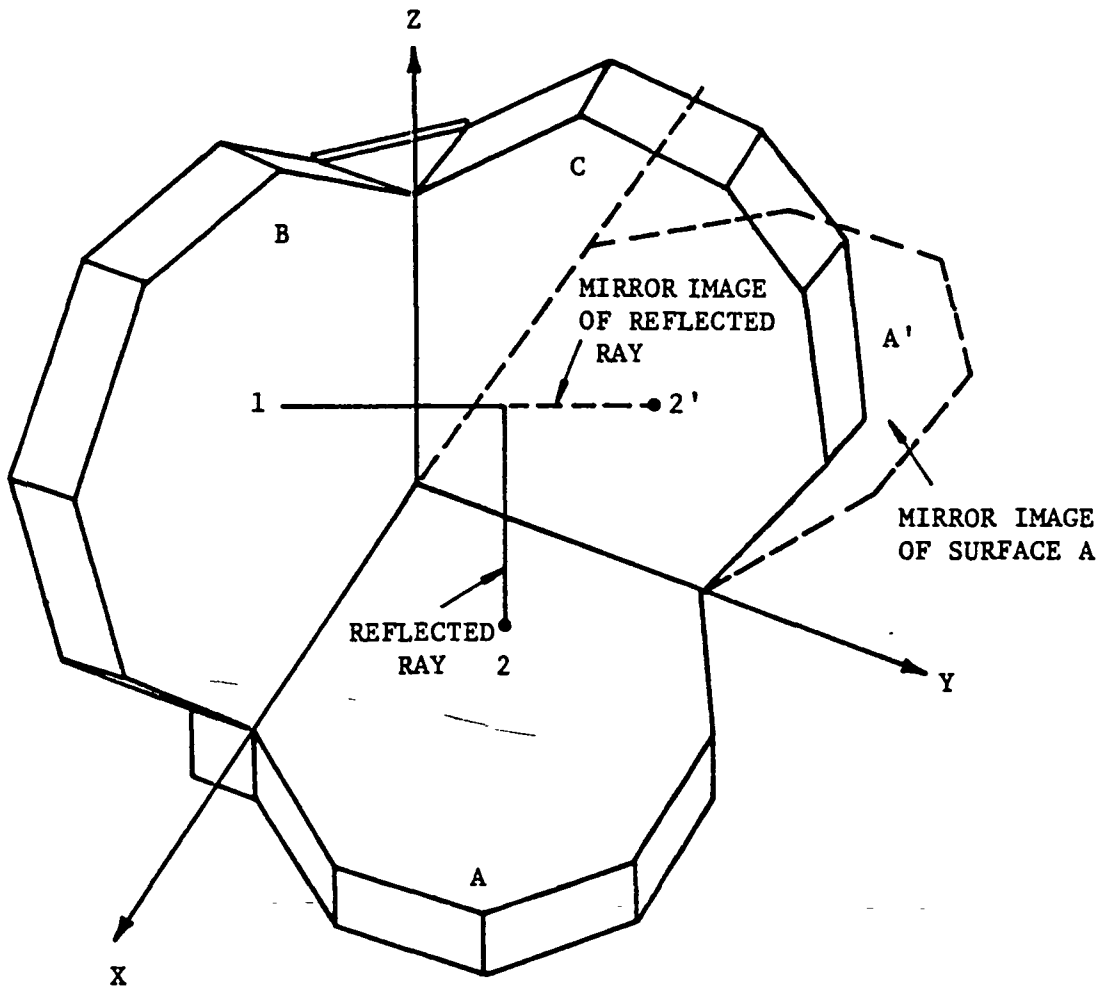


Figure C-3. Mirror Image of Reflected Ray Which Is Emitted by Point 1 and Incident upon Point 2

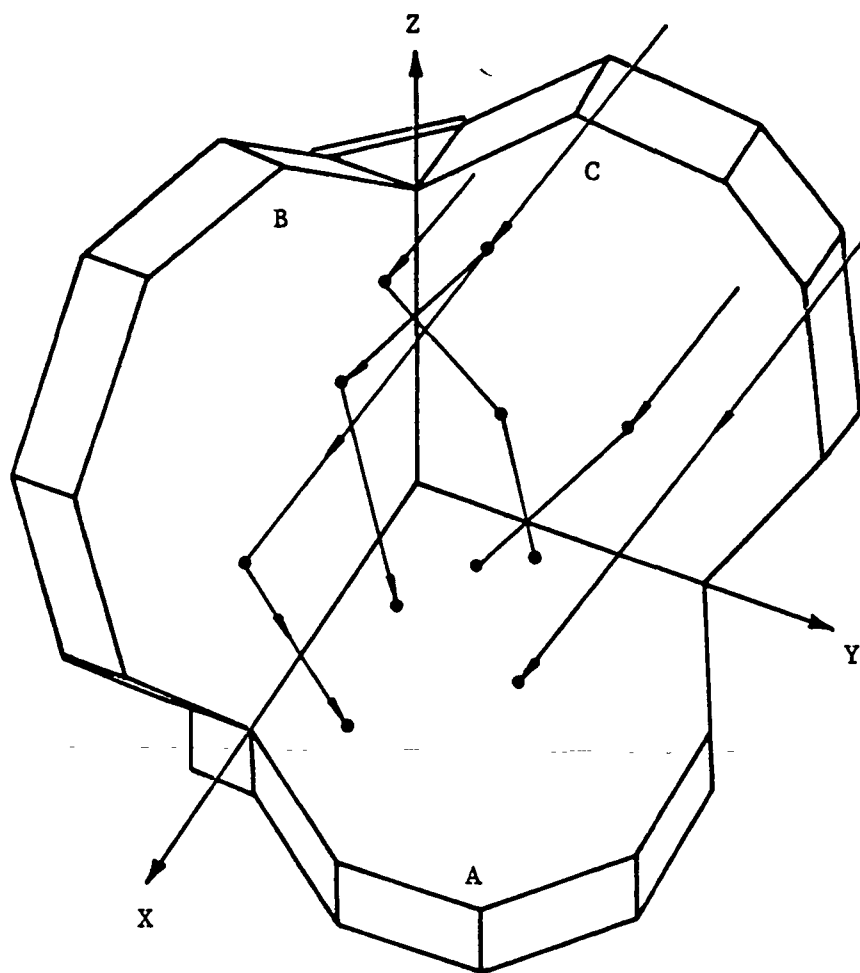


Figure C-4. Energy Incident upon Surface A after 0, 1, and 2 Reflections

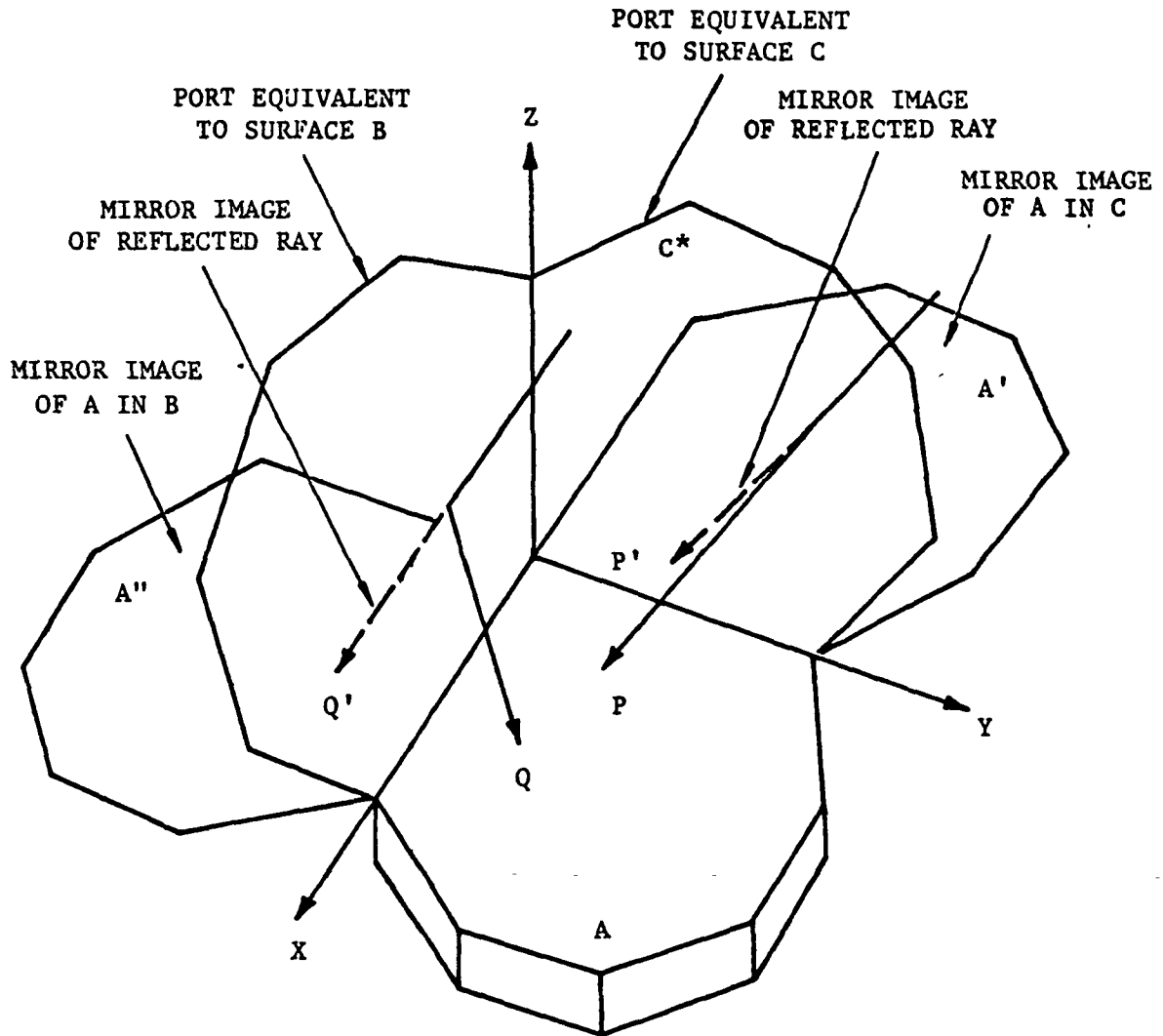


Figure C-5. Paths and Mirror Images of Rays Which Are Incident upon Surface A after 1 Reflection

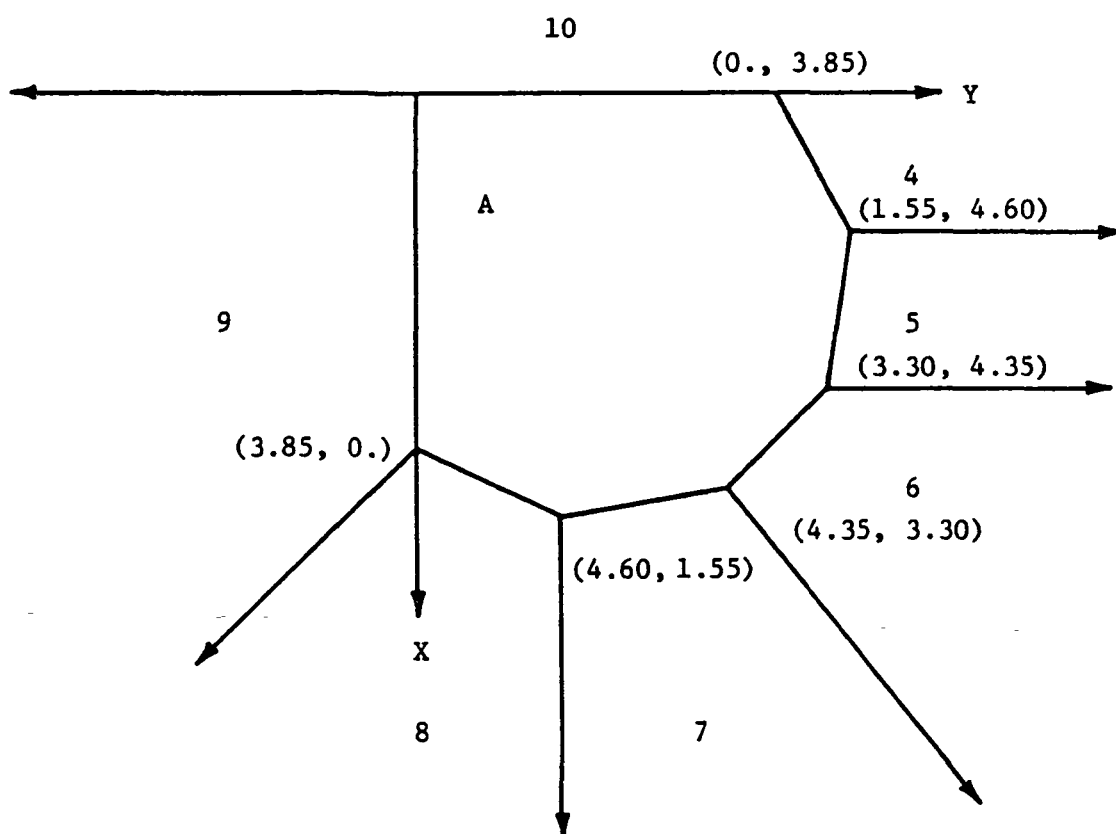


Figure C-6. Coordinates for Generating Minimum Number of Blockage Quadrilaterals for HCR Face

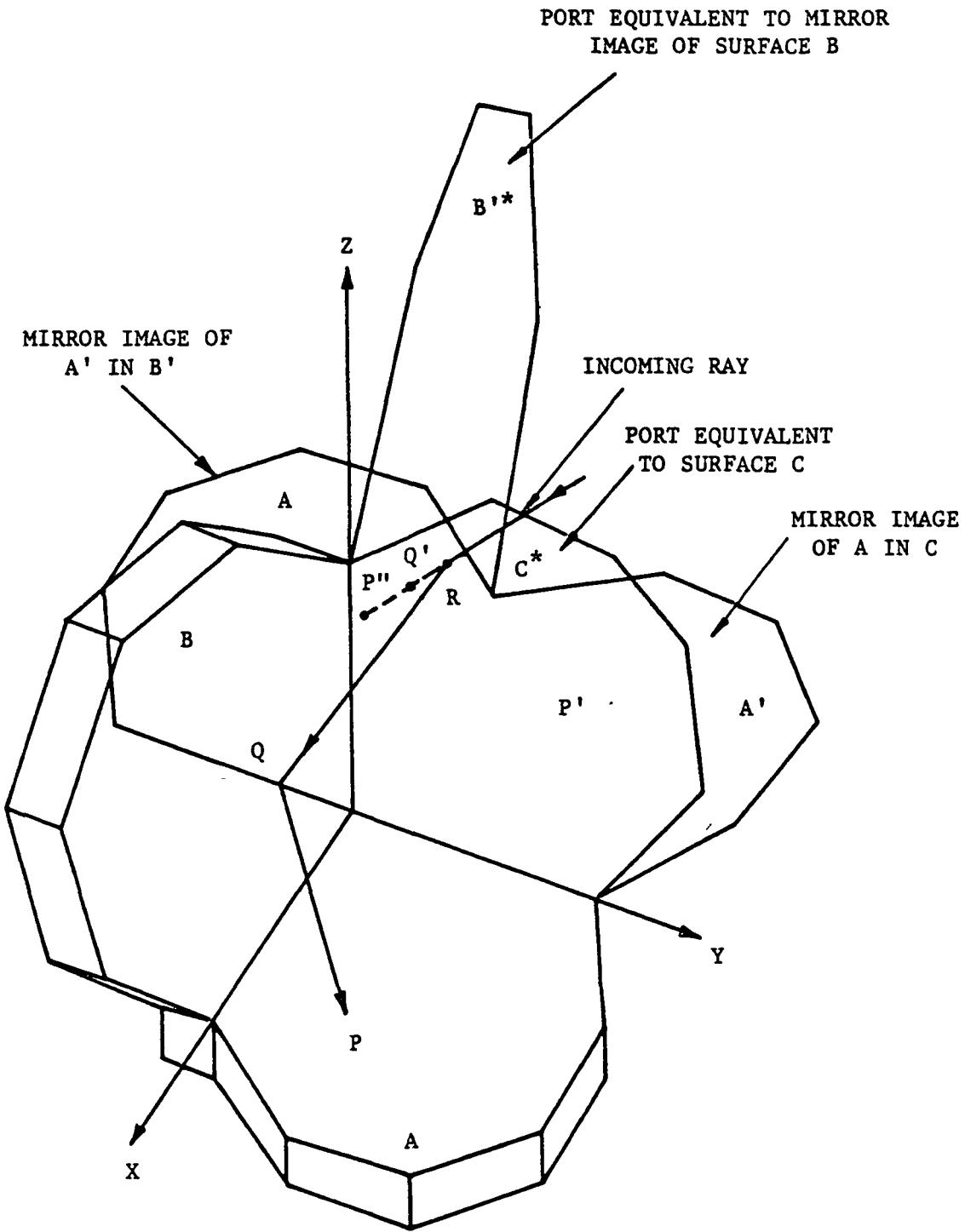


Figure C-7. Paths and Mirror Images of an Incident Ray Which Reaches Surface A after 2 Reflections

point P. The intensity of the fluxes represented by this ray is  $\rho^2$  times the intensity of the fluxes which pass through Port C and through Port B (the mirror image of Port B) and is then incident upon A'', the image of the image A. A similar analysis applies for the other doubly reflected ray.

Once the fluxes and shape factors have been generated, the analysis proceeds in a routine fashion. The calculation of the fluxes, the determination of the mean steady orbital temperature distribution, and the calculation of the transient temperature distribution in a 24 hour orbit, however, would require several hours computation time on the Perkin-Elmer Computer System.

Attachment to CD-LHF-642

Distribution

<u>Addressee</u>	<u>Code</u>	<u>No.</u>
Systems Reliability Director	300	1
Space Application Director	700	1
Publication Branch	251	1
Patent Counsel	204	1
Contracting Officer	287	1
Technical Officer	722	2
Documentation Section	251.2 ✓	Repro

# PERKIN-ELMER

OPTICAL TECHNOLOGY DIVISION  
THE PERKIN-ELMER CORPORATION  
DANBURY, CONNECTICUT 06810  
TELEPHONE (203) 744-4000  
CABLE: PECO-NORWALK

CD-LHF-642  
June 18, 1975

National Aeronautics & Space Administration  
Goddard Space Flight Center  
Greenbelt Road  
Greenbelt, Maryland 20771

Attention: Ms. Rhoda Schwartz, Code 287

Subject: Contract NAS 5-20580 (PE SO 21032);  
Delivery of Final Report

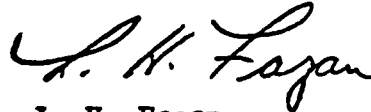
Dear Ms. Schwartz:

In accordance with your telephoned instructions of 9 June, we are delivering the Final Report to the distribution identified in Contract Article XII.

Some changes have been made from the draft copy per a telephone conversation between your Technical Officer, P. Minott and our Program Manager, P. Yoder.

Very truly yours,

THE PERKIN-ELMER CORPORATION



L. H. Fagan  
Contract Administrator

LHF/mw  
Enc:

Distribution: (see attached)